CONTROLLING DEFORMATION IN ELASTIC AND VISCOELASTIC BEAMS DUE TO TEMPERATURE AND MOISTURE CHANGES USING PIEZOELECTRIC ACTUATOR

A Thesis

by

RAMACHANDRA SRINIVASA CHAITANYA KURAVI

Submitted to the Office of Graduate Studies of
Texas A&M University
in partial fulfillment of the requirements for the degree of

MASTER OF SCIENCE

May 2011

Major Subject: Mechanical Engineering

CONTROLLING DEFORMATION IN ELASTIC AND VISCOELASTIC BEAMS DUE TO TEMPERATURE AND MOISTURE CHANGES USING PIEZOELECTRIC ACTUATOR

A Thesis

by

RAMACHANDRA SRINIVASA CHAITANYA KURAVI

Submitted to the Office of Graduate Studies of
Texas A&M University
in partial fulfillment of the requirements for the degree of

MASTER OF SCIENCE

Approved by:

Co-Chairs of Committee,	Kumbakonam Rajagopal
	Anastasia Muliana
Committee Member,	Amine Benzerga
Head of Department,	Dennis O'Neal

May 2011

Major Subject: Mechanical Engineering

ABSTRACT

Controlling Deformation in Elastic and Viscoelastic Beams Due to
Temperature and Moisture Changes Using Piezoelectric Actuator. (May 2011)

Ramachandra Srinivasa Chaitanya Kuravi, B.Tech, Indian Institute of Technology,
Guwahati

Co–Chairs of Advisory Committee: Dr. Kumbakonam Rajagopal
Dr. Anastasia Muliana

This thesis analyzes the implementation of surface bonded piezoelectric actuators to control or minimize the deformation in elastic or viscoelastic cantilever beams due to simultaneous heat and moisture diffusion. The problem is addressed in the context of linearized elasticity and linearized viscoelasticity. The constitutive equations are derived from the balance laws for mass, linear and angular momenta, energy, entropy and the second law of thermodynamics. The constitutive equations for linearized elasticity are then obtained as a consequence of small deformation assumption. The temperature and moisture induced deformation is introduced through the coefficient of thermal expansion CTE and coefficient of moisture expansion CME. The constitutive equations for linearized viscoelasticity are obtained by correspondence principle. The coupled temperature and moisture diffusion equations are obtained as a consequence of Clausius-Duhem inequality. The extent of coupling between heat conduction and moisture diffusion phenomena is studied by varying the ratio of their diffusivities and a non-dimensional coupling parameter. The effect of coupled unsteady heat conduction and moisture diffusion phenomena on the short and long term response characteristics of the beam such as displacement, stress and strain fields is studied. Based on these response characteristics, the magnitude of external actuating voltage required to minimize deformation is predicted. This is followed by a comparative study of the field variables in cases of actuated and unactuated beams. Four materials are chosen for this study; aluminium, epoxy, carbon fiber reinforced polymer with fiber volume fraction of 60%, and an epoxy-like viscoelastic material. The viscoelastic material is assumed to be thermorheologically simple. The shift factor is assumed to be a linear function of temperature and moisture fields. To address this problem numerically, a finite difference formulation is presented for the field equations and boundary conditions. This numerical scheme is validated by solving the problem of uniformly loaded cantilever beam and comparing the results with the analytical solution known a priori. The results obtained numerically are validated by comparison with experimental results. It is observed that the under the effect of external actuation, the stress and displacement fields are largely minimized in all four cases chosen for study. The bending in the unactuated viscoelastic beam is more pronounced than bending in the unactuated elastic beam. This is due to the softening of the material with time due to evolving temperature and moisture fields. However, relatively lesser external actuating voltage is necessary to minimize bending in the former case compared to the latter. The magnitude of actuating electric field required in the piezoelectric layer suggests a need to address the problem with in a non-linear framework, no such attempt is made in this study.

ACKNOWLEDGMENTS

”Matrudevobhava. Pitrudevobhava.” I dedicate this work to my parents who have been a constant source of encouragement and inspiration in my quest to learn the meaning of life. *”Acharadevobhava.”* I am ever grateful to Dr. Kumbakonam Rajagopal, who as a mentor and a philosopher, has guided me with his vision to those horizons of science and philosophy previously unknown to me. I am ever grateful to Dr. Anastasia Muliana for patiently supporting me through the course of my first step to research and teaching me invaluable lessons for my future endeavors. I am indebted to my friend, Yuval Doron, for supporting me and encouraging me through all the ups and downs that I encountered during my stay at Texas A&M University. I am grateful to Dr. Satish Karra for sharing his ideas with me through numerous productive discussions.

TABLE OF CONTENTS

LIST OF TABLES

LIST OF FIGURES

CHAPTER I

INTRODUCTION

Polymers, polymer composites and aluminium are widely used in structural components due to light weight, low manufacturing cost and the ease to shape. Polymer composites also offer high corrosion resistance, high strength to weight ratio and high material moduli. The mechanical and physical properties of polymer and polymer composites such as material modulus, strength, thermal stability and coefficient of thermal expansion can be engineered to meet the requirements of specific applications in space craft and automotive industries, medical devices applications, electronic components, off shore and on shore oil exploration applications [1]. Aluminium, due to its low density, high strength to weight ratio, high corrosion resistance and high thermal conductivity is widely used in automobile industry, shipbuilding industry, heat exchangers, aircraft and railway industries to illustrate a few [4].

These materials while in use as structural components are subjected to several mechanical loading cycles, environmental effects such as extreme temperature changes and humid conditions during their life time. For instance, rotary blades in helicopters or wind turbines are subjected to continuous temperature and humidity changes. These effects might pose a detrimental effect on these structural components in the form of an excessive deformation, for instance. *Creep* and *stress relaxation* characteristics are generally observed in polymer and polymer composite materials owing to which they exhibit viscoelastic behavior. The continued straining or flow of a material under constant stress is called *creep* whereas the decrease in stress at constant strain is called *stress relaxation* [5]. The viscoelastic response is prominent especially at elevated temperatures. Over a long period of time, the environmental factors might also lead to other effects such as corrosion, oxidation which reduce the load

---

The journal model is *IEEE Transactions on Automatic Control.*

carrying ability of the material and hence forth diminishing the lifetime of the components. Prolonged existence of such loading conditions might also lead the system to the verge of instability, if not failure. For instance, in the case of helicopter blades, a slight change in the blade geometry i.e. blade angle can adversely affect the controllability of the helicopter. External actuating mechanism in the form of surface bonded actuators or embedded actuators offers a solution to control or minimize the deformation and prolong the life of such components. However, decrease in load carrying capacity by deterioration of material properties caused due to corrosion cannot be handled using an external actuating mechanism.

This study examines the use of an external actuating mechanism in the form of surface bonded piezoelectric actuators to control the elastic/viscoelastic deformation in certain structural materials i.e. Aluminium, polymer, particle or fiber reinforced polymer, subjected to transient temperature and moisture fields, in the context of a linearized theory of elasticity or viscoelasticity and piezoelectricity.

A. Piezoelectric Materials

Certain type of materials when pressed are observed to develop electric charges. Such materials are termed as Piezoelectric materials. The word *Piezoelectricity* is derived from the the Greek word *Piezien* which means *to press*. This phenomenon was first experimentally observed by Jacques Curie and Pierie Curie in 1880 AD. Piezoelectric materials are also shown to exhibit an inverse effect, i.e. such materials deform when subjected to external electric fields. The inverse Piezoelectric effect was proposed by Lippman and experimentally confirmed by the Curie brothers. Owing to their electromechanical coupling characteristics, piezoelectric materials are employed in wide range of applications. Direct piezoelectric effect is employed in sensing applications whereas inverse piezoelectric effect is used in applications requiring actuation. As a sensor, the piezoelectric material records an electrical signal from displacement or pressure and is employed in devices such as sonar, ultrasonic imaging technologies. Whereas as an actuator, it supplies electric signals such as applied voltage or electric field for controlling movements in devices such as stepper motors, high precision machining tools, valves etc. They are also used as energy harvesters in flooring systems where electricity is generated when pedestrian or vehicular traffic passes over.

Many natural and man made materials exhibit piezoelectric phenomenon. Some examples of natural piezoelectric materials include cane sugar, rochelle's salt, quartz etc. Barium Titanate ($BaTiO_3$), Lead Titanate ($PbTiO_3$), Lead Zirconate Titanate ($Pb(Ti, Zr)O_3$), Lead niobate ($PbNb_2O_6$) are some examples of piezoelectric ceramics which are man made. Poly-vinyl difluoride (PVDF) is a typical example of polymers exhibiting piezoelectric phenomenon. Among natural piezoelectric materials, quartz (α-Quartz) oscillators are commonly used for frequency control in TVs and computers. In general, natural piezoelectric crystals exhibit inferior piezoelectric properties compared to piezoelectric ceramics and polymers and so their applications are limited.

PVDF is lighter, more flexible and can be manufactured to desired shapes with relative ease compared piezoceramics. It also offers greater resistance to moisture absorption and impact loading than piezoceramics. Its piezoelectric properties and permittivities are inferior compared to piezoceramics, but owing to its better response characteristics to ultrasonic energy applications they are employed in applications such as sonor and imaging transducers. Piezoceramics, in general posses relatively higher piezoelectric properties, dielectric constants, electromechanical coupling coefficients and Curie temperature[1] compared to the other two kinds of materials. They exhibit stable piezoelectric properties even at elevated temperatures (below the curie temperature). Hence, piezo ceramics are widely preferred for commercial purposes. But piezoceramics are brittle in nature and heavy. Among piezoceramics, PZT offers superior piezoelectric properties(electromechanical coupling coef-

---

[1] Curie temperature is the temperature at which the spontaneous polarization of the material becomes zero.

ficients), dielectric properties and coupling constants[2]compared to other piezoceramics such as ($BaTiO_3$). But, ($BaTiO_3$) exhibits greater resistance to depoling effect under compressive stresses compared to PZT. Hence, ($BaTiO_3$) doped with Co is preferred over PZT in high acoustic power applications. In general, the choice of piezoelectric material is made based on the type of requirements of a particular application.

Crawley et al. [6] presented the use of piezoelectric actuators to control the response of cantilever beam like structures under static and dynamic loads. They developed analytical models to predict the static and dynamic response characteristics of simple beams with either surface bonded or embedded piezoelectric actuators. These models were validated experimentally for aluminium, graphite/epoxy and glass epoxy laminates, satisfactorily. In the case of surface bonded actuators they have also accounted for effects of a flexible bonding layer between the actuated beam and the actuator and showed that a thin bonding layer with high shear modulus would offer good approximation for perfectly bonded system. Crawley-Anderson [7] discuss two analytical models (uniform strain model, Bernoulli-Euler model) to predict extension, bending and shearing deformation in one dimensional structures with surface bonded/embedded piezoelectric actuators. Their approach is based on an actuation strain provided by the actuator which causes extension or bending in the beam assembly. The results of these models are compared with the results predicted by (i)a finite element model and experimentally obtained data. Zhou et al. [8] studied the problem of bending in simply supported laminated composite plates under the effect of piezoelectric actuators. The geometry was solved in the context of linearized elasticity. Piezoelectric actuators can also be implemented to control thermal deformations in composite structural elements. Lee and Saravanos [9] numerically simulated the deformation and stress fields in a graphite-epoxy composite beam embedded with surface piezoelectric actuators subjected to (a)a uniform

---

[2] A piezoelectric coupling coefficient is a measure of the ability of a piezoelectric material to transform electrical energy to mechanical energy or vice-versa.

thermal change (b)a uniform thermal gradient throughout the entire beam. The active compensation voltage to minimize the displacement was predicted. A layer wise treatment of the beam assembly was considered for this purpose.

Piezoelectric materials are generally installed in patches at specific locations on the controlled structures in place of including one single layer of piezoelectric material of the same length as the controlled geometry, due to space constraints, cost constraints. Crawley et al. [6] presents a note on the choice of actuator locations when piezoelectric patches are used. In the context of linearized theory, Ahmed et al. [10] showed that piezoelectric patches can be effectively used for control of deformation in structural elements. In the context of linearized piezoelectricity, they numerically solved the problem of deformation in cantilever beams under thermal and mechanical loading with the use of surface bonded piezoelectric actuators. Song et al. [2] numerically simulated the use of piezoelectric patches for active control of thermal deformation of composite beams and validated the results with experiments. Their study includes both transient and steady state temperature loading conditions. Active control of the beam deformation using piezoelectric patches was implemented using a PID (proportional-integral-derivative) controller.

B. Thermal and Moisture Effects on Structural Components

Response characteristics of materials can change due to changes in loading conditions, environmental effects and aging. Aging process can be accelerated due to exposure to severe environmental conditions. Environmental changes could have enhancing or detrimental effect on the material behavior. For instance, carbon/epoxy composites are highly vulnerable to moisture diffusion in humid conditions. Due to presence of absorbed moisture, polymers tend to swell and henceforth unintended dimensional changes might occur. Weitsman [11], Springer et al. [12] have shown that the environmental effects on the response characteristics of many polymer matrix composites is quite significant. In particular, Weitsman [13] proposed a model to account for the moisture effects on the response of polymer composites in a general thermodynamic framework appealing to continuum damage theory. In his work, the material moduli depend on 32 invariants making the model too complicated to work with. Muliana et al. [14] studied the effect of moisture on the material response characteristics by proposing that material properties depend on the concentration of the fluid. In their study, the fluid flow is governed by the advection-diffusion equation. In the problems of thermoelasticity, the temperature dependence of strain and stress fields is accounted by introducing the notion of the *coefficient of thermal expansion* (CTE). Similarly, the effects of moisture on deformation of composites were accounted for through *coefficient of moisture expansion (CME)* in [15], [16]. Such a notion is restricted to small deformation problems. Poenninger [17] experimentally measured the moisture induced deformation for a class of carbon fiber reinforced polymer composites (CFRP) under isothermal conditions. The deformation was small enough to be explained in terms of a CME. The absorbtion of moisture by polymer/polymer composites might also be dependent on factors such as temperature and stress-strain fields in the composite and porosity. Right [18] reported the effect of moisture absorption on several epoxy and CFRP composites. The steady state moisture content in those composites at various temperatures and relative humidities, dimensional changes due absorbed moisture were graphically presented. His work reports that the steady state moisture content and moisture diffusivities of several epoxy resins and CFRP composites are temperature dependent. Viscoelastic material behavior might also play a significant role in the response characteristics of polymers, depending on the working and loading conditions. In particular, the stress relaxation and creep processsess could be sped up at elevated temperatures and slowed down at lower temperatures. In the context of linearized viscoelasticity, certain class of materials whose response stress relaxation and creep characteristics at temperatures other than reference temperature could be evaluated by accounting for a corresponding shift of the time scale are termed as thermo-rheologically simple materials

(TSM) by Schwarzl et.al [19]. For such materials, the shift factor is a material property and a function of the reference temperature and current temperature. Similarly, the viscoelastic material response could also be altered by the changes in moisture content in the material [20]. The author proposed to explain such an effect by choosing the shift factor as a function of the concentration. Flaggs et al. [21] conducted experiments to measure the curvature due to warping in non-symmetric GY70/330 composite laminates exposed to temperatures between 75F to 160F and relative humidity varying from 20%-100%. The material was assumed to be a TSM with the shift factor depending on both temperature and moisture contents. The thermal and moisture induced strains were related to temperature and moisture changes through CTE and CME, respectively. The results predicted by this model were in good agreement with the experimental results.

There have been studies involving both transient thermal and moisture fields in polymers, polymer composites and aluminium. In case of polymer and polymer composites, Fick's law of diffusion and Fourier's law of heat conduction could be employed independently neglecting the velocity of the medium and appealing to small deformation approximation to obtain the temperature and moisture fields. Such an uncoupled theory to evaluate temperature and moisture fields might be inadequate and inaccurate as shown by Sih et al. [22, 23]. Their work indicates that stresses in CFRP due to coupling effect can deviate from the results from uncoupled theory by a minimum of 20% depending on the boundary conditions employed. The extent of coupling between the temperature and moisture fields depends on Lewis number, defined as the ratio of thermal diffusivity to moisture diffusivity. The coupling becomes increasingly significant as the Lewis number approaches unity. For instance, in metals such as aluminium, the coupling effect is insignificant as thermal diffusivity is several orders of magnitude higher than moisture diffusivity. However, for certain polymer and polymer composites coupling becomes important as moisture and thermal diffusivities are comparable. For instance Sih et al. [22] showed the significance of a coupled theory numerically for T300/5208 graphite fiber reinforced epoxy matrix with the Lewis number 10. When the composite plate is subjected to a sudden change in surface temperature with moisture concentration held constant, the stresses due to uncoupled theory varied significantly from the coupled theory depending on the surface temperature gradient. Henry [24] developed a phenomenological model to explain the coupling between temperature and moisture fields. Hartranft and Sih [25] presented several other models for the same. All the models presented in their work are developed from the macroscopic conservation laws and irreversible thermodynamics under the assumption that heat and mass fluxes are linearly dependent of temperature and concentration gradients. The governing equations resulting from all the models are of the same form but with different coefficients which can be related to one another.

C. Objective and Motivation

Piezoelectric actuators employed to control deformation of elastic structures due to thermo-mechanical effects have been extensively studied. Available studies show also that the deformation in polymers and polymer composites depends strongly on absorbed moisture, temperature changes and coupled thermal and moisture fields in the materials. But, little work has been done towards implementing piezoelectric actuators to control the deformation in (i) elastic materials subjected to changes in temperature and moisture fields and (ii) materials whose viscoelastic behavior becomes predominant in the working temperature and moisture conditions. In this regard, the objective of this work is to study the application of linear piezoelectric materials to control the deformation of elastic and viscoelastic structural components that are sensitive to both temperature and moisture changes over time. To this end, piezoelectric materials are employed in the form of external surface bonded actuators to control the deformation of these components. The problem is solved in the context of linearized (i)elasticity/viscoelasticity and (ii)piezoelectricity. The choice of piezoelectric material for this purpose and its justification is presented later in this chapter. A cantilever beam geometry of elastic/viscoelastic material with a surface bonded linear piezoelectric actuator is chosen as the structural component under study. Appropriate initial and boundary conditions for the temperature and moisture fields are employed in the transient heat conduction and fluid diffusion analysis. Based on the transient response characteristics of the beam assembly, an external actuating voltage boundary condition at each instant of time is then employed across the piezoelectric material to minimize the net deformation of the beam assembly.

D. Methodology

The problem of interest involves an elastic or a viscoelastic material beam perfectly glued to a piezoelectric material and subjected to temperature and moisture gradients. As a result, the beam assembly deforms and hence induces a potential difference across the piezoelectric material. This voltage gives a rough estimate of an external voltage required to minimize the deformation. The assumptions made and their justifications are described below. The structural materials chosen for this study are assumed to be linearly elastic/viscoelastic in the chosen temperature and moisture conditions. The piezoelectric material chosen for study is assumed to be linearly piezoelectric. A cantilever beam geometry is chosen for simplicity. Aging of the material is not considered in this study. In the current study, the constitutive equations accounting for the effect of moisture and temperature dependent deformation are obtained in the context of small strain theory appealing to the laws of conservation of mass, linear and angular momenta, energy, entropy and thermodynamic principles. It is assumed that the elastic material properties do not depend on the temperature and moisture for simplicity. The effect of temperature and moisture on the deformation of the beam is incorporated through CTE, CME. In the case of viscoelastic material, the shift factor is assumed to be dependent not only on temperature but also on moisture content. The coupled equations governing the evolution of temperature and moisture fields are obtained by assuming that the moisture and the temperature fluxes are linearly dependent on the gradient temperature and moisture content in the body. The coupling between thermal and moisture fields can be explained in terms of *Dufour and Soret effects.* The *Dufour effect* is defined as the heat flux due to moisture concentration changes . The *Soret effect* is defined as the mass flux caused in a body due to temperature changes. In this context, we define two constants. λ is a measure of the ratio of mass flux to heat flux at a uniform moisture concentration. ν is a measure of the ratio of heat flux to mass flux in an isothermal body. The product of λ, ν is non-dimensional and is defined as coupling constant. It is a material property. Temperature and moisture fields are greatly dependent of the ratio of moisture and thermal diffusivities and the non-dimensional coupling constant. So, a parametric study is first done to examine the evolution of temperature and moisture concentrations with time. This parametric study involves varying the Lewis number from 10^1 to 10^6 and the coupling constant ($\lambda\nu$) varying from 0.25 to .0025. The choice of these parameters is justified as follows. In the materials considered for study i.e. aluminium, epoxy and fiber reinforced polymers the thermal diffusivity is observed to be greater than moisture diffusivity. Therefore, the ratio of thermal to moisture diffusivities is allowed to vary from one order of magnitude (as observed in T300/5208 CFRP) to 6 orders of magnitude as observed in un-reinforced epoxy material. It shall be shown in Chapter II that by thermodynamic limitations, the coupling coefficient $\lambda\nu < 1$. In case of T300/5208 CFRP, the coupling coefficient $\lambda\nu = 0.25$ [26]. Therefore, $\lambda\nu = 0.25$ can be considered as a reasonable starting value for parametric study. It shall be graphically depicted in Chapter III that at a given Lewis number, the smaller the value of $\lambda\nu$, the smaller is the coupling between thermal and moisture fields. Through this parametric study it is concluded that the larger the Lewis number, the smaller the coupling effect. For a given Lewis number, the evolution of temperature and moisture fields is dependent on the constants λ and ν. The following are the cases considered in the current study. Materials considered for study are as follows:

- Linearly elastic materials:
    1. Aluminium-PZT beam assembly subjected to transient temperature field.[3]
    2. Isotropic un-reinforced epoxy-PZT beam assembly subjected to transient thermal and moisture fields.
    3. Anisotropic CFRP-PZT beam assembly subjected to transient thermal and moisture field.
- Linearly viscoelastic material-PZT beam assembly subjected to transient thermal and moisture field.

Crawley et al. [6] presented a study on the choice of actuating materials based on their properties. They assert that piezoelectric materials with high effectiveness, high modulus of elasticity and high curie temperature are suitable for actuating purposes. Effectiveness is the ratio of maximum strain transmitted by the actuator to the beam under perfectly bonded static conditions when maximum allowable electric field (E_C) is applied across the actuator. It is proportional to electro mechanical coupling coefficient[4] (d_{311}) and E_C. PZT 5H is chosen for this purpose as it meets the above mentioned requirements better than other piezoelectric materials such as PVDF, $BaTiO_3$. In the current study, linear piezoelectric equations are employed for PZT 5H actuator. The linearized piezoelectric material behavior is restricted to small electric fields (in general of the order of 0.1MV/m). Crawley-Anderson [7] present an experimental study on G-1195 PZT material to determine the limits of actuating electric

---

[3] The moisture dependent deformation of aluminium is not considered for its moisture absorbability is negligible.

[4] d_{311} in engineering notation represents the strain along direction-1 (ε_{11}) due to unit electric field applied along direction-3 (E_3). Alternatively, it represents polarization in direction-3 (P_3) due to unit stress along direction-1 (σ_{11}).

field for a linear constitutive model to be applicable for the Piezoelectric material. They show that when an electric field of the order of 1MV/m is applied along the polarization direction, the strain in the direction perpendicular to the polarization direction is not proportional to the electric field. This leads the system to the verge of non-linearity.

In this thesis, piezoelectric layer is assumed to be very thin and hence is assumed to be in an isothermal state with constant moisture content. Pyroelectric effect and the effect of moisture on the deformation of PZT 5H material are not considered for simplicity. The geometry of the actuated plate and the PZT actuator is shown in the Figure. 1.1(a). The geometry, the initial and boundary conditions used in the problem are summarized as follows: A thin linearly elastic/viscoelastic beam with length to thickness ratio of $\frac{1}{40}$ is perfectly glued to a PZT beam with length to thickness ratio of $\frac{1}{200}$. The PZT layer rests on the top of the elastic/viscoelastic layer. The width of the beam is assumed to be large enough to solve the problem in the context of plain strain deformation. The length of either layers is represented by L. The thickness of the elastic/viscoelastic beam and PZT beam are represented by h1, h2, respectively. The cantilever beam assembly is fixed along the edge ACE as shown in Figure. 1.1(b). The darkly shaded region corresponds to the PZT layer and the lightly shaded region corresponds to the elastic/viscoelastic material. The surface containing the edge AB is maintained at a temperature of T_f and a moisture content, C_f. The surface containing the edge EF is maintained at a temperature of $T_o < T_f$ and moisture density of $C_o < C_f$. The surfaces containing the edges ACE, BDF are perfectly insulated and the moisture flux is maintained at zero. Displacement and traction continuity is assumed at all times along the common interface CD owing to the perfect bonding between the two layers. Since the thickness to length ratio is $\ll 1$, the heat and moisture are assumed to diffuse only along the thickness direction. Therefore, the temperature and moisture fields are obtained by solving one dimensional coupled diffusion equations through the thickness. Since $T_o < T_f$ and $C_o <$

C_f, heat and moisture diffuse from the surface containing edge AB to the surface containing edge EF. Once the system attains a steady state it is assumed that it remains in that state thereafter. The equations governing the system described above are solved for the displacement and the stress fields in the elastic/viscoelastic beam region and voltage and electric field across the PZT5H beam at various instances of time (starting from initial time to the time at which system attains a steady state), as temperature and moisture fields evolve. At a given instant of time, the voltage and electric field so obtained may vary from location to location along the length of the PZT beam. Since, the objective is to minimize the effect of moisture and temperature fields on the deformation of the beam, an external actuating voltage needs to be applied across the PZT layer which in turn minimizes the deformation of beam assembly. A rough estimate of this actuating voltage for a given instant of time could be obtained from the voltage plot obtained for PZT 5H, from the former analysis. The equations governing the system are then solved again for deformation and stress fields by applying this actuating voltage across the PZT 5H beam with out changing other loading conditions. This procedure is repeated for all time instances chosen for study. By plotting the actuating voltage required to minimize the deformation versus time, one can estimate the actuating voltage for all other intermediate times.

The field equations and the boundary conditions are replaced by their corresponding finite difference equations. This reduces the problem to a set of simultaneous algebraic equations. Finite difference equations are solved explicitly using a Forward-time Centered-Space approximation. Various grid sizes, grid ratios and time steps are considered for the study and an optimum value is chosen based on the convergence of results or comparison of the results with analytical solutions of known test cases. The outline of the thesis is as follows:

In Chapter II, the constitutive equations governing thermal and moisture dependent deformation and coupled temperature and moisture evolution are derived from the conservation principles. These equations are then systematically linearized under small deformation assumption. The equations governing temperature and moisture dependent viscoelastic behavior are then derived following the correspondence principle.

In Chapter III, the material geometry under study is described along with the appropriate initial and boundary conditions. The material parameters chosen for study are presented. A parametric study is presented for the evolution of thermal and moisture fields. The finite difference approximation schemes implemented for solving the constitutive and the governing equations with appropriate initial and boundary conditions are presented. In the case of viscoelastic material, an algorithm that accounts for history dependent response is explained briefly. A convergence study is presented to justify the choice of grid sizes and time steps chosen for computations. The four test cases mentioned above are solved numerically to obtain the voltage necessary to minimize the deformation.

In Chapter IV, conclusions are discussed.

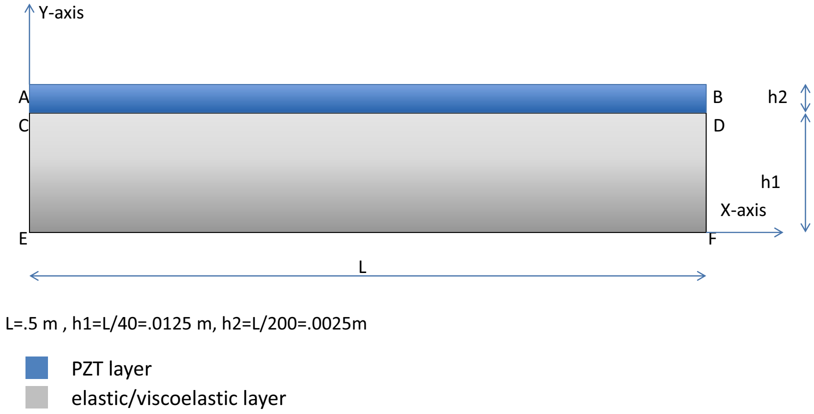

(a) Geometry of the beam assembly

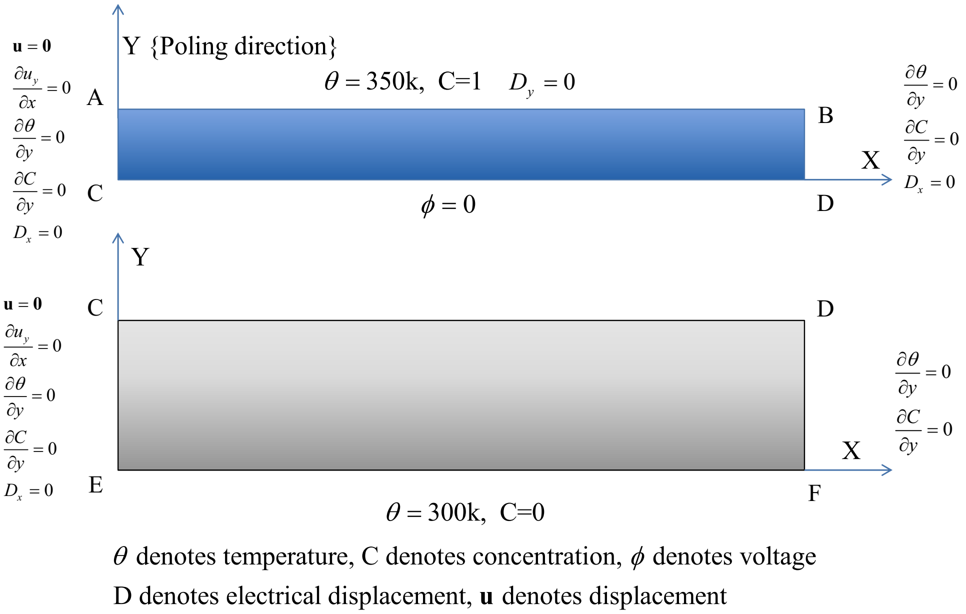

(b) Boundary conditions

Fig. 1.1. (a) Figure shows the geometry of the cantilever beam assembly (b) Figure shows the temperature and moisture boundary conditions of the beam when no external voltage is applied across the PZT 5H layer. The shaded layer refers to the PZT 5H material and the unshaded layer refers to the elastic/viscoealstic material. The surface containing the edge ACE in Figure(a) is rigidly clamped and all other surfaces are traction free.

CHAPTER II

CONSTITUTIVE MODELS FOR LINEARLY ELASTIC AND VISCOELASTIC MATERIAL BEHAVIOR INCORPORATING THERMAL AND MOISTURE EFFECTS

This chapter presents a systematic derivation of the constitutive equations for the deformation of a linearly elastic material incorporating the dependence of stress-strain fields on moisture and temperature changes from the macroscopic conservations laws with the aid of the Clausius-Duhem inequality. The coupling between temperature and moisture fields is derived assuming a linear dependence of moisture and heat fluxes on temperature and moisture gradients. This constitutive model is adopted from the work by Henry [24] and Hartranft et al. [25]. The constitutive model for an isotropic viscoelastic material is also obtained appealing to the correspondence principle. The effects of temperature and moisture fields on the viscoelastic deformation are incorporated by considering the material as a thermorheologically simple material (TSM). Following this, the appropriate constitutive and governing equations for the linear piezoelectric actuator are presented.

A. Constitutive Model for Elastic Deformation Due to Coupled Heat and Moisture Effects

One can model the solid and fluid portions independently accounting for their mutual interactions terms, in the context of mixture theory. But, prescribing boundary conditions in such a setting is a challenging task. In this regard, the solid mass through which heat and moisture diffusion occurs is modeled as follows. The solid and fluid portions are assumed to co-exist at every location in the mixture and their motion is constrained such that these constituents move together at all times. We shall further assume that no chemical reactions occur between the two media. The free energy of the solid mass at every location is assumed to depend on the moisture concentration. The following subsection presents in detail the derivation of the constitutive equations for the solid portion incorporating the effects of heat and moisture diffusion.

1. Kinematics

Let the reference and current configurations of the body be denoted respectively by κ_R and κ_t. A one-one mapping that assigns every single point $\mathbf{X} \epsilon \kappa_R$ to a point $\mathbf{x} \ \epsilon \kappa_t$ is defined as a placer, denoted by χ_{κ_R}. A one parameter(time) family of such placers is defined as motion.

$$\mathbf{x} = \chi_{\kappa_R}(\mathbf{X}, t) \tag{2.1}$$

The gradient of motion/deformation gradient $\mathbf{F}$ is defined by

$$\mathbf{F} := \frac{\partial \chi_{\kappa_R}}{\partial X} \tag{2.2}$$

The displacement $\mathbf{u}$ is defined as follows:

$$\mathbf{u} := \mathbf{x} - \mathbf{X} \tag{2.3}$$

The deformation gradient and the displacement are related as follows from Eq. (2.3):

$$\begin{aligned} \nabla\mathbf{u} &= \mathbf{F} - \mathbf{1} \\ \Rightarrow \mathbf{F} &= \mathbf{1} + \nabla\mathbf{u} \end{aligned} \tag{2.4}$$

where $\mathbf{1}$ denotes the identity tensor. The velocity $\mathbf{v}$ is defined as follows:

$$\mathbf{v} := \frac{\partial \chi_{\kappa_R}}{\partial t} \tag{2.5}$$

The velocity gradient $\mathbf{L}$ is defined by

$$\begin{aligned} \mathbf{L} &:= \frac{\partial \mathbf{v}}{\partial \mathbf{x}} \\ &= \dot{\mathbf{F}}\mathbf{F}^{-1} \end{aligned} \tag{2.6}$$

where$\dot{()}$ denotes the material time derivative. The lagrangian time derivative of det**F** is given by the following equation.

$$\begin{aligned}\overline{\det(\mathbf{F})}^{\cdot} &:= \frac{d(\det(\mathbf{F}))}{dt} \\ &= \det(\mathbf{F})\ \mathrm{div}(\mathbf{v}) \qquad (2.7)\end{aligned}$$

where $\frac{d}{dt}$ represents the Lagrangian time derivative. The Green - St-Venant strain tensor **E** is defined as follows:

$$\mathbf{E} := \frac{\mathbf{F^T F} - \mathbf{1}}{2} \qquad (2.8)$$

Substituting from Eq. (2.4), Eq. (2.8) leads to

$$\mathbf{E} = \frac{\nabla\mathbf{u} + \nabla\mathbf{u}^T + \nabla\mathbf{u}^T\nabla\mathbf{u}}{2} \qquad (2.9)$$

We define the linearized strain $\boldsymbol{\varepsilon}$ as follows:

$$\boldsymbol{\varepsilon} := \frac{\nabla\mathbf{u} + \nabla\mathbf{u}^T}{2} \qquad (2.10)$$

2. Conservation of Mass

In the absence of chemical reactions, the conservation of mass for the solid and fluid portions are written separately. If ρ_R, ρ represent the density of the solid portion in the reference (κ_R) and current configurations (κ_t), then the conservation of mass for solid portion results in the following equation.

$$\rho_R - \rho\det(\mathbf{F}) = 0 \qquad (2.11)$$

$$\text{(or) } \dot{\rho} + \rho\mathrm{div}(\mathbf{v}) = 0 \qquad (2.12)$$

where Eq. (2.11), (2.12) are the Lagrangian and the Eulerian forms of mass conservation, respectively. If ρ_m denotes the density of moisture in the current configuration and the mass flux of the diffusing substance in the solid medium is denoted by **f**, the conservation of mass for the diffusing substance leads to

$$\dot{\rho_m} + \dot{\rho_m}\mathrm{div}(\mathbf{v}) = -\mathrm{div}(\mathbf{f}) \tag{2.13}$$

If we denote the ratio of moisture and solid mass densities in the current configuration by c, then

$$c := \frac{\rho_m}{\rho} \tag{2.14}$$

Substituting from Eq (2.14) into Eq (2.13) we obtain the following:

$$\rho\dot{c} + c(\dot{\rho}_m + \rho\ \mathrm{div}(\mathbf{v})) = -\mathrm{div}(\mathbf{f}) \tag{2.15}$$

Substituting from Eq (2.12) into Eq (2.15) we obtain the following:

$$\rho\dot{c} = -\mathrm{div}(\mathbf{f}) \tag{2.16}$$

3. Conservation of Linear Momentum

Ignoring the amount of momentum transfer to the solid medium due to fluid flow, the conservation of linear momentum equation gives

$$\rho\dot{\mathbf{v}} = \mathrm{div}(\mathbf{T}^T) + \rho\mathbf{b} \tag{2.17}$$

Here, **T** represents the Cauchy Stress Tensor, **b** represents the body force per unit mass.

4. Conservation of Angular Momentum

In absence of the internal body couples and ignoring the contributions due to the moisture flow to the angular momentum of the solid, balance of angular momemtum reduces to the following equation.

$$\mathbf{T} = \mathbf{T}^T \tag{2.18}$$

5. Conservation of Energy

We shall ignore the energy equation of the fluid. However, we shall incorporate the contributions due to interactions between the solid and fluid portions in the conservation of energy equation for the solid portion. In which case, the energy equation for the solid portion in the integral form is written as follows.

$$\frac{d}{dt}\int_{P_t} \rho\varepsilon \, d\nu = -\int_{\partial P_t} \mathbf{q}\cdot\mathbf{n}\, da + \int_{\partial P_t} (\mathbf{t}+\rho\mathbf{b})\cdot\mathbf{v}\, da + \int_{P_t} \rho r\, d\nu - \int_{\partial P_t} \hat{h}\mathbf{f}\cdot\mathbf{n}\, da \tag{2.19}$$

Here, ε,$\hat{h}$, $\mathbf{q}$, $\mathbf{t}$, r denote the specific internal energy of the solid mass, energy flux of moisture per its unit mass, heat flux, boundary traction and specific internal heat source terms, respectively and $P_t, \partial P_t$ represent a control volume and its bounding surface in the current configuration κ_t. Substituting from Eq. (2.17), (2.18) and appealing to divergence theoram[1],the Eq. (2.19) reduces to the following equation.

$$\rho\dot{\varepsilon} = \mathbf{T}\cdot\mathbf{L} + \rho r - \mathrm{div}(\mathbf{q}) - \mathrm{div}(\hat{h}\mathbf{f}) \tag{2.20}$$

The Specific Helmholtz Potential ψ of the solid medium is assumed to depend on the temperature θ, concentration of the diffusing fluid and the deformation gradient of the solid, i.e.,

$$\psi \ := \ \psi(\theta, c, \mathbf{F}) \tag{2.21}$$

The material time derivative of Helmholtz potential ψ is given as

$$\dot{\psi} = \frac{\partial\psi}{\partial\mathbf{F}}\cdot\dot{\mathbf{F}} + \frac{\partial\psi}{\partial\theta}\dot{\theta} + \frac{\partial\psi}{\partial c}\dot{c} \tag{2.22}$$

---

[1] $\int_{\partial P_t} A_{ijk..p}n_p\, ds = \int_{P_t} A_{ijk...p,p}\, d\nu$

But Helmholtz potential is defined in terms of specific internal energy of the solid$u$, specific entropy of the solid η and temperature θ as follows

$$\begin{aligned} \psi &:= \varepsilon - \eta\theta && (2.23) \\ \Rightarrow \varepsilon &= \psi + \theta\eta && (2.24) \\ \Rightarrow \dot{\varepsilon} &= \dot{\psi} + \dot{\theta}\eta + \theta\dot{\eta} && (2.25) \end{aligned}$$

Substituting from Eq. (2.25), Eq. (2.20) is given as

$$\begin{aligned} \rho(\dot{\psi} + \dot{\theta}\eta + \theta\dot{\eta}) &= \mathbf{T}\cdot\mathbf{L} + \rho r - div(\mathbf{q}) - div(\hat{h}\mathbf{f}) && (2.26) \\ \rho\theta\dot{\eta} + \rho(\frac{\partial\psi}{\partial\theta} + \eta)\dot{\theta} + \rho\frac{\partial\psi}{\partial c}\dot{c} &= (\mathbf{T} - \rho\frac{\partial\psi}{\partial\mathbf{F}}\mathbf{F}^T)\cdot\mathbf{L} - div(\mathbf{q}) + \rho r - div(\hat{h}\mathbf{f}) && (2.27) \end{aligned}$$

Here we have used the fact that $\dot{\mathbf{F}}$=$\mathbf{LF}$.

6. Balance of Entropy

Though the balance of entropy is not considered for the fluid portion, the irreversibility associated with the diffusion of fluid is incorporated in the balance of entropy equation written for the solid mass. In integral form the entropy equation for the solid portion is expressed as follows:

$$\frac{d}{dt}\int_{P_t} \rho\eta\, d\nu = -\int_{\partial P_t} \frac{\mathbf{q}}{\theta}\cdot\mathbf{n}\, da + \int_{P_t} \frac{\rho r}{\theta}\, d\nu - \int_{\partial P_t} \hat{\eta}\mathbf{f}\cdot\mathbf{n}\, da + \int_{P_t} \rho\zeta\, d\nu \qquad (2.28)$$

Appealing to the divergence theorem Eq. (2.28) in the local form reduces to the following equation

$$\rho\dot{\eta} = -div(\frac{\mathbf{q}}{\theta}) + \frac{\rho r}{\theta} - div(\hat{\eta}\mathbf{f}) + \rho\zeta \qquad (2.29)$$

Here $\hat{\eta}$ denotes the entropy of moisture per its unit mass and ζ denotes the rate of entropy generation per unit mass of solid. Substituting from Eq. (2.29) the Eq. (2.27) leads to the following equation.

$$\begin{aligned} \rho\zeta\theta &= -\frac{\mathbf{q}\cdot\nabla\theta}{\theta} + (\theta\ \nabla\hat{\eta}\ \mathbf{f} + \theta\hat{\eta}\ \mathrm{div}(\mathbf{f})) - (\hat{h}\ \mathrm{div}(\mathbf{f}) + \nabla\hat{h}\cdot\mathbf{f}) + \\ & (\mathbf{T} - \rho\frac{\partial\psi}{\partial\mathbf{F}}\mathbf{F}^T)\cdot\mathbf{L} - \rho\frac{\partial\psi}{\partial c}\dot{c} - \rho\dot{\theta}(\eta + \frac{\partial\psi}{\partial\theta}) \end{aligned} \tag{2.30}$$

We introduce the variable $\hat{\mu}$, which is defined as follows:

$$\hat{\mu} = \hat{h} - \theta\hat{\eta} \tag{2.31a}$$

$$\nabla\hat{\mu}_{\theta=const} = \nabla\hat{h} - \theta\nabla\hat{\eta} \tag{2.31b}$$

Substituting from Eq. (2.31b) in Eq. (2.30), the rate of dissipation $\rho\dot{\zeta}\theta$ can be written as follows:

$$\begin{aligned} \rho\zeta\theta &= -\frac{\mathbf{q}\cdot\nabla\theta}{\theta} + (-\hat{\mu} + \rho\frac{\partial\psi}{\partial c})\ \mathrm{div}(\mathbf{f}) + (\theta\nabla\hat{\eta} - \nabla\hat{h})\cdot\mathbf{f} \\ & +(\mathbf{T} - \rho\frac{\partial\psi}{\partial\mathbf{F}})\cdot\mathbf{L} - \rho\theta(\frac{\partial\psi}{\partial\theta} + \eta) \end{aligned} \tag{2.32}$$

The terms on the right hand side are defined as follows

$$\begin{aligned} \frac{\mathbf{q}\cdot\nabla\theta}{\theta} &\equiv \text{entropy generation due to heat tranfer} \\ (\mathbf{T} - \rho\frac{\partial\psi}{\partial\mathbf{F}})\cdot\mathbf{L} &\equiv \text{entropy generation due to Mechanical working} \\ (\theta\nabla\hat{\eta} - \nabla\hat{h})\cdot\mathbf{f} &\equiv \text{entropy generation due to diffusion of fluid} \end{aligned}$$

We shall define

$$\hat{\mu} := \frac{\partial\psi}{\partial c} \tag{2.33}$$

The specific entropy of the solid portion η is related the Helmholtz potential ψ as follows:

$$\eta = -\frac{\partial\psi}{\partial\theta} \tag{2.34}$$

If entropy generation due to mechanical working is assumed to be zero then the Cauchy stress tensor can be defined as

$$\mathbf{T} := \rho \frac{\partial \psi}{\partial \mathbf{F}} \mathbf{F}^T \tag{2.35}$$

Then the Eq. (2.32) subject to Eq. (2.33), (2.31b) reduces to the following equation

$$\rho \zeta \theta = -\frac{\mathbf{q}.\nabla \theta}{\theta} - \nabla \hat{\mu}_{\theta=const} \cdot \mathbf{f} \tag{2.36}$$

The Clausius-Duhem Inequality states that

$$\rho \zeta \geq 0 \tag{2.37}$$

$$\Rightarrow -\frac{\mathbf{q}.\nabla \theta}{\theta} - \nabla \hat{\mu}_{\theta=const} \cdot \mathbf{f} \geq 0 \tag{2.38}$$

7. Linearization of the Constitutive Equations

In this subsection we obtain expressions for the Cauchy stress tensor, specific entropy of the solid mass and $\hat{\mu}$ in the context of a linearized theory. This is achieved by assuming that the body undergoes an infinitesimal deformation due to mechanical loads, temperature and moisture changes. The changes in temperature and moisture concentration are assumed to be small enough to be addressed by a linearized theory. To this end, we introduce the linearized strain ε. This is done as follows:

The Cauchy stress tensor $\mathbf{T}$ can be expressed in terms of Green - St-Venant strain tensor $\mathbf{E}$ by substituting from Eq.(2.8) in Eq. (2.35). This results in the following equation.

$$\Rightarrow \mathbf{T} = \rho \mathbf{F} \frac{\partial \psi}{\partial \mathbf{E}} \mathbf{F}^T \tag{2.39}$$

For Small strain problems i.e. when $||\nabla \mathbf{u}|| \ll 1$, The Green-St Venant strain tensor from

Eq. (2.9) and the Cauchy Stress Tensor transform as follows:

$$\mathbf{E} \approx \frac{\nabla\mathbf{u} + \nabla\mathbf{u}^T}{2} = \boldsymbol{\varepsilon} \tag{2.40}$$

$$\mathbf{T} \approx \rho\,\frac{\partial\psi}{\partial\boldsymbol{\varepsilon}} \tag{2.41}$$

The Taylor Series expansion of ψ in the neighbourhood of the reference configuration can be written as follows:

$$\begin{aligned}\psi(\mathbf{F},\theta,c) = \psi_o &+ \frac{\partial\psi}{\partial\boldsymbol{\varepsilon}}\cdot\boldsymbol{\varepsilon} + \frac{\partial\psi}{\partial\theta}\Delta\theta + \frac{\partial\psi}{\partial c}\Delta c \\ &+ \frac{1}{2}\frac{\partial^2\psi}{\partial\boldsymbol{\varepsilon}\partial\boldsymbol{\varepsilon}}\cdot\boldsymbol{\varepsilon}\otimes\boldsymbol{\varepsilon} + \frac{1}{2}\frac{\partial^2\psi}{\partial\theta^2}(\Delta\theta)^2 + \frac{1}{2}\frac{\partial^2\psi}{\partial c^2}(\Delta c)^2 + \\ &\frac{\partial^2\psi}{\partial\theta\partial\boldsymbol{\varepsilon}}\cdot(\Delta\theta)\boldsymbol{\varepsilon} + \frac{\partial^2\psi}{\partial c\partial\boldsymbol{\varepsilon}}\cdot(\Delta c)\boldsymbol{\varepsilon} + \frac{\partial^2\psi}{\partial\theta\partial c}\cdot(\Delta c)\boldsymbol{\varepsilon}\end{aligned} \tag{2.42}$$

Appealing to Eq. (2.33), (2.34), (2.41), Eq. (2.42) can be written as follows:

$$\begin{aligned}\Rightarrow \psi(\mathbf{F},\theta,c) = \psi_o &+ \frac{\mathbf{T_o}}{\rho}\cdot\boldsymbol{\varepsilon} - \eta_o\Delta\theta + \mu_o\Delta c \\ &\frac{1}{2\rho}\frac{\partial\mathbf{T}}{\partial\boldsymbol{\varepsilon}}\cdot\boldsymbol{\varepsilon}\otimes\boldsymbol{\varepsilon} - \frac{1}{2}\frac{\partial\eta}{\partial\theta}(\Delta\theta)^2 + \frac{1}{2}\frac{\partial\hat{\mu}}{\partial c}(\Delta c)^2 \\ &+ \frac{1}{\rho}\frac{\partial\mathbf{T}}{\partial\theta}\cdot(\Delta\theta)\boldsymbol{\varepsilon} + \frac{1}{\rho}\frac{\partial\mathbf{T}}{\partial c}\cdot(\Delta c)\boldsymbol{\varepsilon} - \frac{\partial\eta}{\partial c}(\Delta c)(\boldsymbol{\Delta}\theta)\end{aligned} \tag{2.43}$$

where ψ_o, η_o, μ_o, $\mathbf{T}_o$ denote values in the reference configuration. We assume that in the reference configuration, $\boldsymbol{\varepsilon} = 0$, $\Delta c = 0$. We further assume that the reference configuration is a stress free configuration i.e. $\mathbf{T}_o$=0. Under these assumptions, Eq. (2.43) reduces to the following form:

$$\Rightarrow \psi(\mathbf{F},\theta,c) = \psi_o - \eta_o\Delta\theta + \mu_o\Delta c + \frac{1}{2\rho}\frac{\partial\mathbf{T}}{\partial\boldsymbol{\varepsilon}}\cdot\boldsymbol{\varepsilon}\otimes\boldsymbol{\varepsilon} - \frac{1}{2}\frac{\partial\eta}{\partial\theta}(\Delta\theta)^2 + \frac{1}{2}\frac{\partial\hat{\mu}}{\partial c}(\Delta c)^2 \tag{2.44}$$

$$+\frac{1}{\rho}\frac{\partial\mathbf{T}}{\partial\theta}\cdot(\Delta\theta)\boldsymbol{\varepsilon} + \frac{1}{\rho}\frac{\partial\mathbf{T}}{\partial c}\cdot(\Delta c)\boldsymbol{\varepsilon} - \frac{\partial\eta}{\partial c}(\Delta c)(\Delta\theta) \tag{2.45}$$

We define the elastic modulus ($\mathbf{C}$), the linear thermomechanical coupling coefficient ($\hat{\boldsymbol{\alpha}}$) and the linear moisture-mechanical coupling coefficient ($\hat{\boldsymbol{\beta}}$) as follows:

$$\begin{aligned} \mathbf{C} &:= \frac{\partial \mathbf{T}}{\partial \boldsymbol{\varepsilon}} && (2.46a) \\ \hat{\boldsymbol{\alpha}} &:= -\frac{\partial \mathbf{T}}{\partial \theta} && (2.46b) \\ \hat{\boldsymbol{\beta}} &:= -\frac{\partial \mathbf{T}}{\partial c} && (2.46c) \end{aligned}$$

We further introduce the following variables

$$\begin{aligned} \hat{\gamma} &:= -\frac{\partial \eta}{\partial c} && (2.47a) \\ \hat{\delta} &:= -\frac{\partial \hat{\mu}}{\partial c} && (2.47b) \\ \omega &:= \frac{\partial \eta}{\partial \theta} && (2.47c) \end{aligned}$$

From Eq. (2.41), (2.46c), (2.47c), (2.33), we obtain expressions for the Cauchy Stress $\mathbf{T}$, the specific entropy η and $\hat{\mu}$ as follows:

$$\begin{aligned} \mathbf{T} &= \mathbf{C}\boldsymbol{\varepsilon} - \hat{\boldsymbol{\alpha}}\Delta\theta - \hat{\boldsymbol{\beta}}\Delta c && (2.48) \\ \eta &= \eta_o + \omega\Delta\theta + \frac{\boldsymbol{\varepsilon} \cdot \hat{\boldsymbol{\alpha}}}{\rho} + \frac{\hat{\gamma}\ \Delta c}{\rho} && (2.49) \\ \hat{\mu} &= \hat{\mu}_o + \delta\Delta c + \hat{\gamma}\ \Delta\theta - \frac{\boldsymbol{\varepsilon} \cdot \hat{\boldsymbol{\beta}}}{\rho} && (2.50) \end{aligned}$$

B. Coupled Temperature and Moisture Fields

In this section, we obtain the expressions that govern the coupled heat and moisture transport phenomena in the solid medium. To this end, we begin by assuming a form for heat and moisture flux in the solid medium based on the mathematical form of Fourier's heat conduction and Fickian mass diffusion. The coefficients introduced in these equations are evaluated by using the Eq. (2.38), which is a consequence of Clausius-Duhem inequality. This is achieved as follows:

In the Eq. (2.50), we shall ignore the dependence of chemical potential $\hat{\mu}$ on the strain $\boldsymbol{\varepsilon}$ for simplicity. Thus, Eq. (2.50) reduces to the following form:

$$\begin{aligned} \hat{\mu} &= \hat{\mu}_o + \hat{\delta}\Delta c + \hat{\gamma}\ \Delta\theta \\ \Rightarrow \nabla\hat{\mu}|_{\theta=constant} &= \hat{\delta}\nabla c \end{aligned} \tag{2.51a}$$

Thus, the Eq. (2.52) reduces to the following form

$$-\frac{\mathbf{q}.\nabla\theta}{\theta} - \hat{\delta}\nabla c \cdot \mathbf{f} \geq 0 \tag{2.52}$$

The Eq. (2.52) be is assumed to be satisfied with the following forms for heat and moisture fluxes as suggested by Henry [24], Hartranft et al. [25].[2].

$$\begin{aligned} \mathbf{q} &= -k_{11}\frac{\nabla\theta}{\theta} - \hat{k}_{12}\hat{\delta}\nabla c = -k_{11}\frac{\nabla\theta}{\theta} - k_{12}\nabla c \\ \mathbf{f} &= -k_{21}\frac{\nabla\theta}{\theta} - \hat{k}_{22}\hat{\delta}\nabla c = -k_{21}\frac{\nabla\theta}{\theta} - k_{22}\nabla c \end{aligned} \tag{2.53a}$$

Substituting Eq. (2.60b) into Eq. (2.52) we obtain the following inequality.

$$(k_{12} + k_{21})^2 \leq 4k_{11}k_{22} \tag{2.54}$$

Setting the concentration gradient and mass flux are set to zero, equations (2.60b), (2.52) require that

$$k_{11} > 0 \tag{2.55}$$

Similarly, setting the temperature gradient and heat flux to zero, equations (2.60b), (2.52) require that

$$k_{22} > 0 \tag{2.56}$$

---

[2] By setting the constants k_{12}, k_{21} to zero, Eq. (2.60b) reduce to Fourier's Heat conduction and Fickian diffusion equations respectively

Since, we require that the inequality in Eq. (2.52) to hold even when **q=0**, **f=0**, we obtain the following relation between the coefficients.

$$k_{11}k_{22} = k_{21}k_{12} \tag{2.57}$$

Substituting from Eq. (2.54), Eq. (2.57) leads to

$$k_{21} = k_{12} \tag{2.58}$$

We assume that the density of the solid mass doesn't change significantly due to the diffusion of heat and moisture. In this regard, we ignore the spatial and temporal variation of solid mass density due to the diffusion. Therefore, the gradient of c can be written as follows:

$$\nabla c \approx \frac{\nabla \rho_c}{\rho} \tag{2.59}$$

Substituting from Eq. (2.59), Eq. (2.65b) can be re-written as follows:

$$\mathbf{q} = -k_{11}\frac{\nabla\theta}{\theta} - \frac{k_{12}}{\rho}\nabla\rho_m \tag{2.60a}$$

$$\mathbf{f} = -k_{21}\frac{\nabla\theta}{\theta} - \frac{k_{22}}{\rho}\nabla\rho_m \tag{2.60b}$$

Let, D_m be defined as the coefficient of moisture diffusivity of the fluid in the solid in an isothermal state and $\hat{k}$ be the thermal conductivity of the solid medium in dry state. Then,

$$D_m := \frac{k_{22}}{\rho} \tag{2.61a}$$

$$\hat{k} := \frac{k_{11}}{\theta} \tag{2.61b}$$

Let Q^* be defined as the ratio of isothermal heat flux to mass flux. Therefore

$$Q^* := \frac{k_{12}}{k_{22}} \tag{2.62}$$

The thermal diffusivity of the solid medium denoted by D_h is defined as follows

$$D_h := \frac{\hat{k}}{\rho C_v} \tag{2.63}$$

where C$_v$ denotes the specific heat capacity of the solid mass which is defined as follows:

$$C_v := \frac{\partial \varepsilon}{\partial \theta} \tag{2.64}$$

Substituting from Equations (2.61b), (2.62) and (2.63), the Eq. (2.60b) reduces to the following form:

$$\begin{aligned} \mathbf{f} &= -D_m \nabla \rho_m - \frac{Q^* D_m \rho}{\theta} \nabla \theta && (2.65a) \\ \frac{\mathbf{q}}{\rho C_v} &= -D_h \nabla \theta - \frac{Q^* D_m}{\rho C_\theta} \nabla \rho_m && (2.65b) \end{aligned}$$

Let coupling constants ν, λ be defined as follows:

$$\begin{aligned} \nu &:= \frac{Q^*}{\rho C_v} && (2.66a) \\ \lambda &:= \frac{Q^* D_m \rho}{D_h \theta} && (2.66b) \end{aligned}$$

Using the equations 2.65b, 2.66b and 2.54 we obtain

$$\begin{aligned} \mathbf{f} &= -D_m \nabla c - \lambda D_h \nabla \theta && (2.67) \\ \frac{\mathbf{q}}{\rho C_v} &= -D_h \nabla \theta - \nu D_m \nabla c && (2.68) \\ \lambda \nu &< 1 && (2.69) \end{aligned}$$

Substituting from Eq. (2.16) and replacing with ρ_m with C, Eq. (2.67) reduces to the following form:

$$\rho \dot{c} = D_m \nabla^2 C + \lambda D_h \nabla^2 \theta \tag{2.70a}$$

$$\Rightarrow \dot{C} = D_m \nabla^2 C + \lambda D_h \nabla^2 \theta \tag{2.70b}$$

If the velocity of the body, the amount of energy supplied supplied by the moisture and the internal heat source terms are neglected, the energy equation Eq. (2.20) reduces to the following equation.

$$\rho\dot{\varepsilon} \approx -\mathrm{div}(\mathbf{q}) \tag{2.71}$$

Substituting from Eq. (2.68), the Eq. (2.71) leads to the following equation:

$$\rho\dot{\varepsilon} = \rho C_v(D_h\nabla^2\theta + \nu D_m\nabla^2 C) \tag{2.72a}$$

$$\Rightarrow \dot{\varepsilon} = C_v(D_h\nabla^2\theta + \nu D_m\nabla^2 C) \tag{2.72b}$$

Substituting from the definition of specific heat capacity in Eq. (2.64), the Eq. (2.72b) reduces to the following form.

$$\dot{\theta} = D_h\nabla^2\theta + \nu D_m\nabla^2 C \tag{2.73}$$

The equations (2.73), (2.70b) can be equivalently written as follows:

$$D\nabla^2 C \;=\; \dot{C} - \lambda\dot{\theta} \tag{2.74a}$$

$$\mathsf{D}\nabla^2\theta \;=\; \dot{\theta} - \nu\dot{C} \tag{2.74b}$$

where

$$D = (1-\lambda\nu)D_m \;, \mathsf{D} = (1-\lambda\nu)D_h \tag{2.75}$$

This concludes the derivation of the equations incorporating the effects of heat and moisture diffusion in the context of linearized elasticity.

C. Constitutive Equations for an Isotropic, Homogeneous Linearly Elastic Material

In this section, the constitutive and governing field equations for an isotropic, homogeneous linearly elastic material are presented taking into account the temperature and moisture effects. Since, a plane strain deformation field is assumed for the current study, the relevant equations for this special case are presented.

The displacement field in for plane strain deformation is given as follows:

$$\mathbf{u} = (u(x,y), v(x,y)) \tag{2.76}$$

The constitutive equations for a linearly elastic material are written as follows from Eq. (2.48):

$$\mathbf{T} = \mathbf{C}\boldsymbol{\varepsilon} - \hat{\boldsymbol{\alpha}}\Delta\theta - \hat{\boldsymbol{\beta}}\Delta c \tag{2.77}$$

where $\hat{\boldsymbol{\alpha}}$ and $\hat{\boldsymbol{\beta}}$ are second order tensors representing thermo-mechanical and hygro-mechanical coupling coefficients. These coefficients are related to CTE ($\boldsymbol{\alpha}$) and CME ($\boldsymbol{\beta}$) as follows:

$$\hat{\boldsymbol{\alpha}} = \mathbf{C}\boldsymbol{\alpha} \tag{2.78}$$

$$\hat{\boldsymbol{\beta}} = \mathbf{C}\boldsymbol{\beta} \tag{2.79}$$

In the absence of temperature and moisture effects this equation reduces to the following form:

$$\mathbf{T} = \mathbf{C}\boldsymbol{\varepsilon} \tag{2.80}$$

The elastic modulus $\mathbf{C}$ in Eq. (2.48) is a fourth order tensor with 81 independent entries. Appealing to the symmetry of stress and strain tensors, the number of independent entries reduce to 36. For an isotropic material the number of independent coefficients further reduce just 2. In this case, the constitutive equation Eq. (2.80) reduces to the following form:

$$\mathbf{T} = 2\mu\boldsymbol{\varepsilon} + \hat{\lambda}\mathrm{tr}\boldsymbol{\varepsilon}\mathbf{1} \tag{2.81}$$

where μ, $\hat{\lambda}$ are known as Lamé constants. The Eq. (2.81) can be written equivalently in terms of the Young's modulus (E) and the poisson ratio ($\hat{\nu}$) as follows:

$$\mathbf{T} = \frac{E}{(1+\hat{\nu})}\boldsymbol{\varepsilon} + \frac{E\hat{\nu}}{(1+\hat{\nu})(1-2\hat{\nu})}\mathrm{tr}\boldsymbol{\varepsilon}\mathbf{1} \tag{2.82}$$

where the Lamé constants are related to E, $\hat{\nu}$ as follows:

$$\mu = \frac{E\hat{\nu}}{2(1+\hat{\nu})} \tag{2.83}$$

$$\hat{\lambda} = \frac{E\hat{\nu}}{(1+\hat{\nu})(1-2\hat{\nu})} \tag{2.84}$$

When the temperature and moisture effects are also incorporated and further assuming that the material response is assumed to be isotropic when subjected to temperature and moisture changes then the Eq. (2.80) takes the following form:

$$\mathbf{T} = \frac{E}{(1+\hat{\nu})}\boldsymbol{\varepsilon} + \frac{E\nu}{(1+\hat{\nu})(1-2\hat{\nu})}\mathrm{tr}\boldsymbol{\varepsilon}\mathbf{1} - \frac{E}{(1-2\hat{\nu})}(\alpha\Delta\theta + \beta\Delta C)\mathbf{1} \tag{2.85}$$

where α and β are the CTE and the CME, respectively. In case of plane strain deformation, the stress components σ_{xx}, σ_{yy}, σ_{xy} can be expressed in terms of displacements appealing to Eq. (2.82), (2.10) as follows:

$$\sigma_{xx} = \frac{E(1-\hat{\nu})}{(1+\hat{\nu})(1-2\hat{\nu})}u_{,x} + \frac{E\hat{\nu}}{(1+\hat{\nu})(1-2\hat{\nu})}v_{,y} - \frac{E}{(1-2\hat{\nu})}(\alpha\Delta\theta + \beta\Delta C) \tag{2.86a}$$

$$\sigma_{yy} = \frac{E(1-\hat{\nu})}{(1+\hat{\nu})(1-2\hat{\nu})}v_{,y} + \frac{E\hat{\nu}}{(1+\hat{\nu})(1-2\hat{\nu})}u_{,x} - \frac{E}{(1-2\hat{\nu})}(\alpha\Delta\theta + \beta\Delta C) \tag{2.86b}$$

$$\sigma_{xy} = \frac{E}{2(1+\hat{\nu})}(u_{,y} + v_{,x}) \tag{2.86c}$$

The conservation of linear momemtum Eq. (2.17) for plane strain deformation leads to the following equations:

$$\sigma_{xx,x} + \sigma_{xy,y} = 0 \tag{2.87a}$$

$$\sigma_{xy,x} + \sigma_{yy,y} = 0 \tag{2.87b}$$

Substituting from the Eq. (2.86c), the Eq. (2.87b) leads to the following equations:

$$\frac{E(1-\hat{\nu})}{(1+\hat{\nu})(1-2\hat{\nu})}u_{,xx}+\frac{E}{2(1+\hat{\nu})(1-2\hat{\nu})}v_{,xy}+\frac{E}{2(1+\hat{\nu})}u_{,yy}-\frac{E}{(1-2\hat{\nu})}(\alpha\theta_{,x}+\beta C_{,x})=0 \tag{2.88a}$$

$$\frac{E(1-\hat{\nu})}{(1+\hat{\nu})(1-2\hat{\nu})}v_{,yy}+\frac{E}{2(1+\hat{\nu})(1-2\hat{\nu})}u_{,xy}+\frac{E}{2(1+\hat{\nu})}v_{,xx}-\frac{E}{(1-2\hat{\nu})}(\alpha\theta_{,y}+\beta C_{,y})=0 \tag{2.88b}$$

Thus the equations (2.86c) and (2.88b)represent the field equations that shall be employed for the elastic portion of the beam assembly.

D. Constitutive Equations for Viscoelastic Materials With and Without Temperature and Moisture Effects

In this section, the constitutive and governing equations for a linear viscoelastic material for 2 cases are presented. In the first case, temperature and moisture effects are not considered, and in the second case where temperature and moisture effects are incorporated, the viscoelastic material is assumed to be a thermo-rheologically simple material.

For a class of problems in linearized viscoelasticity, the solution can be constructed from the solution of a corresponding boundary value problem in linearized elasticity. This approach is known as the *Correspondence Principle* and is discussed in detail by Rajagopal and Wineman [5]. However, there exist certain limitations to this principle. This principle can be appealed to only under the following conditions:

1. All material points must belong to the body for all times $t \geq 0$.
2. The motion of the viscoelastic body is quasi-static.
3. During the deformation, the boundary condition at a point on the boundary cannot be changed from displacement being specified to traction being specified.

For problems in linearized viscoelasticity where the above conditions are met with, the solution is constructed from the corresponding boundary value problem in linearized elasticity. The constitutive and governing field equations along with the boundary conditions in case of linearized viscoelasticity when transformed into laplace domain result in equations that are similar to in linearized elasticity. Thus from the solution obtained in the latter case, the solution for the former case can be obtained as follows: the field variables such as displacements, stresses, strains are replaced by their appropriate forms in laplace domain while the material properties of the elastic medium are replaced the laplace parameter times the laplace transform of the viscoelastic medium properties[3]. The geometry used for the current study as depicted in Figure 2.1(a) meets all conditions imposed by the correspondence principle to be used. Hence for the case where viscoelastic beam is perfectly bonded to the PZT layer, the constitutive and governing equations are obtained from the corresponding equations in linearized elasticity, appealing to the correspondence principle.

In what follows, the constitutive and governing equations for the viscoelastic part of the beam assembly are presented for plane strain deformation with out incorporating temperature and moisture effects. For simplicity, the linear viscoelastic material is assumed to be isotropic and homogeneous. Let E_s and E_c denote the stress relaxation modulus and creep compliance of the viscoelastic material respectively. For simplicity, the Poisson ratio ν is assumed to be a constant. Then constitutive equations in Laplace domain for an isotropic, homogeneous linearly viscoelastic material appealing to correspondence principle

---

[3] For a field variable $\mathbf{A}$ and material property E, the replacement is done follows: $A(\mathbf{x},t) \rightarrow \bar{A}(\mathbf{x},s)$; $E_s(\mathbf{x},t) \rightarrow s\bar{E}(\mathbf{x},s)$ where $\bar{A}$ and $\bar{E}$ denote the laplace transform of $\mathbf{A}$ and the viscoelastic material modulus E_s

can be written from Eq. (2.86c) as follows:

$$\bar{\sigma}_{xx} = \frac{s\bar{E}_s(1-\hat{\nu})}{(1+\hat{\nu})(1-2\hat{\nu})}\bar{u}_{,x} + \frac{s\bar{E}_s\hat{\nu}}{(1+\hat{\nu})(1-2\hat{\nu})}\bar{v}_{,y} \tag{2.89}$$

$$\bar{\sigma}_{yy} = \frac{s\bar{E}_s(1-\hat{\nu})}{(1+\hat{\nu})(1-2\hat{\nu})}\bar{v}_{,y} + \frac{s\bar{E}_s\hat{\nu}}{(1+\hat{\nu})(1-2\hat{\nu})}\bar{u}_{,x} \tag{2.90}$$

$$\bar{\sigma}_{xy} = \frac{s\bar{E}_s}{2(1+\hat{\nu})}(\bar{u}_{,y} + \bar{v}_{,x}) \tag{2.91}$$

On inversion, these equations transform as follows:

$$\begin{aligned}
\sigma_{xx} &= \frac{(1-\hat{\nu})}{(1+\hat{\nu})(1-2\hat{\nu})}\int_{0-}^{t} E_s(t-s)\,\frac{\partial u_{,x}}{\partial s}ds + \frac{\hat{\nu}}{(1+\hat{\nu})(1-2\hat{\nu})}\int_{0-}^{t} E_s(t-s)\,\frac{\partial v_{,y}}{\partial s}ds \\
\sigma_{yy} &= \frac{(1-\hat{\nu})}{(1+\hat{\nu})(1-2\hat{\nu})}\int_{0-}^{t} E_s(t-s)\,\frac{\partial v_{,y}}{\partial s}ds + \frac{\hat{\nu}}{(1+\hat{\nu})(1-2\hat{\nu})}\int_{0-}^{t} E_s(t-s)\,\frac{\partial u_{,x}}{\partial s}ds \\
\sigma_{xy} &= \frac{1}{2(1+\hat{\nu})}\int_{0-}^{t} E_s(t-s)\,(\frac{\partial u_{,y}}{\partial s} + \frac{\partial v_{,x}}{\partial s})ds
\end{aligned} \tag{2.92}$$

where $\int_{0-}^{t} E_s(t-s)\,\frac{\partial f}{\partial s}ds := E_s(t)f(0) + \int_{0}^{t} E(t-s)\frac{\partial f}{\partial s}\,ds.$

Similarly, on applying laplace transform to Eq. (2.88b) we obtain the following equations:

$$\begin{aligned}
\frac{s\bar{E}_s(1-\hat{\nu})}{(1+\hat{\nu})(1-2\hat{\nu})}\bar{u}_{,xx} + \frac{s\bar{E}_s}{2(1+\hat{\nu})(1-2\hat{\nu})}\bar{v}_{,xy} + \frac{s\bar{E}_s}{2(1+\hat{\nu})}\bar{u}_{,yy} &= 0 \\
\frac{s\bar{E}_s(1-\hat{\nu})}{(1+\hat{\nu})(1-2\hat{\nu})}\bar{v}_{,yy} + \frac{s\bar{E}_s}{2(1+\hat{\nu})(1-2\hat{\nu})}\bar{u}_{,xy} + \frac{s\bar{E}_s}{2(1+\hat{\nu})}\bar{v}_{,xx} &= 0
\end{aligned} \tag{2.93}$$

On inversion, these equations transform as follows:

$$\begin{aligned}
&\frac{(1-\hat{\nu})}{(1+\hat{\nu})(1-2\hat{\nu})}\int_{0-}^{t} E_s(t-s)\,\frac{\partial u_{,xx}}{\partial s}ds + \frac{1}{2(1+\hat{\nu})(1-2\hat{\nu})}\int_{0-}^{t} E_s(t-s)\,\frac{\partial v_{,xy}}{\partial s}ds \\
&\qquad + \frac{1}{(1+\hat{\nu})}\int_{0-}^{t} E_s(t-s)\,\frac{\partial u_{yy}}{\partial s}ds = 0
\end{aligned} \tag{2.94}$$

$$\begin{aligned}
&\frac{(1-\hat{\nu})}{(1+\hat{\nu})(1-2\hat{\nu})}\int_{0-}^{t} E_s(t-s)\,\frac{\partial v_{,yy}}{\partial s}ds + \frac{1}{2(1+\hat{\nu})(1-2\hat{\nu})}\int_{0-}^{t} E_s(t-s)\,\frac{\partial u_{,xy}}{\partial s}ds \\
&\qquad + \frac{1}{2(1+\hat{\nu})}\int_{0-}^{t} E_s(t-s)\,\frac{\partial v_{,xx}}{\partial s}ds = 0
\end{aligned} \tag{2.95}$$

Thus equations (2.92), represent the field equations for an isotropic, homogeneous lineraly viscoelastic material due to mechanical loads.

1. Temperature and Moisture Dependent Response of Viscoelastic Materials

The response of viscoelastic materials is strongly dependent on the temperature changes to which the material is subjected. The stress relaxation or creep phenomena can either be sped up or slowed down depending on the change in temperature. For a class of materials for which such a change can be accounted for by a corresponding change in the time scale are termed as thermo-rheologically simple materials (TSM) by Schwarzl and Staverman [19]. For these materials, the change in the time scale is quantified in terms of *shift factor*(a), which is a material property. The shift factor is a function of the working temperature θ and the reference temperature θ_o. This theoretical model that describes the viscoelastic behavior with respect to time and temperature is known as *time-temperature superposition.*

The TSM materials exhibit the following features:

- The relaxation/creep curves when plotted on logarithmic time scale have same shape for all temperatures.
- The initial and long time values of relaxation modulus/creep compliance are independent of temperature.
- Same rearrangements of macromolecules occur during creep and stress relaxation processes but the speed of such rearrangements is temperature dependent.

Time-temperature superposition allows to evaluate the creep compliance/relaxation modulus of TSM at a temperature other than the reference temperature from (i) the creep compliance/relaxation modulus at reference temperature and (ii) the temperature dependent shift factor a. For instance, the stress relaxation modulus E_s at temperature θ is given as follows

follows:

$$E_s(t,\theta) = E_s(\frac{t}{a(\theta,\theta_o)}, \theta_o) \tag{2.96}$$

$$\text{if} \;\; \theta > \theta_o \Rightarrow a < 1 \tag{2.97}$$

$$\text{if} \;\; \theta < \theta_o \Rightarrow a > 1 \tag{2.98}$$

$$\text{if} \;\; \theta = \theta_o \Rightarrow a = 1 \tag{2.99}$$

Rajagopal and Wineman [5] discuss the extension of time-temperature superposition to time varying temperature histories. In this case, the creep compliance/relaxation modulus in Eq. (2.96) takes the following form.

$$E_s(t,\theta) = E_s(\int_o^t \frac{ds}{a(\theta,\theta_o)}, \theta_o) \tag{2.100}$$

where the integral $\int_o^t \frac{ds}{a(\theta,\theta_o)}$ is termed as *intrinsic time/reduced time* and is denoted by $\phi(t)$ i.e.

$$\phi(t) = \int_o^t \frac{ds}{a(\theta,\theta_o)} \tag{2.101}$$

Viscoelastic material behavior can also be affected due to the diffusion of a fluid in the material, such as moisture. The diffusing fluid can either soften the material or harden it. In either case the material response is influenced due to the presence of the fluid. The effect of diffusing fluid such as a medical drug on the response characteristics of the viscoelastic materials such as muscles was studied by Rajagopal and Wineman [20]. Towards this end, the shift function (a) is assumed to be a function of the fluid/drug concentration as follows:

$$E_s(t,\theta) = E_s(\int_o^t \frac{ds}{a(C,C_o)}, C_o) \tag{2.102}$$

Since, the current study is intended to incorporate the effects of temperature and moisture on the response characteristics of a viscoelastic material, to address this the shift factor is assumed to be a function of temperature and fluid concentration as follows:

$$E_s(t,\theta,C) = E_s(\int_o^t \frac{ds}{a(\theta,C,\theta_o,C_o)},\theta_o,C_o) \tag{2.103}$$

in which case the intrinsic time is given as follows:

$$\phi(t) := \int_0^t \frac{ds}{a(\theta(s),C(s),\theta_o,C_o)} \tag{2.104}$$

The constitutive equations for viscoelastic plane strain deformation incorporating thermal and moisture effects can be obtained from the corresponding equations in linearized elasticity Eq. (2.86c) by the same procedure described in the earlier subsection. The summary of the equations so obtained is as follows:

$$\begin{aligned}
\sigma_{xx} = & \frac{(1-\hat{\nu})}{(1+\hat{\nu})(1-2\hat{\nu})} \int_{0-}^t E_s(\phi(t)-\phi(s))\,\frac{\partial u_{,x}}{\partial s} ds \\
& + \frac{\hat{\nu}}{(1+\hat{\nu})(1-2\hat{\nu})} \int_{0-}^t E_s(\phi(t)-\phi(s))\,\frac{\partial v_{,y}}{\partial s} ds \\
& - \frac{1}{(1-2\hat{\nu})} \int_{0-}^t E_s(\phi(t)-\phi(s))\,(\alpha\frac{\partial \theta}{\partial s} + \beta\frac{\partial C}{\partial s}) ds \qquad (2.105) \\
\sigma_{yy} = & \frac{(1-\hat{\nu})}{(1+\hat{\nu})(1-2\hat{\nu})} \int_{0-}^t E_s(\phi(t)-\phi(s))\,\frac{\partial v_{,y}}{\partial s} ds \\
& + \frac{\hat{\nu}}{(1+\hat{\nu})(1-2\hat{\nu})} \int_{0-}^t E_s(\phi(t)-\phi(s))\,\frac{\partial u_{,x}}{\partial s} ds \\
& - \frac{1}{(1-2\hat{\nu})} \int_{0-}^t E_s(\phi(t)-\phi(s))\,(\alpha\frac{\partial \theta}{\partial s} + \beta\frac{\partial C}{\partial s}) ds \qquad (2.106) \\
\sigma_{xy} = & \frac{1}{2(1+\hat{\nu})} \int_{0-}^t E_s(\phi(t)-\phi(s))\,(\frac{\partial u_{,y}}{\partial s} + \frac{\partial v_{,x}}{\partial s}) ds \qquad (2.107)
\end{aligned}$$

Similarly, the equilibrium equations can be summarized as follows:

$$\begin{aligned}
&\frac{(1-\hat{\nu})}{(1+\hat{\nu})(1-2\hat{\nu})}\int_{0-}^{t} E_s(\phi(t)-\phi(s))\,\frac{\partial u_{,xx}}{\partial s}ds \\
&+\frac{1}{2(1+\hat{\nu})(1-2\hat{\nu})}\int_{0-}^{t} E_s(\phi(t)-\phi(s))\,\frac{\partial v_{,xy}}{\partial s}ds \\
&+\frac{1}{(1+\hat{\nu})}\int_{0-}^{t} E_s(\phi(t)-\phi(s))\,\frac{\partial u_{,yy}}{\partial s}ds \\
&-\frac{1}{(1-2\hat{\nu})}\int_{0-}^{t} E_s(\phi(t)-\phi(s))\,(\alpha\frac{\partial \theta_{,x}}{\partial s}+\beta\frac{\partial C_{,x}}{\partial s})ds = 0 \qquad (2.108)
\end{aligned}$$

$$\begin{aligned}
&\frac{(1-\hat{\nu})}{(1+\hat{\nu})(1-2\hat{\nu})}\int_{0-}^{t} E_s(\phi(t)-\phi(s))\,\frac{\partial v_{,yy}}{\partial s}ds \\
&+\frac{1}{2(1+\hat{\nu})(1-2\hat{\nu})}\int_{0-}^{t} E_s(\phi(t)-\phi(s))\,\frac{\partial u_{,xy}}{\partial s}ds \\
&+\frac{1}{2(1+\hat{\nu})}\int_{0-}^{t} E_s(\phi(t)-\phi(s))\,\frac{\partial v_{,xx}}{\partial s}ds \\
&-\frac{1}{(1-2\hat{\nu})}\int_{0-}^{t} E_s(\phi(t)-\phi(s))\,(\alpha\frac{\partial \theta_{,y}}{\partial s}+\beta\frac{\partial C_{,y}}{\partial s})ds = 0 \qquad (2.109)
\end{aligned}$$

This concludes the constitutive and governing field equations for the linearly viscoelastic portion of the beam incorporating temperature and moisture effects.

E. Constitutive Equations for the PZT Layer

The derivation of the field equations in the context of coupled eletro-thermo-elasticity from the fundamental principles of conservation of mass, linear momemtum, angular momemtum, energy and charge followed by the use of second law of thermodynamics are presented by H.F.Tiersten et.al. in [27]. Due to the interaction between electric field ($\hat{\mathbf{E}}$) and polarization ($\mathbf{P}$) the stress tensor($\mathbf{T}$) is shown to be non-symmetric and non linearly dependent on the electric field ($\hat{\mathbf{E}}$) as shown in Eq. (2.110b). If ψ, ρ, $\mathbf{F}$, $\boldsymbol{\pi}$ denote specific Helmholtz potential, density, deformation gradient and polarization per unit mass respectively, then

$$\mathbf{T} = \rho\, \mathbf{F}\frac{\partial \psi}{\partial \hat{\mathbf{E}}}\, \mathbf{F}^T - \mathbf{P} \otimes \hat{\mathbf{E}} \tag{2.110a}$$

$$\boldsymbol{\pi} = -\frac{\partial \psi}{\partial \hat{\mathbf{E}}} \tag{2.110b}$$

where

$$\boldsymbol{\pi} := \frac{\mathbf{P}}{\rho} \tag{2.111}$$

The electric displacement $\mathbf{D}$ is related to the electric field $\hat{\mathbf{E}}$ and the polarization $\mathbf{P}$ as follows:

$$\mathbf{D} = \boldsymbol{\epsilon}\hat{\mathbf{E}} + \mathbf{P} \tag{2.112}$$

where $\boldsymbol{\epsilon}$ denotes the permittivity of the medium. If the deformation and electric fields are assumed to be small enough to linearize the equations of the stress($\mathbf{T}$) and electric displacement($\mathbf{D}$) and if the pyroelectric effects are ignored, then the Eq. (2.110b) reduces to the following set of equations [28]:

$$\mathbf{T} = \mathbf{C}\, \boldsymbol{\varepsilon} - \mathbf{e}^{\mathbf{T}}\, \hat{\mathbf{E}} - \boldsymbol{\alpha}\Delta\theta \tag{2.113}$$

$$\mathbf{D} = \mathbf{e}\, \boldsymbol{\varepsilon} + \boldsymbol{\epsilon}\, \hat{\mathbf{E}} \tag{2.114}$$

where $\mathbf{e}$ denotes the piezoelectric tensor and $\boldsymbol{\varepsilon}$ denotes the linearized strain. The electric field can be expressed in terms of the voltage φ in the PZT material as follows:

$$\hat{\mathbf{E}} := -\text{grad}\varphi \tag{2.115}$$

The conservation of charge and the conservation of linear momemtum result in the following equations:

$$\begin{aligned} \text{div}\mathbf{D} &= 0 \\ \text{div}\mathbf{T} &= \mathbf{0} \end{aligned} \tag{2.116}$$

Thus equations (2.113) through (2.116) represent field equations employed for the PZT layer of the beam assembly.

.

CHAPTER III

NUMERICAL SOLUTION AND ANALYSIS OF THE ELASTIC OR VISCOELASTIC BEAM ASSEMBLY

The geometry of the structure considered for study is summarized as follows. A thin linearly elastic/viscoelastic beam with length to thickness ratio of $\frac{1}{40}$ is perfectly bonded to a PZT beam with length to thickness ratio of $\frac{1}{200}$. The PZT layer rests on the top of the elastic/viscoelastic layer. The length of either layers is represented by L. The thickness of the elastic/viscoelastic beam and PZT beam are represented by h1, h2, respectively. The cantilever beam assembly is fixed along the edge ACE as shown in Figure 3.1(b). The shaded region corresponds to the PZT 5H layer and the unshaded region corresponds to the elastic/viscoelastic material. The surface containing the edge AB is maintained at a temperature of T_f and a moisture concentration of C_f. The surface containing the edge EF is maintained at a temperature of $T_o < T_f$ and moisture density of $C_o < C_f$. The surfaces containing the edges ACE, BDF are perfectly insulated and the moisture flux is maintained at zero. Displacement and traction continuity is assumed at all times along the common interface CD owing to the rigid bonding between the two layers. Since the thickness to length ratio is $\ll 1$, the heat and moisture are assumed to diffuse only along the thickness direction. Therefore, the temperature and moisture fields are obtained by solving one dimensional coupled diffusion equations. Since $T_o < T_f$ and $C_o < C_f$, heat and moisture diffuse from the surface containing edge AB to the surface containing edge EF. Once the system attains a steady state, it is assumed that it remains in that state thereafter.

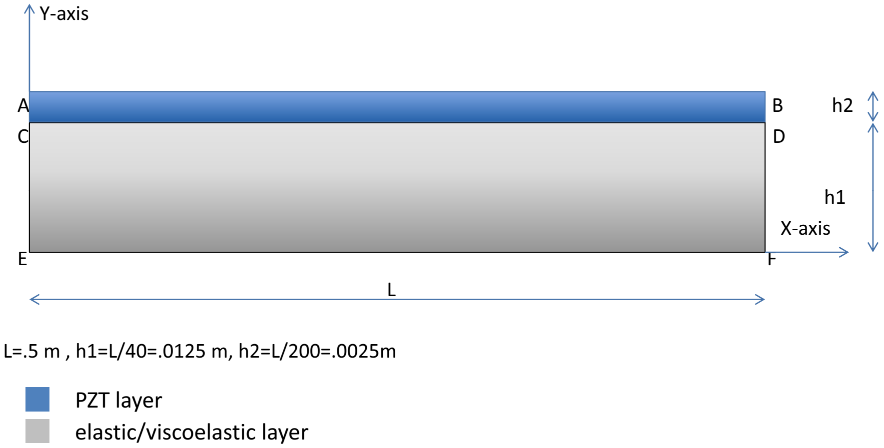

(a) Geometry of the beam assembly

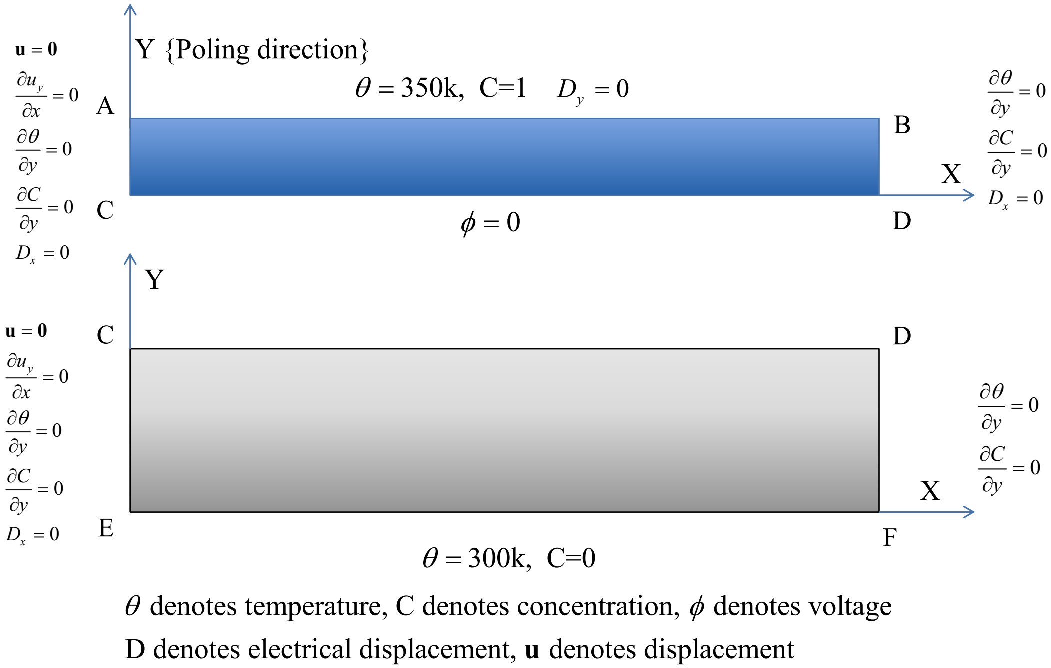

(b) Boundary conditions

Fig. 3.1. Figure depicting the geometry and of the cantilever beam assembly and the boundary conditions for the case where no external voltage is applied across the PZT layer. The blue layer corresponds to the PZT material and the ash colored layer corresponds to the elastic/viscoealstic material. The surface containing the edge ACE is clamped and all other surfaces are traction free.

The first section presents a detailed description of the problem under study. The geometry considered for study and the corresponding initial and boundary conditions are specified in this section. The second section is divided into two subsections. In the first subsection finite difference equations for coupled heat and moisture diffusion equations are presented. This is followed by a study to determine an optimal choice of grid size and time step values required to solve these finite difference equations. In the second subsection, temperature and moisture field characteristics for a range of values of moisture and thermal properties are presented in the form of a parametric study. This is followed by a discussion on the choice of thermal and moisture material properties considered for the problem. The third section is divided into two subsections. In the first subsection, finite difference equations are obtained for the governing and constitutive equations employed in the current study. In the second subsection the optimal grid size values required to solve these finite difference equations are obtained. In the fourth section, numerical solutions are obtained for the displacement characteristics and the corresponding required active voltage control for the four different material specimens considered for study. This is followed by a discussion on the results and plots obtained. The materials chosen for the host structure and the actuator are summarized as follows:

- Linearly elastic materials:
    1. Aluminium-PZT 5H beam assembly subjected to transient thermal field.[1]
    2. Isotropic un-reinforced epoxy-PZT beam assembly subjected to transient thermal and moisture fields.
    3. Anisotropic CFRP-PZT beam assembly subjected to transient thermal and moisture fields.

---

[1] The moisture dependent deformation of Al is not considered for the moisture diffusion in Aluminium is negligible compared to the diffusion of heat.

- Linearly viscoelastic material-PZT beam assembly subjected to transient thermal and moisture fields.

A. Description of the Problem

As described earlier, the cantilever beam assembly consists of an elastic/viscoelastic beam perfectly glued to the PZT 5H layer which rests on the top of the beam as depicted in Figure 3.1(b). Heat and moisture diffusion are assumed to occur predominantly along the thickness direction, for simplicity. The assembly is clamped rigidly to a wall at one end and all other surfaces are assumed to be traction free. The length of the beam is chosen to be 0.5m. The length to thickness ratio for the elastic/viscoelatic beam and the PZT 5H layer are chosen as 40 and 200 respectively. The width of the beam is assumed to be large enough to solve the problem in the context of plane strain deformation. Therefore, the displacement field can be chosen as follows:

$$\mathbf{u} = \mathbf{u}(\mathrm{u},\ \mathrm{v}) \tag{3.1}$$

The boundary conditions for both the sections of the beam assembly referring to the Figure 3.1(a) are summarized as follows:

$$u = v = 0 \text{ along the edge ACE} \tag{3.2a}$$

$$\frac{\partial v}{\partial x} = 0 \text{ along the edge ACE} \tag{3.2b}$$

Traction free boundary conditions along the surfaces BDF, AB and EF result in the following equations:

$$\sigma_{xx} = \sigma_{xy} = 0 \tag{3.3a}$$

$$\sigma_{yy} = \sigma_{xy} = 0 \tag{3.3b}$$

Traction and displacement continuity conditions along the surface CD can be summarized as follows:

$$\mathbf{u}^e(x, h_2, t) = \mathbf{u}^p(x, h_2, t) \tag{3.4a}$$

$$\sigma^e_{yy}(x, h_2, t) = \sigma^p_{yy}(x, h_2, t) \tag{3.4b}$$

$$\sigma^e_{xy}(x, h_2, t) = \sigma^p_{xy}(x, h_2, t) \tag{3.4c}$$

Other boundary conditions are summarized as follows:

$$\varphi = 0 \quad \text{along the edge CD} \tag{3.5a}$$

$$D_y = 0 \;\; \text{along the edge AB when no voltage is applied across PZT layer} \tag{3.5b}$$

$$D_x = 0 \;\; \text{along the edges ACE, BDF} \tag{3.5c}$$

$$\varphi = \varphi_o \;\; \text{along the edge AB when voltage } \varphi_o \text{ is applied across PZT layer} \tag{3.5d}$$

The boundary temperatures T$_f$, T$_o$ are chosen to be 350 k and 300 k, respectively. The moisture content in a structural component at steady state largely depends on the humidity level of the surroundings. If W$_o$ denotes the initial weight of T300/5208 CFRP sample placed in an environment with relative humidity RH, then the final weight W$_f$ of the sample when completely saturated with moisture is reported to be 0.015 x RH x W$_o$% heavier than its initial weight. AS/3501-5 carbon/epoxy composite is reported to be 0.017 x RH x W$_o$% heavier than its initial weight [26]. Therefore the amount of moisture in T300/5208 and AS/3501-5 in saturated state is given by 0.015 x RH % and 0.017 x RH % of their initial weights, respectively. For instance if the relative humidity RH=60% then the over all weight of T300/5208 and AS/3501-5 would be increased by 0.9% and 1.02% respectively. When completely immersed in distilled water, the absorbed moisture content for both these materials is reported to be 1-2 % of initial weights at steady state [26]. The absorbed moisture content in various epoxy resins and CFRP composites is also shown to be dependent on the temperature conditions [18]. In the Figure 3.1(a), boundaries AB and EF are assumed to be saturated with moisture content C_f, C_o respectively. For the current problem, we shall assume $C_f=1$ and $C_o=0$ i.e. the surface EF is assumed to be in dry state. Here, C_f and C_o denote the % of moisture by weight in the saturated and dry states of the solid respectively. In the equations, (2.74b) which govern the coupled moisture and heat transport, the properties that are material specific are thermal diffusivity D_h, moisture diffusivity D_m, non-dimensional coupling constant $\lambda\nu$. The coupling between temperature and moisture diffusion phenomena is strongly dependent on the ratio of their diffusivities and the coupling constant $\lambda\nu$.

Diffusion of moisture through polymer/polymer composites is a relatively slower process compared to the diffusion of temperature. It is almost negligible in the case of metals. The ratio of thermal to moisture diffusivity (defined as Lewis number) in the case of composites can differ directionally. For instance in the case of carbon fiber reinforced epoxy composite, the thermal diffusivity along the fiber direction is much higher than in the direction perpendicular to it. Similarly, moisture diffusivity is much less along the fiber direction than in the direction perpendicular to it. Since, the current study is intended to capture the effects of simultaneous heat and moisture diffusion, the direction of these diffusive phenomena and ratio of their diffusivities is chosen such that both the effects are predominant for the time period under consideration. It has been established in Chapter II that the value of the coupling constant, $\lambda\nu <1$ due to thermodynamic considerations. The interdependency of temperature and moisture fields is governed by the constants λ, ν. Therefore a parametric study is presented in the second section of this chapter, where temperature and moisture field plots are obtained by varying the values of the Lewis number, the coupling constant$(\lambda\nu)$ and the constants λ, ν over a certain range. Based on the results thus obtained a choice of values for Lewis number, $\lambda\nu$, λ and ν that would be apt for a strong coupling between temperature and moisture fields.

B. Coupled Thermal and Moisture Diffusion Equations

In the current study, we consider a one dimensional treatment to the diffusion problem for both thermal and moisture fields. The derivation of the equations used in this section were presented in Chapter II and shall not be repeated here. The coupled heat and moisture diffusion equations are as follows:

$$\frac{\partial C}{\partial t} = D\Delta C + \lambda \frac{\partial \theta}{\partial t} \tag{3.6}$$

$$\frac{\partial \theta}{\partial t} = \mathsf{D}\Delta \theta + \nu \frac{\partial C}{\partial t} \tag{3.7}$$

where D and D are related to the moisture diffusivity and thermal diffusivity respectively by the dimensionless coupling constant $\lambda\nu$ as follows:

$$D = (1-\lambda\nu)D_m \tag{3.8}$$

$$\mathsf{D} = (1-\lambda\nu)\mathsf{D_h} \tag{3.9}$$

The equations (3.6) and (3.7) can be re-written as follows:

$$\frac{\partial C}{\partial t} = D\Delta C + \lambda\Delta\theta \tag{3.10}$$

$$\frac{\partial \theta}{\partial t} = \mathsf{D}\Delta\theta + \nu\Delta C \tag{3.11}$$

The following non-dimensional parameters and functions f, g are introduced to rewrite equations (3.10) and (3.11).

$$\hat{u} = D_m/\mathsf{D_h} \text{ (u is the inverse of Lewis number)} \tag{3.12}$$

$$\hat{\theta} = \frac{D_m t}{h^2} \tag{3.13}$$

$$\xi = \frac{y}{h} \tag{3.14}$$

$$C(\xi,\hat{\theta}) = C_0 + \nu f(\xi,\hat{\theta}) \tag{3.15}$$

$$\theta(\xi,\hat{\theta}) = \theta_0 + \nu g(\xi,\hat{\theta}) \tag{3.16}$$

The transformed equations are as follows:

$$\begin{aligned} \frac{\partial f}{\partial \hat{\theta}} &= \frac{\partial^2 f}{\partial \xi^2} + \frac{\lambda \nu}{u} \frac{\partial^2 g}{\partial \xi^2} \qquad (3.17) \\ \frac{\partial g}{\partial \hat{\theta}} &= \frac{1}{\hat{u}} \frac{\partial^2 g}{\partial \xi^2} + \frac{\partial^2 f}{\partial \xi^2} \qquad (3.18) \end{aligned}$$

The initial and boundary conditions for temperature and moisture fields are summarized as follows:

$$\begin{aligned} \forall\ t > 0,\ \theta(0,t) &= \theta_o \qquad (3.19a) \\ \forall\ t > 0,\ \theta(h,t) &= \theta_f \qquad (3.19b) \\ \forall\ 0 \geq \xi \leq 1,\ \theta(y,0) &= \theta_o \qquad (3.19c) \\ \forall\ \theta > 0,\ C(0,t) &= C_o \qquad (3.19d) \\ \forall\ \theta > 0,\ C(h,t) &= C_f \qquad (3.19e) \\ \forall\ 0 \geq \xi \leq 1,\ C(y,0) &= C_o \qquad (3.19f) \end{aligned}$$

Equations (3.20a) to (3.20f) when expressed using equations (3.12)-(3.16) transform to the following form:

$$\begin{aligned} \forall\ \theta > 0,\ g(0,\hat{\theta}) &= 0 \qquad (3.20a) \\ \forall\ \theta > 0,\ g(1,\hat{\theta}) &= \frac{\theta_f - \theta_0}{\nu} \qquad (3.20b) \\ \forall\ 0 \leq \xi \leq 1,\ g(\xi,0) &= 0 \qquad (3.20c) \\ \forall\ \theta > 0,\ f(0,\hat{\theta}) &= 0 \qquad (3.20d) \\ \forall\ \theta > 0,\ f(1,\hat{\theta}) &= C_f - C_0 \qquad (3.20e) \\ \forall\ 0 \leq \xi \leq 1,\ f(\xi,0) &= 0 \qquad (3.20f) \end{aligned}$$

1. Finite Difference Formulation and Convergence Study for Temperature and Moisture Fields

The partial differential equations (3.17) and (3.18) and the corresponding boundary conditions are replaced by their corresponding finite difference equations. This reduces the problem to a set of simultaneous algebraic equations which can solved with ease. Finite difference equations are solved explicitly using forward difference for temporal component and central difference for spatial component. Hence, equations (3.17), (3.18) are written in finite difference form as follows:

$$\frac{f_i^{k+1} - f_i^k}{\Delta\theta} = \frac{f_{i+1}^k - 2f_i^k + f_{i-1}^k}{(\Delta\xi)^2} + \frac{\lambda\nu}{\hat{u}}\,\frac{g_{i+1}^k - 2g_i^k + g_{i-1}^k}{(\Delta\xi)^2} \tag{3.21}$$

$$\frac{g_i^{k+1} - g_i^k}{\Delta\theta} = \frac{1}{u}\,\frac{g_{i+1}^k - 2g_i^k + g_{i-1}^k}{(\Delta\xi)^2} + \frac{f_{i+1}^k - 2f_i^k + f_{i-1}^k}{(\Delta\xi)^2} \tag{3.22}$$

In order for the solution obtained using the finite difference expressed in equations (3.30) and (3.31d) to be acceptably accurate, grid sizes $\Delta\xi$, and $\Delta\theta$, must be sufficiently small and satisfy the following condition for convergence:

$$\frac{\Delta\theta}{\hat{u}\,(\Delta\xi)^2} \leq 0.2 \tag{3.23}$$

The following values are used as boundary conditions considered for the current study:

$$C_o = 0 \tag{3.24a}$$

$$C_f = 1 \tag{3.24b}$$

$$\theta_o = 300\ K \tag{3.24c}$$

$$\theta_f = 350\ K \tag{3.24d}$$

To ensure that the condition (3.23) is good enough to predict the evolution of temperature and moisture fields with desired accuracy, temperature and moisture plots are obtained by varying the non-dimensional grid size $\Delta\xi$ and the non-dimensional time increment $\Delta\theta$. The results of the same are presented below. For convergence analysis, the values for u, $\lambda\nu$, λ are chosen for the CFRP material T300/5208 from [26].

$$\hat{u} = 10^{-1} \text{ (in the direction normal to fiber direction)} \tag{3.25a}$$

$$\lambda\nu = 0.25 \tag{3.25b}$$

$$\lambda = 0.122 \tag{3.25c}$$

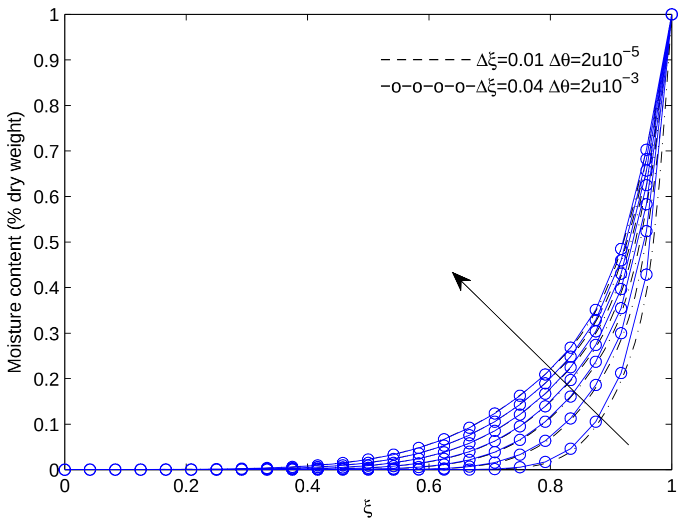

(a) Moisture Field

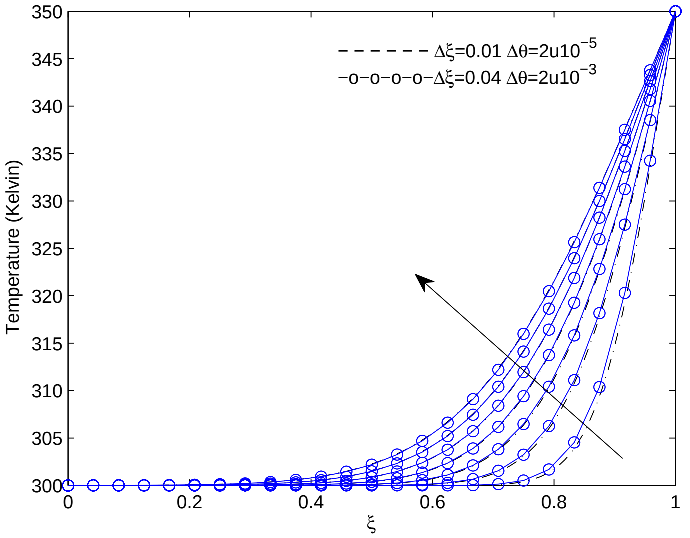

(b) Temperature Field

Fig. 3.2. Figure shows moisture and temperature fields by varying the spatial grid size($\Delta\xi$) and time increment($\Delta\theta$). Arrow indicates the direction of evolution of both the fields with time.

From the Figure 3.2, it can be concluded that temperature and moisture fields can be accurately predicted for a choice of $\Delta\xi \leq 0.04$ and $\Delta\theta \leq 2$ x10^{-3}û.

2. Parametric Study for Moisture and Temperature Fields

Since, the current study is focussed towards understanding the simultaneous effects of temperature and moisture fields in polymer/polymer composites, it is essential to understand the coupling between heat and moisture diffusion phenomena. The Lewis number(û$^{-1}$) and the coupling constant($\lambda\nu$) are the material parameters which quantify this coupling. It was established in Chapter II that the coupling constant ($\lambda\nu$ <1). It was mentioned earlier that the thermal and moisture diffusion phenomena in polymers/polymer composites occur at different time scales, the latter phenomena being slower than the former. This is identified by comparing the thermal and moisture diffusivities of materials. For instance, the Lewis number in case of T300/5208 carbon/epoxy composite in the direction normal to the fibers is 10. Whereas, referring to the table in page 82, the Lewis number for epoxy when calculated is of the order of 10^6. The coupling constant also differs from material to material. So, in order to quantitatively study the effect of these constants on the coupling between thermal and moisture diffusion is necessary to conduct a parametric study by allowing these properties to vary and study the outcome. To this end, Table 3.1 summarizes the values considered for the parametric study. For simplicity, the properties of T300/5208 polymer composite are chosen for a standard case. The boundary conditions used for the parametric study are summarized in Eq (3.24). Alternatively, mixed boundary conditions can be chosen for the problem. The consequences of this are illustrated at the end of the parametric study.

Table 3.1. Summary of the range of parameters considered for study

û	$\lambda\nu$	λ	ν
10^{-6}	.25	.122	2.05
	.25	.0122	20.5
	.25	1.22	.205
	.025	.122	.205
	.025	.0122	2.05
	.0025	.122	.0205
	.0025	.0122	.205

û	$\lambda\nu$	λ	ν
10^{-3}	.25	.122	2.05
	.25	.0122	20.5
	.25	1.22	.205
	.025	.122	.205
	.025	.0122	2.05
	.0025	.122	.0205
	.0025	.0122	.205

û	$\lambda\nu$	λ	ν
10^{-1}	.25	.122	2.05
	.25	.0122	20.5
	.25	1.22	.205
	.25	.00122	205.0
	.025	.122	.205
	.025	.0122	2.05
	.025	.00122	20.5
	.025	1.22	.0205
	.0025	.122	.0205
	.0025	.0122	.205
	.0025	.00122	2.05

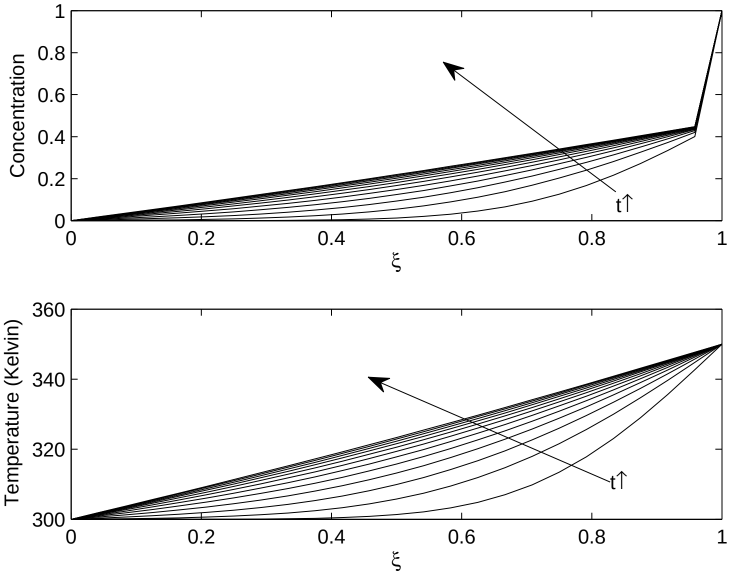

(a) Plot showing evolution of temperature and moisture fields(λ=0.122, ν=2.05)

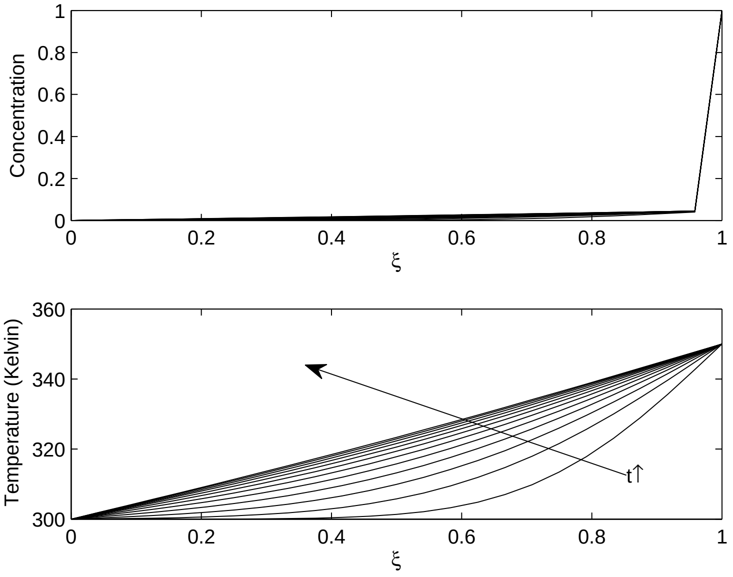

(b) Plot showing evolution of temperature and moisture fields (λ=0.0122, ν=20.5)

Fig. 3.3. Evolution of moisture and temperature fields when $\hat{u}$=10^{-6} and $\lambda\nu$=0.25 for various choices of λ, ν. The non-dimensional time parameter $\hat{\theta}$ varies from 0 to 3x10^{-7}.

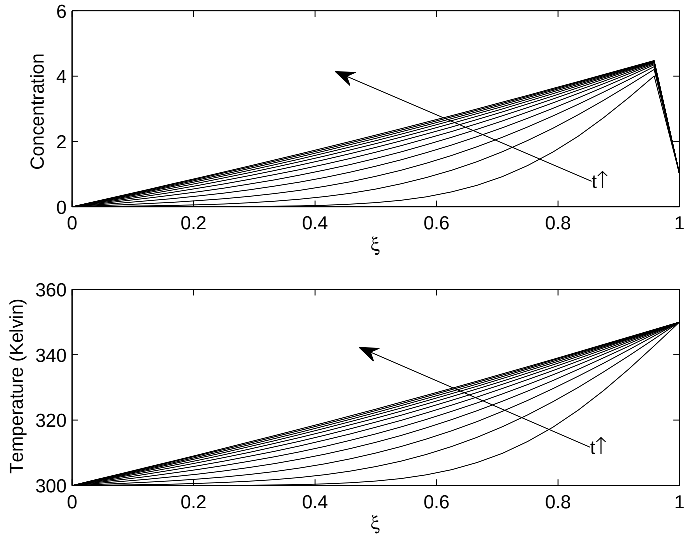

Fig. 3.4. Evolution of moisture and temperature fields when $\hat{u}$=10^{-6} and $\lambda\nu$=0.25 and (λ=1.22, ν=0.205). The non-dimensional time parameter $\hat{\theta}$ varies from 0 to 3x10^{-7}.

It is observed from Figures (3.3) through (3.6) that for a very low value of u=10^{-6}, the effect of moisture field on the temperature field is negligible irrespective of the value of coupling constant $\lambda\nu$. But, the dependence of the moisture field on the temperature field is strongly governed by the value of λ. This can be noted from Figures 3.3(b), 3.5(b) and 3.6(b).

When the value of λ is decreased by one order of magnitude from its base value of 0.122, the dependence of moisture field on the temperature field is reduced greatly. It is observed from Figure 3.4 that when the value of λ is increased by one order of magnitude from its base value, the moisture concentration inside the material exceeds the boundary values of moisture concentration. This is non-physical because, in such a case there should be an outflow of moisture from the material (which is initially assumed to be dry) to the surroundings, even in the absence of internal moisture source. The sharp changes in the slope of the concentration curve is because of the following reasons: A jump discontinuity is observed in the value of concentration at ξ=0 and t=0 due to the limitations of the numerical scheme. Grid size considered for the parametric study is not fine enough to capture large gradients in concentration near $\xi = 1$ at early times. This problem can be avoided by using finer grids for the study. Since the parametric study is dedicated to quantitatively examine the coupling effect, a coarser grid was implemented. However, while studying the effect of hygrothermal deformation a finer grid was implemented.

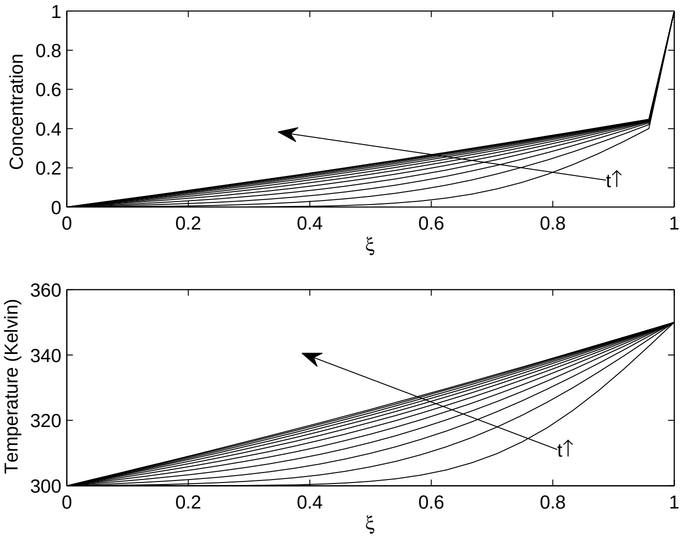

(a) Plot showing evolution of temperature and moisture fields (λ=0.122, ν=0.205)

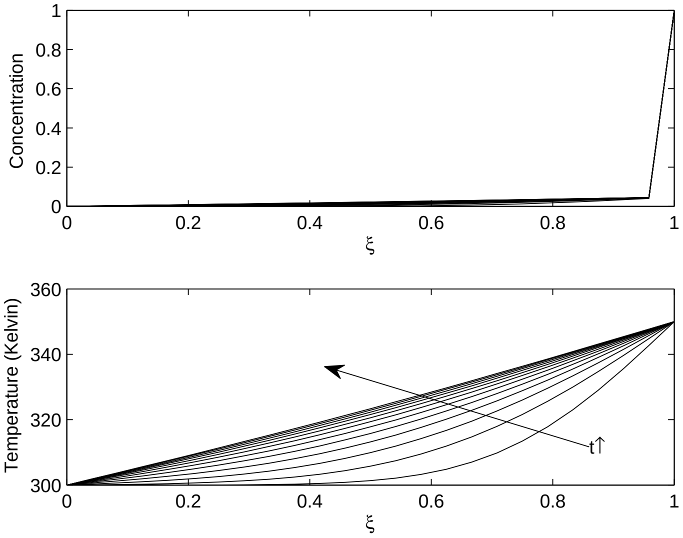

(b) Plot showing evolution of temperature and moisture fields (λ=0.0122, ν=2.05)

Fig. 3.5. Evolution of moisture and temperature fields when $\hat{u}$=10^{-6} and $\lambda\nu$=0.025 for various choices of λ, ν. The non-dimensional time parameter $\hat{\theta}$ varies from 0 to 3x10^{-7}.

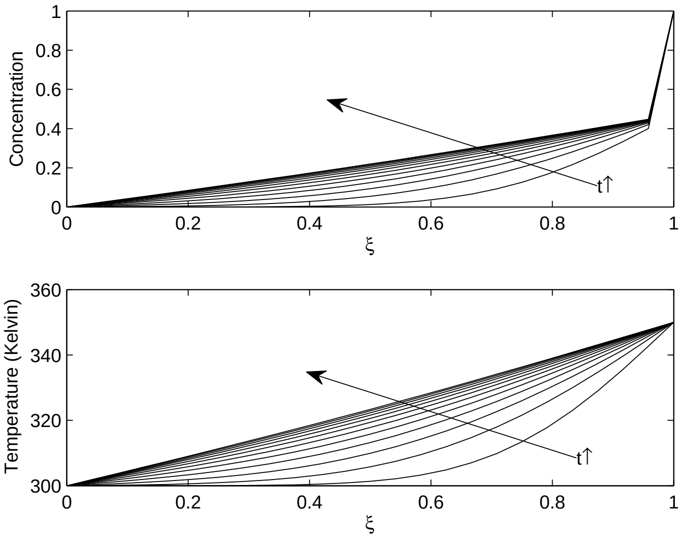

(a) Plot showing evolution of temperature and moisture fields (λ=0.122, ν=0.0205)

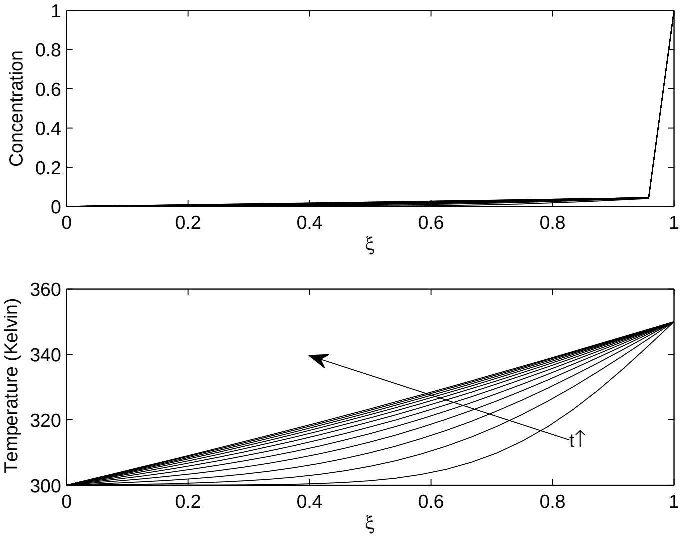

(b) Plot showing evolution of temperature and moisture fields (λ=0.0122, ν=0.205)

Fig. 3.6. Evolution of moisture and temperature fields when $\hat{u}$=10^{-6} and $\lambda\nu$=0.0025 for various choices of λ, ν. The non-dimensional time parameter $\hat{\theta}$ varies from 0 to 3x10^{-7}.

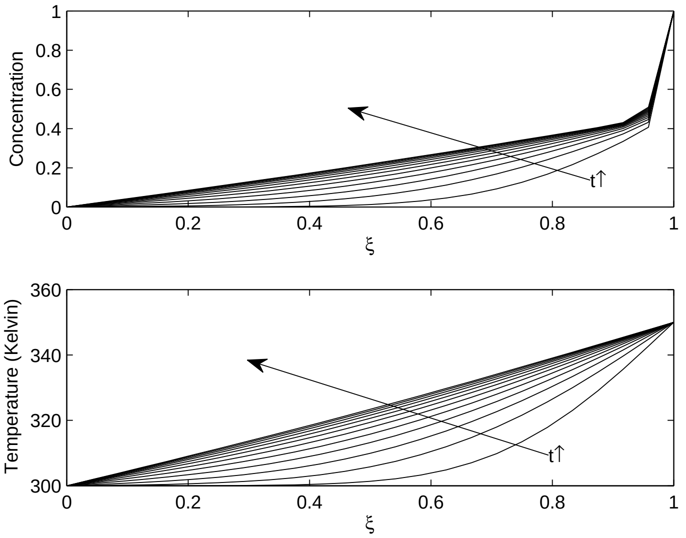

(a) Plot showing evolution of temperature and moisture fields(λ=0.122, ν=2.05)

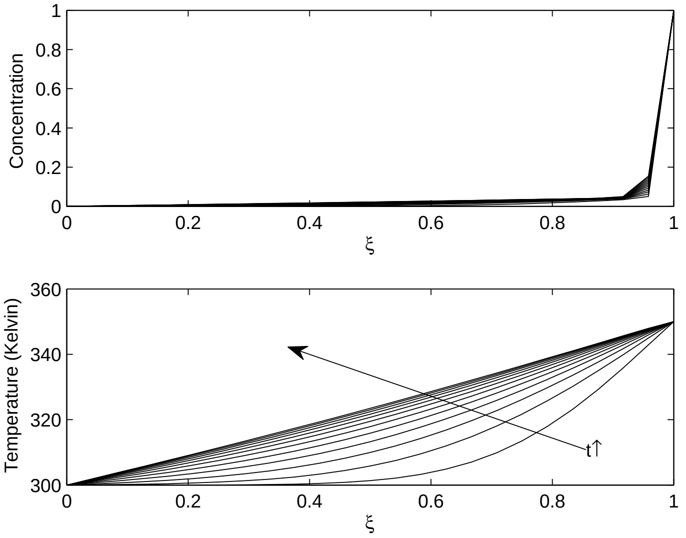

(b) Plot showing evolution of temperature and moisture fields (λ=0.0122, ν=20.5)

Fig. 3.7. Evolution of moisture and temperature fields when $\hat{u}$=10^{-3} and $\lambda\nu$=0.25 for various choices of λ, ν. The non-dimensional time parameter $\hat{\theta}$ varies from 0 to 3x10^{-4}.

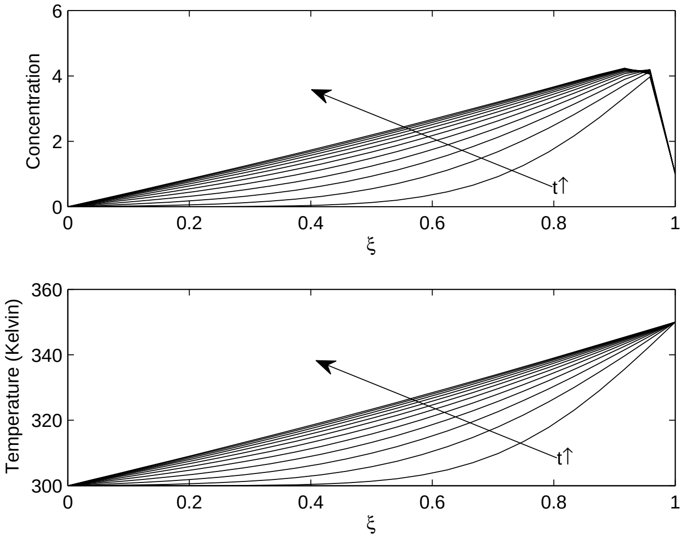

Fig. 3.8. Evolution of moisture and temperature fields when $\hat{u}$=10^{-3} and $\lambda\nu$=0.25 and (λ=1.22, ν=0.205). The non-dimensional time parameter $\hat{\theta}$ varies from 0 to 3x10^{-4}.

It is observed from Figures 3.7, 3.8 and 3.10 that when u=10^{-3}, the evolution trend of moisture and temperature fields is similar to the case where u=10^{-6}. The effect of moisture field on the temperature field is negligible irrespective of the value of coupling constant $\lambda\nu$. Whereas, the value of λ quantifies the dependence of the moisture field on the temperature field. This is noted from Figures 3.7(b), 3.9(b) and 3.10(b). When the value of λ is decreased by one order of magnitude from its base value of 0.122, the dependence of moisture field on the temperature field is reduced, significantly. It can be noted from Figure 3.8 that when the value of λ is increased by one order of magnitude from its base value, the moisture concentration inside the material exceeds the boundary values. This is non-physical and the explanation offered earlier holds here as well.

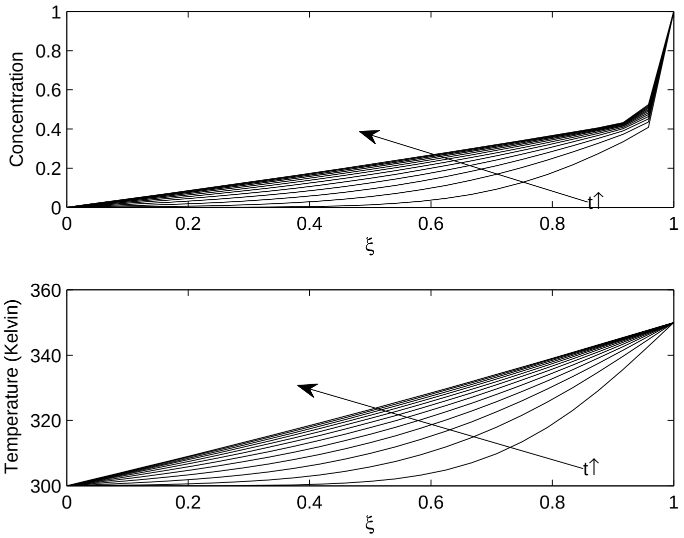

(a) Plot showing evolution of temperature and moisture fields (λ=0.122, ν=0.205)

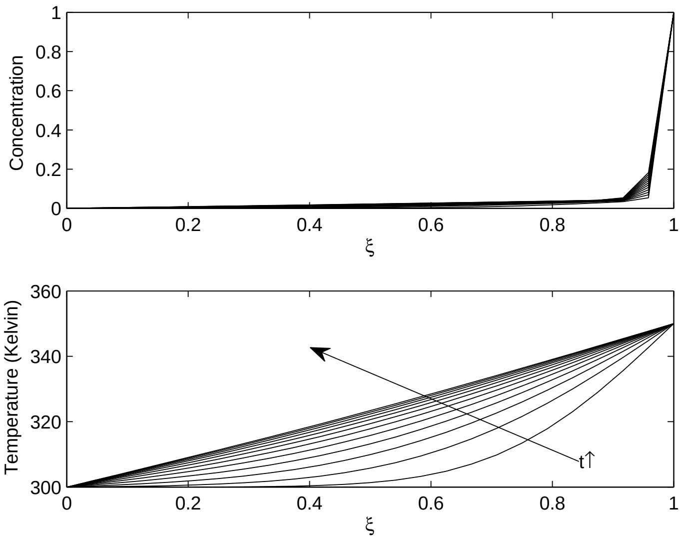

(b) Plot showing evolution of temperature and moisture fields (λ=0.0122, ν=2.05)

Fig. 3.9. Evolution of moisture and temperature fields when $\hat{u}$=10^{-3} and $\lambda\nu$=0.025 for various choices of λ, ν. The non-dimensional time parameter $\hat{\theta}$ varies from 0 to 3x10^{-4}.

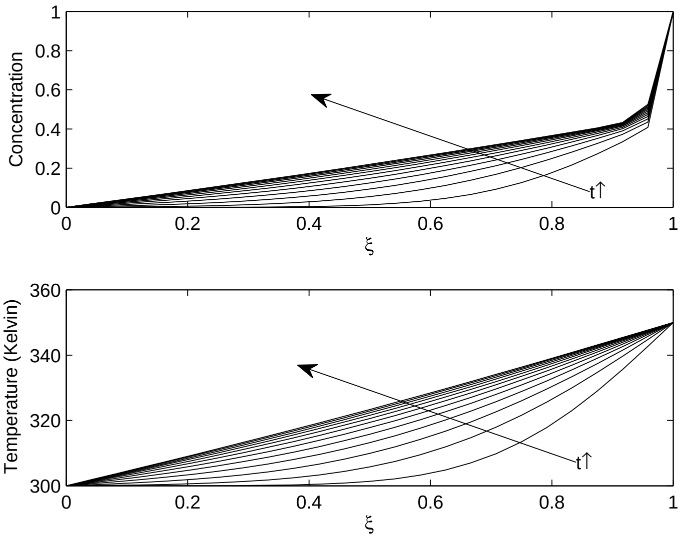

(a) Plot showing evolution of temperature and moisture fields (λ=0.122, ν=0.0205)

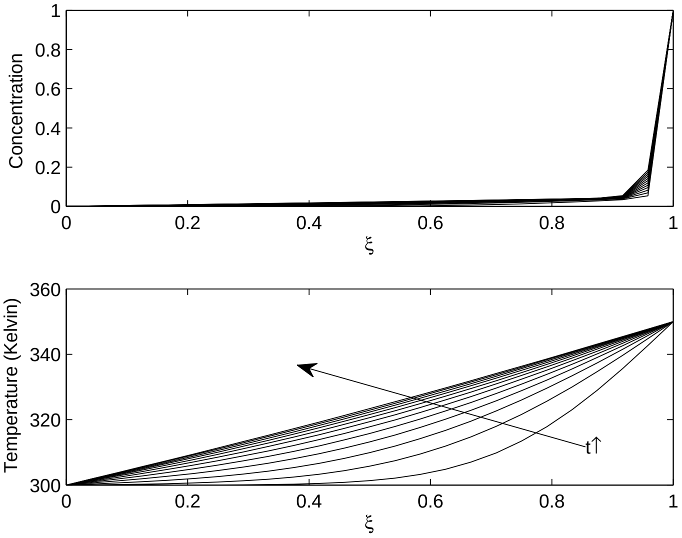

(b) Plot showing evolution of temperature and moisture fields (λ=0.0122, ν=0.205)

Fig. 3.10. Evolution of moisture and temperature fields when $\hat{u}$=10^{-3} and $\lambda\nu$=0.0025 for various choices of λ, ν. The non-dimensional time parameter $\hat{\theta}$ varies from 0 to 3x10^{-4}.

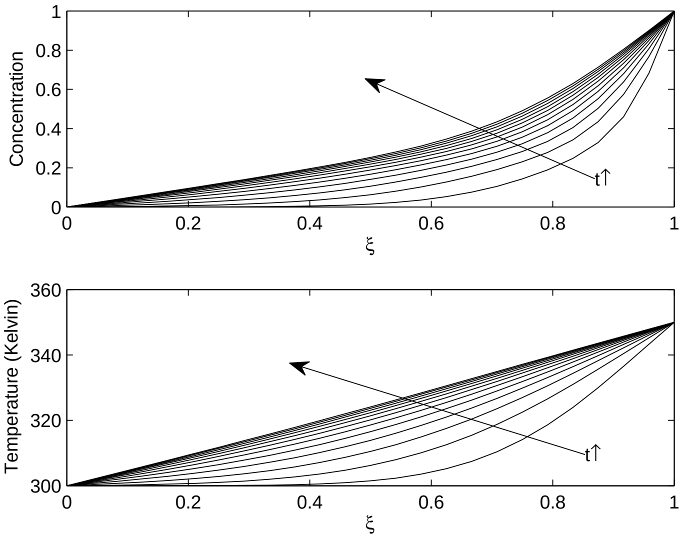

(a) Plot showing evolution of temperature and moisture fields (λ=0.122, ν=2.05)

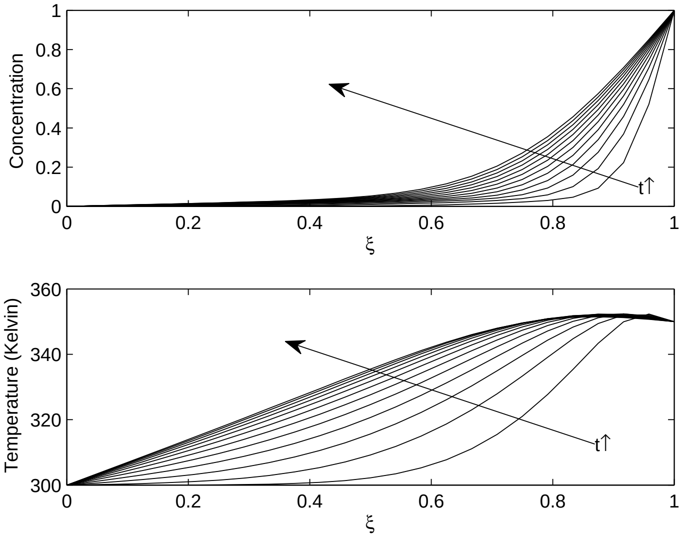

(b) Plot showing evolution of temperature and moisture fields (λ=0.0122, ν=20.5)

Fig. 3.11. Evolution of moisture and temperature fields when $\hat{u}$=10^{-1} and $\lambda\nu$=0.25 for various choices of λ, ν. The non-dimensional time parameter $\hat{\theta}$ varies from 0 to 3x10^{-1}.

When u=0.1, the effect of coupling between temperature and moisture fields is prominent. The interdependence of both the fields is strongly governed by the values of λ, ν. Figure 3.11(a) represents the temperature and moisture fields for the base values of λ and ν. From Figures 3.11(b) and 3.12 it is observed that when the values of λ, ν are changed by an order of magnitude from their base values, temperature and moisture fields differ significantly from the Figure 3.11(a). When these constants are changed by two orders of magnitude, the result is non-physical as depicted in Figure 3.12(b). Figures 3.13 and 3.14 are obtained when the $\lambda\nu$ is reduced by one order of magnitude from its base value and Figures 3.14 and 3.15 are obtained by reducing $\lambda\nu$ by two orders of magnitude from its base value. From Figures 3.13, 3.14(b) and 3.15 it is observed that temperature dependency on moisture is not affected by any decrease in the value ν from its base value. Whereas any increase in the value of ν is reflected in the drastic change in temperature profile as shown in Figures 3.11(b), 3.12(b)and 3.14(a). Moisture field is sensitive to both increase and decrease of the value of λ from its base value as shown in Figures 3.11 to 3.15.

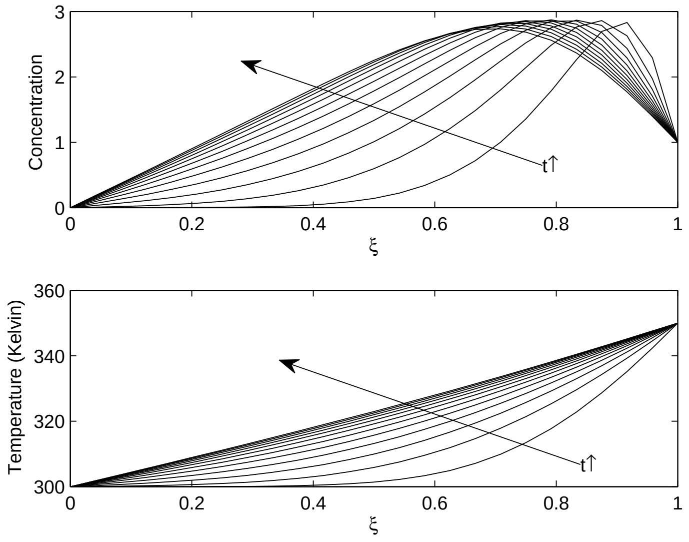

(a) Plot showing evolution of temperature and moisture fields (λ=1.22, ν=0.205)

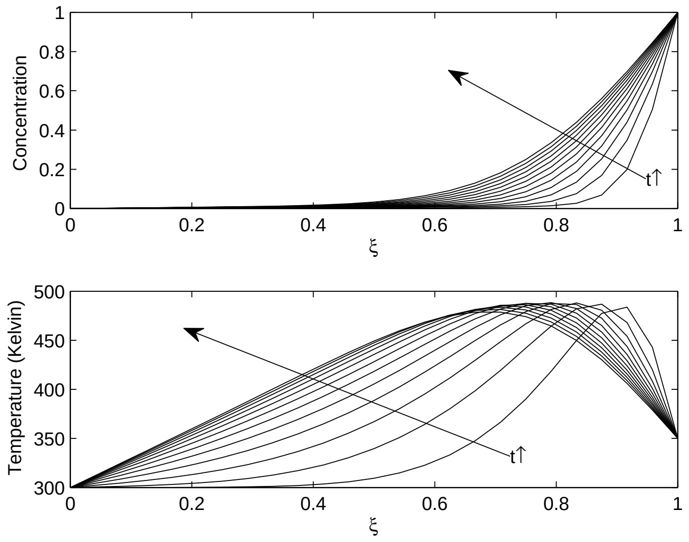

(b) Plot showing evolution of temperature and moisture fields (λ=0.00122, ν=205.0)

Fig. 3.12. Evolution of moisture and temperature fields when $\hat{u}$=10^{-1}, $\lambda\nu$=0.25 and (a)λ=1.22, ν=0.205 (b) λ=0.00122, ν=205.0. The non-dimensional time parameter $\hat{\theta}$ varies from 0 to 3x10^{-1}.

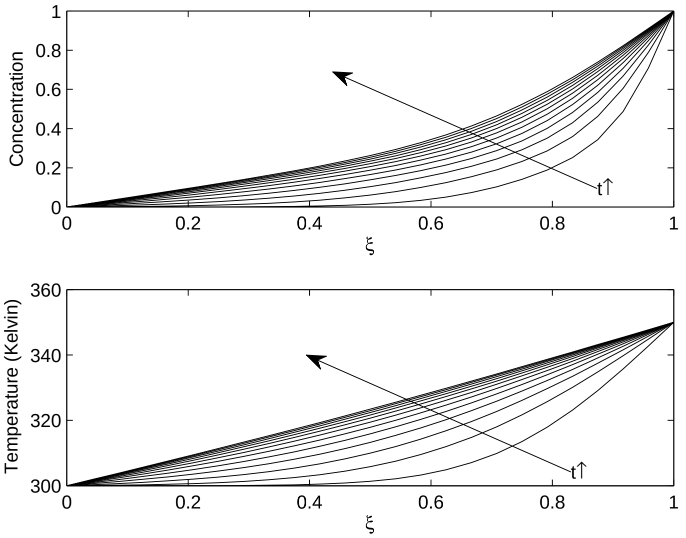

(a) Plot showing evolution of temperature and moisture fields (λ=0.122, ν=0.205)

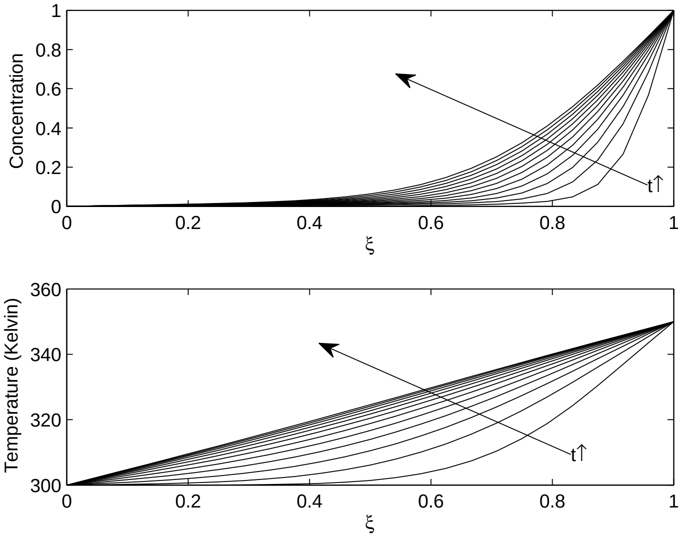

(b) Plot showing evolution of temperature and moisture fields (λ=0.0122, ν=2.05)

Fig. 3.13. Evolution of moisture and temperature fields when $\hat{u}$=10^{-1} and $\lambda\nu$=0.025 for various choices of λ, ν. The non-dimensional time parameter $\hat{\theta}$ varies from 0 to 3x10^{-1}.

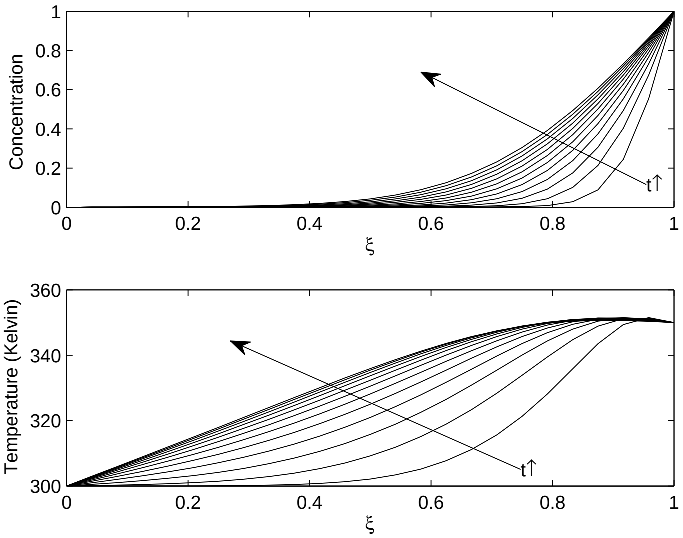

(a) Plot showing evolution of temperature and moisture fields (λ=0.00122, ν=20.5)

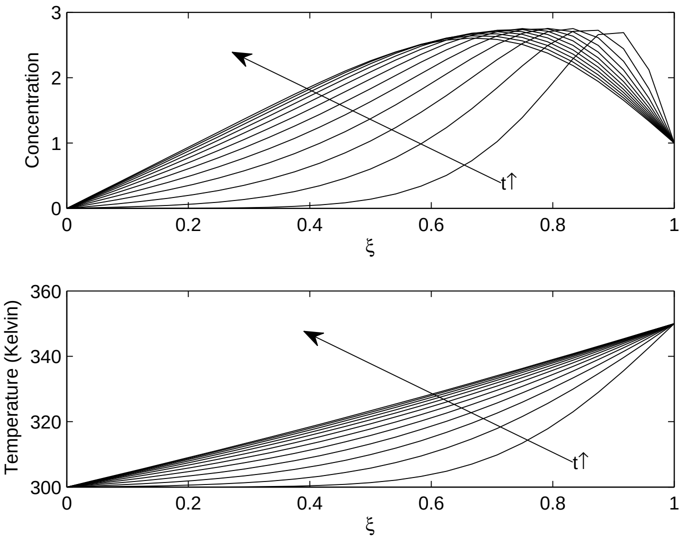

(b) Plot showing evolution of temperature and moisture fields (λ=1.22, ν=0.0205)

Fig. 3.14. Evolution of moisture and temperature fields when $\hat{u}$=10^{-1}, $\lambda\nu$=0.025 and (a)λ=0.00122, ν=20.5, (b)λ=1.22, ν=0.0205. The non-dimensional time parameter $\hat{\theta}$ varies from 0 to 3x10^{-1}.

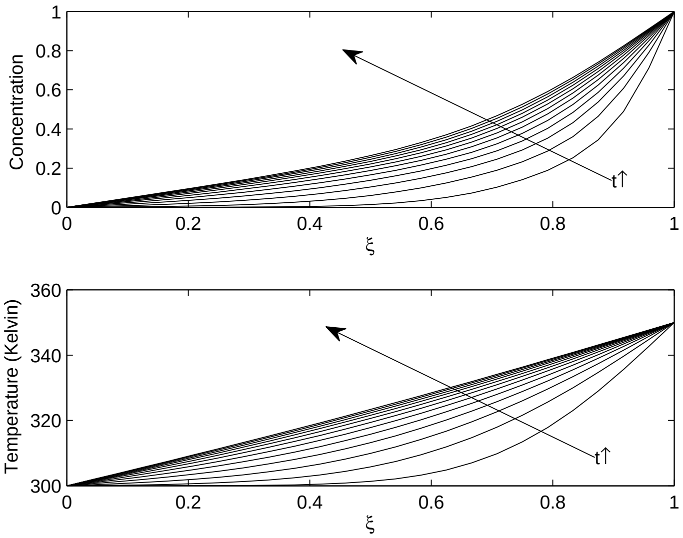

(a) Plot showing evolution of temperature and moisture fields (λ=0.122, ν=0.0205)

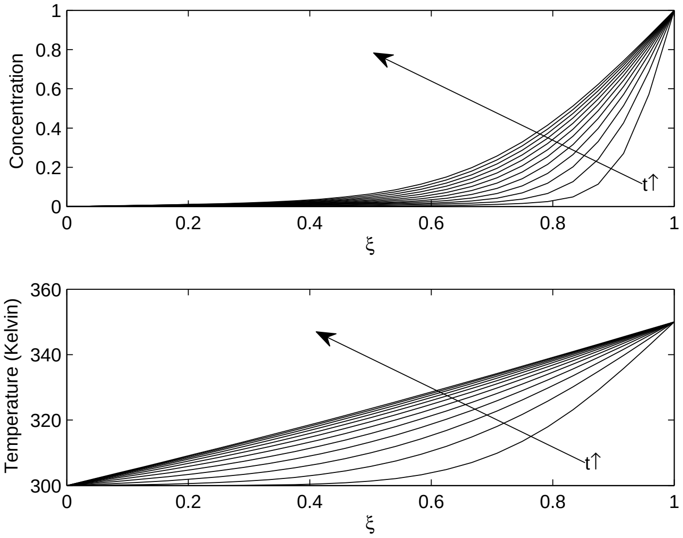

(b) Plot showing evolution of temperature and moisture fields (λ=0.0122, ν=0.205)

Fig. 3.15. Evolution of moisture and temperature fields when $\hat{u}$=10^{-1} and $\lambda\nu$=0.0025 for various choices of λ, ν. The non-dimensional time parameter $\hat{\theta}$ varies from 0 to 3x10^{-1}.

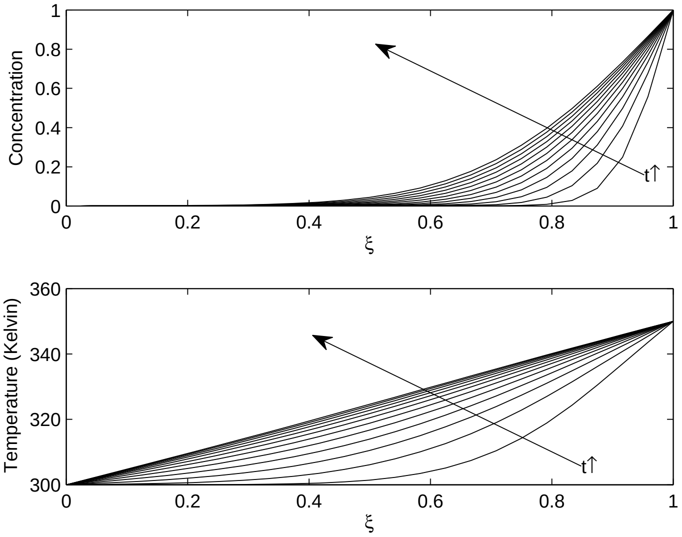

Fig. 3.16. Evolution of moisture and temperature fields when $\hat{u}$=10^{-1}, $\lambda\nu$=0.0025 and λ=0.00122, ν=2.05. The non-dimensional time parameter $\hat{\theta}$ varies from 0 to 3x10^{-1}.

From the plots obtained for the choice of parameters summarized in Table 3.1, it can be noted that the coupling between moisture and temperature fields increases with u and is predominant when û=0.1. At û=0.1, it is observed from Figures 3.11 through 3.16 that the interdependency of temperature and moisture fields is significant when the coupling constant $\lambda\nu$, the constants λ, ν are at their base values. Towards this end the following is the choice of constants made for the problem under study:

$$\hat{u} = 0.1 \tag{3.26a}$$

$$\lambda\nu = 0.25 \tag{3.26b}$$

$$\lambda = 0.122 \tag{3.26c}$$

A similar study can be performed by implementing mixed boundary conditions for temperature and moisture concentration. For instance, boundary EF can be assumed to be thermally insulated and with zero moisture gradient. Figure 3.17 depicts the evolution of the temperature and the moisture concentration evolve in the medium. It is observed that the average rise in temperature and the amount of absorbed moisture and in the medium is more in this case than in the cases discussed earlier. Therefore the hygrothermal deformation and hence the external actuating voltage in this case are expected to be more than in the earlier cases. Therefore, boundary conditions play a critical role in determining the external actuating voltage to minimize the deformation of the geometry.

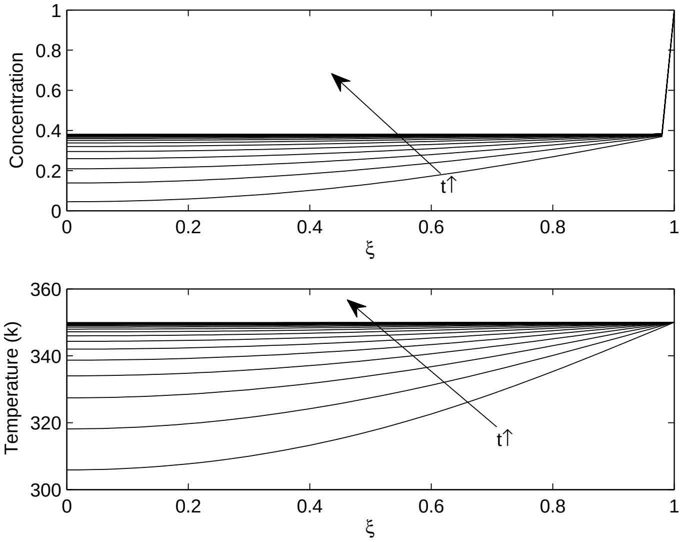

Fig. 3.17. Evolution of temperature and moisture fields when û=10^{-6}, $\lambda\nu$=0.25 and λ=0.122. The non-dimensional time parameter $\hat{\theta}$ varies from 0 to 3x10^{-7}.

C. Finite Difference Formulation of Governing Equations and Convergence Study for the Beam Assembly

1. Finite Difference Formulation of Field Equations for Viscoelastic Material

In this section, the finite difference formulation for the field equations derived in Chapter II, will be presented. The finite difference equations for isotropic viscoelastic material field equations are presented and those for the elastic material field equations can be obtained by ignoring the history dependent terms.

At a fixed time t_m, the first term of Eq. (2.108) can be expanded as follows:

$$\int_{0-}^{t_m} E_s(\phi(t_m)-\phi(s))\,\frac{\partial u_{,xx}}{\partial s}ds = E_s u_{,xx}(t_m) - \int_{0}^{t_m} u_{,xx}(s)\frac{\partial E_s(\phi^m-\phi^s)}{\partial s}\,ds \tag{3.27}$$

which can be approximated as follows:

$$\begin{aligned}\int_{0-}^{t} E_s(\phi(t)-\phi(s))\,\frac{\partial u_{,xx}}{\partial s}ds &\approx E_s u_{,xx}(t_m) - \sum_{k=0}^{m-1} u_{,xx}(t_k)[E_s(\phi^m-\phi^{k+1})-E_s(\phi^m-\phi^k)] \\ &= E_s u_{,xx}^m - \sum_{k=0}^{m-1} u_{,xx}^k[E_s(\phi^m-\phi^{k+1})-E_s(\phi^m-\phi^k)] \qquad (3.28)\end{aligned}$$

where,

$$u(t_m)=u^m;\ \phi(t_m)=\phi^m \tag{3.29a}$$

$$\phi^m=\sum_{k=0}^{m-1}\frac{t_{k+1}-t_k}{a(c_{k+1},\theta_{k+1})} \tag{3.29b}$$

$$\phi^{k+1}=\sum_{p=0}^{k}\frac{t_{p+1}-t_p}{a(c_{p+1},\theta_{p+1})} \tag{3.29c}$$

The spatial derivatives are approximated as follows: We use a mid point rule in obtaining the finite difference equations for nodes other than those on the boundary which results in the following equations.

$$\xi,_x^m \approx \frac{\xi_{i+1,j}^m - \xi_{i-1,j}^m}{2\Delta x} \tag{3.30a}$$

$$\xi,_y^m \approx \frac{\xi_{i,j+1}^m - \xi_{i,j-1}^m}{2\Delta y} \tag{3.30b}$$

$$\xi,_{xx}^m \approx \frac{\xi_{i+1,j}^m - 2\xi_{i,j}^m + \xi_{i-1,j}^m}{2\Delta x^2} \tag{3.30c}$$

$$\xi,_{xy}^m \approx \frac{\xi_{i+1,j+1}^m + \xi_{i-1,j-1}^m - \xi_{i+1,j-1}^m - \xi_{i-1,j+1}^m}{4\Delta x\Delta y} \tag{3.30d}$$

$$\xi,_{yy}^m \approx \frac{\xi_{i,j+1}^m - 2\xi_{i,j}^m + \xi_{i,j-1}^m}{2\Delta y^2} \tag{3.30e}$$

where i, j denote the node numbers along the x and y directions, respectively. For the boundary nodes a quadratic approximation is used which is described as follows:

$$\text{if i=1, } \xi,_x^m \approx \frac{-3\xi_{i,j}^m + 4\xi_{i+1,j}^m - \xi_{i+2,j}^m}{2\Delta x} \tag{3.31a}$$

$$\text{if i=M, } \xi,_x^m \approx \frac{-3\xi_{i,j}^m + 4\xi_{i+1,j}^m - \xi_{i+2,j}^m}{2\Delta x} \tag{3.31b}$$

$$\text{if j=1, } \xi,_y^m \approx \frac{-3\xi_{i,j}^m + 4\xi_{i,j+1}^m - \xi_{i,j+2}^m}{2\Delta y} \tag{3.31c}$$

$$\text{if j=N, } \xi,_y^m \approx \frac{3\xi_{i,j}^m - 4\xi_{i,j-1}^m + \xi_{i,j-2}^m}{2\Delta y} \tag{3.31d}$$

where ξ denotes the field variables such as displacement components u,v and voltage φ. M and N denote the maximum number of nodes chosen along x and y directions.

At a fixed time t_m Eq. (2.105) can be expanded as follows:

$$\begin{aligned}
\sigma_{xx}^m &= \frac{(1-\hat{\nu})}{(1+\hat{\nu})(1-2\hat{\nu})}(E_s u,_x(t_m) - \int_0^{t_m} u,_x(s)\frac{\partial E_s(\phi^m - \phi^s)}{\partial s}\,ds) \\
&+ \frac{\hat{\nu}}{(1+\hat{\nu})(1-2\hat{\nu})}(E_s v,_y(t_m) - \int_0^{t_m} v,_y(s)\frac{\partial E_s(\phi^m - \phi^s)}{\partial s}\,ds) \\
&- \frac{1}{(1-2\hat{\nu})}\{E_s(\alpha\theta(t_m) + \beta c(t_m)) - \int_0^{t_m}(\alpha\theta(s) + \beta c(s))\frac{\partial E_s(\phi^m - \phi^s)}{\partial s}\,ds\} \\
&\approx \frac{(1-\hat{\nu})}{(1+\hat{\nu})(1-2\hat{\nu})}(E_s\frac{u_{i+1,j}^m - u_{i-1,j}^m}{2\Delta x} - \int_0^{t_m} u,_x(s)\frac{\partial E_s(\phi^m - \phi^s)}{\partial s}\,ds)
\end{aligned} \tag{3.32}$$

which referring to Eq. (3.28) and Eq. (3.30) can be approximated as follows:

$$\begin{aligned}
\sigma_{xx}^{m} \approx\ & \frac{(1-\hat{\nu})}{(1+\hat{\nu})(1-2\hat{\nu})}\{E_s u,_{x}^{m} - \sum_{k=0}^{m-1} u,_{x}^{k}[E_s(\phi^m - \phi^{k+1}) - E_s(\phi^m - \phi^k)]\} \\
& + \frac{\hat{\nu}}{(1+\hat{\nu})(1-2\hat{\nu})}\{E_s v,_{y}^{m} - \sum_{k=0}^{m-1} v,_{y}^{k}[E_s(\phi^m - \phi^{k+1}) - E_s(\phi^m - \phi^k)]\} \\
& - \frac{1}{(1-2\hat{\nu})}\{E_s(\alpha\theta^m + \beta c^m) - \sum_{k=0}^{m-1}(\alpha\theta^k + \beta c^k)[E_s(\phi^m - \phi^{k+1}) - E_s(\phi^m - \phi^k)]\}
\end{aligned} \tag{3.33}$$

$$\begin{aligned}
& \approx \frac{(1-\hat{\nu})}{(1+\hat{\nu})(1-2\hat{\nu})}\{E_s \frac{u_{i+1,j}^{m} - u_{i-1,j}^{m}}{2\Delta x} \\
& - \sum_{k=0}^{m-1} \frac{u_{i+1,j}^{k} - u_{i-1,j}^{k}}{2\Delta x}[E_s(\phi^m - \phi^{k+1}) - E_s(\phi^m - \phi^k)]\} \\
& + \frac{\hat{\nu}}{(1+\hat{\nu})(1-2\hat{\nu})}\{E_s \frac{v_{i,j+1}^{m} - v_{i,j-1}^{m}}{2\Delta y} \\
& - \sum_{k=0}^{m-1} \frac{v_{i,j+1}^{k} - v_{i,j-1}^{k}}{2\Delta y}[E_s(\phi^m - \phi^{k+1}) - E_s(\phi^m - \phi^k)]\} \\
& - \frac{1}{(1-2\hat{\nu})}\{E_s(\alpha\theta^m + \beta c^m) \\
& - \sum_{k=0}^{m-1}(\alpha\theta^k + \beta c^k)[E_s(\phi^m - \phi^{k+1}) - E_s(\phi^m - \phi^k)]\}
\end{aligned} \tag{3.34}$$

In the same way, the Equation (2.106), (2.107) can be approximated by their finite difference formulations. The governing equation Equation (2.108) can be expanded as follows:

$$\frac{(1-\hat{\nu})}{(1+\hat{\nu})(1-2\hat{\nu})}(E_s u,_{xx}^m - \sum_{k=0}^{m-1} u,_{xx}^k [E_s(\phi^m - \phi^{k+1}) - E_s(\phi^m - \phi^k)])$$
$$+ \frac{1}{2(1+\nu)(1-2\nu)}(E_s v,_{xy}^m - \sum_{k=0}^{m-1} v,_{xy}^k [E_s(\phi^m - \phi^{k+1}) - E_s(\phi^m - \phi^k)])$$
$$+ \frac{1}{(1+\hat{\nu})}(E_s u,_{yy}^m - \sum_{k=0}^{m-1} u,_{yy}^k [E_s(\phi^m - \phi^{k+1}) - E_s(\phi^m - \phi^k)])$$
$$- \frac{1}{(1-2\hat{\nu})}\{E_s(\alpha\theta,_x^m + \beta c,_x^m) - \sum_{k=0}^{m-1} (\alpha\theta,_x^k + \beta c,_x^k)[E_s(\phi^m - \phi^{k+1}) - E_s(\phi^m - \phi^k)]\} = 0 \tag{3.35}$$

which referring to Eq. (3.30) can be approximated as follows:

$$\frac{(1-\hat{\nu})}{(1+\hat{\nu})(1-2\hat{\nu})}\{E_s \frac{u_{i+1,j}^m - 2u_{i,j}^m + u_{i-1,j}^m}{2\Delta x^2}$$
$$- \sum_{k=0}^{m-1} \frac{u_{i+1,j}^k - 2u_{i,j}^k + u_{i-1,j}^k}{2\Delta x^2}[E_s(\phi^m - \phi^{k+1}) - E_s(\phi^m - \phi^k)]\}$$
$$+ \frac{1}{2(1+\hat{\nu})(1-2\hat{\nu})}\{E_s \frac{v_{i+1,j+1}^m + v_{i-1,j-1}^m - v_{i+1,j-1}^m - v_{i-1,j+1}^m}{4\Delta x\Delta y}$$
$$- \sum_{k=0}^{m-1} \frac{v_{i+1,j+1}^k + v_{i-1,j-1}^k - v_{i+1,j-1}^k - v_{i-1,j+1}^k}{4\Delta x\Delta y}[E_s(\phi^m - \phi^{k+1}) - E_s(\phi^m - \phi^k)]\}$$
$$+ \frac{1}{(1+\hat{\nu})}\{E_s \frac{u_{i,j+1}^m - 2u_{i,j}^m + u_{i,j-1}^m}{2\Delta y^2}$$
$$- \sum_{k=0}^{m-1} \frac{u_{i,j+1}^k - 2u_{i,j}^k + u_{i,j-1}^k}{2\Delta y^2}[E_s(\phi^m - \phi^{k+1}) - E_s(\phi^m - \phi^k)]\}$$
$$- \frac{1}{(1-2\hat{\nu})}\{E_s(\alpha\frac{\theta_{i+1,j}^m - \theta_{i-1,j}^m}{2\Delta x} + \beta\frac{c_{i+1,j}^m - c_{i-1,j}^m}{2\Delta x})$$
$$- \sum_{k=0}^{m-1} (\alpha\frac{\theta_{i+1,j}^k - \theta_{i-1,j}^k}{2\Delta x} + \beta\frac{c_{i+1,j}^k - c_{i-1,j}^k}{2\Delta x})[E_s(\phi^m - \phi^{k+1}) - E_s(\phi^m - \phi^k)]\} = 0 \tag{3.36}$$

The Eq. (2.109) can be approximated in similar manner. Since, in the current problem temperature and moisture fields vary only along the y-direction their derivatives along x-direction can be dropped from Eq. (3.36). The boundary conditions specified in Eq. (3.5d) lead to the following set of equations. Along the edge DF, $\sigma_{xx} = 0$ transforms as follows:

$$\begin{aligned}
&\frac{(1-\hat{\nu})}{(1+\hat{\nu})(1-2\hat{\nu})}(E_s u,_x^m - \sum_{k=0}^{m-1} u,_x^k[E_s(\phi^m-\phi^{k+1}) - E_s(\phi^m-\phi^k)]) \\
&+ \frac{\hat{\nu}}{(1+\hat{\nu})(1-2\hat{\nu})}(E_s v,_y^m - \sum_{k=0}^{m-1} v,_y^k[E_s(\phi^m-\phi^{k+1}) - E_s(\phi^m-\phi^k)]) \\
&- \frac{1}{(1-2\hat{\nu})}\{E_s(\alpha\theta^m+\beta c^m) - \sum_{k=0}^{m-1}(\alpha\theta^k+\beta c^k)[E_s(\phi^m-\phi^{k+1}) - E_s(\phi^m-\phi^k)]\} = 0 \quad (3.37)
\end{aligned}$$

$$\begin{aligned}
\Rightarrow&\frac{(1-\hat{\nu})}{(1+\hat{\nu})(1-2\hat{\nu})}\{E_s\frac{3u_{i,j}^m - 4u_{i-1,j}^m + u_{i-2,j}^m}{2\Delta x} \\
&- \sum_{k=0}^{m-1}\frac{3u_{i,j}^k - 4u_{i-1,j}^k + u_{i-2,j}^k}{2\Delta x}[E_s(\phi^m-\phi^{k+1}) - E_s(\phi^m-\phi^k)]\} \\
&+ \frac{\hat{\nu}}{(1+\hat{\nu})(1-2\hat{\nu})}\{E_s\frac{v_{i,j+1}^m - v_{i,j-1}^m}{2\Delta y} \\
&- \sum_{k=0}^{m-1}\frac{v_{i,j+1}^k - v_{i,j-1}^k}{2\Delta y}[E_s(\phi^m-\phi^{k+1}) - E_s(\phi^m-\phi^k)]\} \\
&- \frac{1}{(1-2\hat{\nu})}\{E_s(\alpha\theta^m+\beta c^m) - \sum_{k=0}^{m-1}(\alpha\theta^k+\beta c^k)[E_s(\phi^m-\phi^{k+1}) - E_s(\phi^m-\phi^k)]\} = 0
\end{aligned} \quad (3.38)$$

Along the edge EF, $\sigma_{yy} = 0$ transforms as follows:

$$\begin{aligned}
&\frac{(1-\hat{\nu})}{(1+\hat{\nu})(1-2\hat{\nu})}(E_s v,_y^m - \sum_{k=0}^{m-1} v,_y^k[E_s(\phi^m-\phi^{k+1}) - E_s(\phi^m-\phi^k)]) \\
&+ \frac{\hat{\nu}}{(1+\hat{\nu})(1-2\hat{\nu})}(E_s u_x^m - \sum_{k=0}^{m-1} u,_x^k[E_s(\phi^m-\phi^{k+1}) - E_s(\phi^m-\phi^k)]) \\
&- \frac{1}{(1-2\hat{\nu})}\{E_s(\alpha\theta^m+\beta c^m) - \sum_{k=0}^{m-1}(\alpha\theta^k+\beta c^k)[E_s(\phi^m-\phi^{k+1}) - E_s(\phi^m-\phi^k)]\} = 0 \quad (3.39)
\end{aligned}$$

$$\begin{aligned}
\Rightarrow &\frac{(1-\hat{\nu})}{(1+\hat{\nu})(1-2\hat{\nu})}\{E_s\frac{-3v_{i,j}^m+4v_{i,j+1}^m-v_{i,j+2}^m}{2\Delta y} \\
&-\sum_{k=0}^{m-1}\frac{-3v_{i,j}^k+4v_{i,j+1}^k-v_{i,j+2}^k}{2\Delta y}[E_s(\phi^m-\phi^{k+1})-E_s(\phi^m-\phi^k)]\} \\
&+\frac{\hat{\nu}}{(1+\hat{\nu})(1-2\hat{\nu})}\{E_s\frac{u_{i+1,j}^m-u_{i-1,j}^m}{2\Delta x} \\
&-\sum_{k=0}^{m-1}\frac{u_{i+1,j}^k-u_{i-1,j}^k}{2\Delta x}[E_s(\phi^m-\phi^{k+1})-E_s(\phi^m-\phi^k)]\} \\
&-\frac{1}{(1-2\hat{\nu})}\{E_s(\alpha\theta^m+\beta c^m)-\sum_{k=0}^{m-1}(\alpha\theta^k+\beta c^k)[E_s(\phi^m-\phi^{k+1})-E_s(\phi^m-\phi^k)]\}=0
\end{aligned} \tag{3.40}$$

Along the edge DF, $\sigma_{xy}=0$ transforms as follows:

$$\begin{aligned}
&\frac{1}{2(1+\hat{\nu})}\{E_s(u,_y^m+v,_x^m)-\sum_{k=0}^{m-1}(u,_y^k+v,_x^k)[E_s(\phi^m-\phi^{k+1})-E_s(\phi^m-\phi^k)]\}=0 \\
\Rightarrow &\frac{1}{2(1+\hat{\nu})}\{E_s(\frac{u_{i,j+1}^m-u_{i,j-1}^m}{2\Delta y}+\frac{3v_{i,j}^m-4v_{i-1,j}^m+v_{i-2,j}^m}{2\Delta x}) \\
&-\sum_{k=0}^{m-1}(\frac{u_{i,j+1}^k-u_{i,j-1}^k}{2\Delta y}+\frac{3v_{i,j}^k-4v_{i-1,j}^k+v_{i-2,j}^k}{2\Delta x})[E_s(\phi^m-\phi^{k+1})-E_s(\phi^m-\phi^k)]\}=0
\end{aligned} \tag{3.41}$$

Along the edge EF, $\sigma_{xy}=0$ transforms as follows:

$$\begin{aligned}
&\frac{1}{2(1+\hat{\nu})}\{E_s(u,_y^m+v,_x^m)-\sum_{k=0}^{m-1}(u,_y^k+v,_x^k)[E_s(\phi^m-\phi^{k+1})-E_s(\phi^m-\phi^k)]\}=0 \\
\Rightarrow &\frac{1}{2(1+\hat{\nu})}\{E_s(\frac{-3u_{i,j}^m+4u_{i,j+1}^m-u_{i,j+2}^m}{2\Delta y}+\frac{v_{i+1,j}^m-v_{i-1,j}^m}{2\Delta x}) \\
&-\sum_{k=0}^{m-1}(\frac{-3u_{i,j}^k+4u_{i,j+1}^k-u_{i,j+2}^k}{2\Delta y}+\frac{v_{i+1,j}^k-v_{i-1,j}^k}{2\Delta x})[E_s(\phi^m-\phi^{k+1})-E_s(\phi^m-\phi^k)]\}=0
\end{aligned} \tag{3.42}$$

2. Finite Difference Formulation of Field Equations for Piezoelectric Material

The field equations ((2.113), (2.114)) for the PZT layer were summarized in previous section. Since, the PZT layer is a transversely isotropic material poled along y-axis, the number of independent coefficients on the elastic modulus tensor is 5 and can be noted from page 93. In the context of plane strain deformation, the stress components σ_{xx}, σ_{xy} and σ_{yy} in PZT layer are as follows:

$$\sigma_{xx} = c_{11}u_{,x} + c_{12}v_{,y} + e_{21}\varphi_{,y} - \hat{\alpha}_1\Delta\theta \tag{3.43a}$$

$$\sigma_{xy} = c_{66}(u_{,y} + v_{,x}) + e_{16}\varphi_{,x} \tag{3.43b}$$

$$\sigma_{yy} = c_{21}u_{,x} + c_{22}v_{,y} + e_{22}\varphi_{,y} - \hat{\alpha}_2\Delta\theta \tag{3.43c}$$

The electric displacement component equations are as follows:

$$D_x = e_{16}(u_{,y} + v_{,x}) - \varepsilon_{11}\varphi_{,x} \tag{3.44a}$$

$$D_y = e_{21}u_{,x} + e_{22}v_{,y} - \varepsilon_{22}\varphi_{,y} \tag{3.44b}$$

The equilibrium condition (Eq. (2.116)) results in the following equations:

$$\sigma_{xx,x} + \sigma_{xy,y} = 0$$

$$\Rightarrow c_{11}u_{,xx} + c_{66}u_{,yy} + (c_{12} + c_{66})v_{,xy} + (e_{16} + e_{21})\varphi_{,xy} = 0 \tag{3.45a}$$

$$\sigma_{xy,x} + \sigma_{yy,y} = 0$$

$$\Rightarrow c_{66}v_{,xx} + c_{22}v_{,yy} + (c_{21} + c_{66})u_{,xy} + e_{16}\varphi_{,x}x + e_{22}\varphi_{,y}y - \hat{\alpha}_1\Delta\theta_{,y} = 0 \tag{3.45b}$$

$$D_{xx} + D_{yy} = 0$$

$$\Rightarrow e_{16}v_{,xx} + e_{22}v_{,yy} + (e_{21} + e_{16})u_{,xy} - \varepsilon_{11}\varphi_{,xx} - \varepsilon_{22}\varphi_{,yy} = 0 \tag{3.45c}$$

The finite difference equations of the field equations Eq. (3.45c) are as follows:

$$\begin{aligned} & c_{11}\frac{u_{i+1,j}-2u_{i,j}+u_{i-1,j}}{2\Delta x^2}+c_{66}\frac{u_{i,j+1}-2u_{i,j}+u_{i,j-1}}{2\Delta y^2} \\ & +(c_{12}+c_{66})\frac{v_{i+1,j+1}+v_{i-1,j-1}-v_{i+1,j-1}-v_{i-1,j+1}}{4\Delta x\Delta y} \\ & +(e_{16}+e_{21})\frac{\varphi_{i+1,j+1}+\varphi_{i-1,j-1}-\varphi_{i+1,j-1}-\varphi_{i-1,j+1}}{4\Delta x\Delta y}=0 \end{aligned} \tag{3.46}$$

$$\begin{aligned} & c_{66}\frac{v_{i+1,j}-2v_{i,j}+v_{i-1,j}}{2\Delta x^2}+c_{22}\frac{v_{i,j+1}-2v_{i,j}+v_{i,j-1}}{2\Delta y^2} \\ & +(c_{21}+c_{66})\frac{u_{i+1,j+1}+u_{i-1,j-1}-u_{i+1,j-1}-u_{i-1,j+1}}{4\Delta x\Delta y} \\ & +e_{16}\frac{\varphi_{i+1,j}-2\varphi_{i,j}+\varphi_{i-1,j}}{2\Delta x^2}+e_{22}\frac{\varphi_{i,j+1}-2\varphi_{i,j}+\varphi_{i,j-1}}{2\Delta y^2}-\hat{\alpha}_1\frac{\theta_{i,j+1}-\theta_{i,j-1}}{2\Delta y}=0 \end{aligned} \tag{3.47}$$

$$\begin{aligned} & e_{16}\frac{v_{i+1,j}-2v_{i,j}+v_{i-1,j}}{2\Delta x^2}+e_{22}\frac{v_{i,j+1}-2v_{i,j}+v_{i,j-1}}{2\Delta y^2} \\ & +(e_{21}+e_{16})\frac{u_{i+1,j+1}+u_{i-1,j-1}-u_{i+1,j-1}-u_{i-1,j+1}}{4\Delta x\Delta y} \\ & -\varepsilon_{11}\frac{\varphi_{i+1,j}-2\varphi_{i,j}+\varphi_{i-1,j}}{2\Delta x^2}-\varepsilon_{22}\frac{\varphi_{i,j+1}-2\varphi_{i,j}+\varphi_{i,j-1}}{2\Delta y^2}=0 \end{aligned} \tag{3.48}$$

The boundary conditions for the PZT material in finite difference formulation are as follows:

$$\begin{aligned} & \text{Along the egde BD} \quad \sigma_{xx}=0 \\ & \Rightarrow c_{11}\frac{u_{i+1,j}-u_{i-1,j}}{2\Delta x}+c_{12}\frac{3v_{i,j}-4v_{i,j-1}+v_{i,j-2}}{2\Delta y} \\ & +e_{21}\frac{3\varphi_{i,j}-4\varphi_{i,j-1}+\varphi_{i,j-2}}{2\Delta y}-\hat{\alpha}_1\Delta\theta=0 \\ & \text{Along the edge AB} \quad \sigma_{yy}=0 \\ & \Rightarrow c_{21}\frac{3u_{i,j}-4u_{i-1,j}+u_{i-2,j}}{2\Delta x}+c_{22}\frac{v_{i,j+1}-v_{i,j-1}}{2\Delta y}+e_{22}\frac{\varphi_{i,j+1}-\varphi_{i,j-1}}{2\Delta y}-\hat{\alpha}_2\Delta\theta=0 \end{aligned} \tag{3.49}$$

Along the edge AB $\sigma_{xy} = 0$

$$\Rightarrow c_{66}(\frac{3u_{i,j} - 4u_{i,j-1} + u_{i,j-2}}{2\Delta y} + \frac{v_{i+1,j} - v_{i-1,j}}{2\Delta x}) + e_{16}\frac{\varphi_{i+1,j} - \varphi_{i-1,j}}{2\Delta x} = 0$$

Along the edge BD $\sigma_{xy} = 0$

$$\Rightarrow c_{66}(\frac{u_{i,j+1} - u_{i,j-1}}{2\Delta y} + \frac{3v_{i,j} - 4v_{i-1,j} + v_{i-2,j}}{2\Delta x}) + e_{16}\frac{3\varphi_{i,j} - 4\varphi_{i-1,j} + \varphi_{i-2,j}}{2\Delta x} = 0 \qquad (3.50)$$

Along the boundary CD, we require the displacement and the traction to be continuous. The traction continuity results in the following equations.

$$\begin{aligned}
&\sigma^e_{yy} = \sigma^p_{yy} \\
&\Rightarrow \frac{(1-\hat{\nu})}{(1+\hat{\nu})(1-2\hat{\nu})}\{E_s\frac{u^m_{i+1,j} - u^m_{i-1,j}}{2\Delta x} - \sum_{k=0}^{m-1}\frac{u^k_{i+1,j} - u^k_{i-1,j}}{2\Delta x}[E_s(\phi^m - \phi^{k+1}) - E_s(\phi^m - \phi^k)]\} \\
&\quad + \frac{\hat{\nu}}{(1+\hat{\nu})(1-2\hat{\nu})}\{E_s\frac{3v^m_{i,j} - 4v^m_{i,j-1} + v^m_{i,j-2}}{2\Delta y} \\
&\quad - \sum_{k=0}^{m-1}\frac{3v^k_{i,j} - 4v^k_{i,j-1} + v^k_{i,j-2}}{2\Delta y}[E_s(\phi^m - \phi^{k+1}) - E_s(\phi^m - \phi^k)]\} \\
&\quad - \frac{1}{(1-2\hat{\nu})}\{E_s(\alpha\theta^m + \beta c^m) - \sum_{k=0}^{m-1}(\alpha\theta^k + \beta c^k)[E_s(\phi^m - \phi^{k+1}) - E_s(\phi^m - \phi^k)]\} \\
&\qquad = c_{11}\frac{u_{i+1,j} - u_{i-1,j}}{2\Delta x} + c_{12}\frac{-3v_{i,j} + 4v_{i,j+1} - v_{i,j+2}}{2\Delta y} \\
&\quad + e_{21}\frac{-3\varphi_{i,j} + 4\varphi_{i,j+1} - \varphi_{i,j+2}}{2\Delta y} - \hat{\alpha}_1\Delta\theta
\end{aligned} \qquad (3.51)$$

$$\begin{aligned}
&\sigma^e_{xy} = \sigma^p_{xy} \\
&\Rightarrow \frac{1}{2(1+\hat{\nu})}\{E_s(\frac{3u^m_{i,j} - 4u^m_{i,j-1} + u^m_{i,j-2}}{2\Delta y} + \frac{v^m_{i+1,j} - v^m_{i-1,j}}{2\Delta x}) \\
&\quad - \sum_{k=0}^{m-1}(\frac{3u^k_{i,j} - 4u^k_{i,j-1} + u^k_{i,j-2}}{2\Delta y} + \frac{v^k_{i+1,j} - v^k_{i-1,j}}{2\Delta x})[E_s(\phi^m - \phi^{k+1}) - E_s(\phi^m - \phi^k)]\} \\
&\qquad = c_{66}(\frac{-3u_{i,j} + 4u_{i,j+1} - u_{i,j+2}}{2\Delta y} + \frac{v_{i+1,j} - v_{i-1,j}}{2\Delta x}) + e_{16}\frac{\varphi_{i+1,j} - \varphi_{i-1,j}}{2\Delta x}
\end{aligned} \qquad (3.52)$$

σ^e_{yy}, σ^e_{xy} denote transverse and shear stresses in the elastic/viscoelastic portion of the beam.

σ^p_{yy}, σ^p_{xy} denote transverse and shear stresses in the piezoelectric layer of the beam.

Using the equations (3.36), (3.40), (3.41), (3.42), (3.46), (3.47) to (3.52) we form a set of linear equations with $(u^k_{i,j}, v^k_{i,j}, \varphi)$ as independent variables where $1 \leq i \leq M$, $i \leq j \leq N$ and $0 \leq k \leq m$. By solving these equations we obtain the displacement field. The axial, transverse and shear stress fields can then be evaluated from the following equations. In the PZT region, the stress fields can be calculated as follows:

$$\begin{aligned}
\sigma_{xx} &\approx c_{11}\frac{u_{i+1,j} - u_{i-1,j}}{2\Delta x} + c_{12}\frac{v_{i,j+1} - v_{i,j-1}}{2\Delta y} + e_{21}\frac{\varphi_{i,j+1} - \varphi_{i,j-1}}{2\Delta y} - \hat{\alpha}_1 \Delta\theta \\
\sigma_{yy} &\approx c_{21}\frac{u_{i+1,j} - u_{i-1,j}}{2\Delta x} + c_{22}\frac{v_{i,j+1} - v_{i,j-1}}{2\Delta y} + e_{22}\frac{\varphi_{i,j+1} - \varphi_{i,j-1}}{2\Delta y} - \hat{\alpha}_2 \Delta\theta \\
\sigma_{xy} &\approx c_{66}(\frac{u_{i,j+1} - u_{i,j-1}}{2\Delta y} + \frac{v_{i+1,j} - v_{i-1,j}}{2\Delta x}) + e_{16}\frac{\varphi_{i+1,j} - \varphi_{i-1,j}}{2\Delta x}
\end{aligned} \tag{3.53}$$

In the elastic/viscoelastic region, the stress fields can be calculated as follows:

$$\begin{aligned}
\sigma^m_{xx} \approx & \frac{(1-\hat{\nu})}{(1+\hat{\nu})(1-2\hat{\nu})}\{E_s\frac{u^m_{i+1,j} - u^m_{i-1,j}}{2\Delta x} \\
& - \sum_{k=0}^{m-1}\frac{u^k_{i+1,j} - u^k_{i-1,j}}{2\Delta x}[E_s(\phi^m - \phi^{k+1}) - E_s(\phi^m - \phi^k)]\} \\
& + \frac{\nu}{(1+\hat{\nu})(1-2\hat{\nu})}\{E_s\frac{v^m_{i,j+1} - v^m_{i,j-1}}{2\Delta y} \\
& - \sum_{k=0}^{m-1}\frac{v^k_{i,j+1} - v^k_{i,j-1}}{2\Delta y}[E_s(\phi^m - \phi^{k+1}) - E_s(\phi^m - \phi^k)]\} \\
& - \frac{1}{(1-2\hat{\nu})}\{E_s(\alpha\theta^m + \beta c^m) - \sum_{k=0}^{m-1}(\alpha\theta^k + \beta c^k)[E_s(\phi^m - \phi^{k+1}) - E_s(\phi^m - \phi^k)]\} = 0
\end{aligned} \tag{3.54}$$

$$\begin{aligned}
\sigma^m_{yy} \approx & \frac{1}{2(1+\hat{\nu})}\{E_s(\frac{u^m_{i,j+1} - u^m_{i,j-1}}{2\Delta y} + \frac{v^m_{i+1,j} - v^m_{i-1,j}}{2\Delta x}) \\
& - \sum_{k=0}^{m-1}(\frac{u^k_{i,j+1} - u^k_{i,j-1}}{2\Delta y} + \frac{v^k_{i+1,j} - v^k_{i-1,j}}{2\Delta x})[E_s(\phi^m - \phi^{k+1}) - E_s(\phi^m - \phi^k)]\}
\end{aligned} \tag{3.55}$$

$$\sigma_{xy}^m \approx \frac{1}{2(1+\hat{\nu})}\{E_s(\frac{u_{i,j+1}^m - u_{i,j-1}^m}{2\Delta y} + \frac{v_{i+1,j}^m - v_{i-1,j}^m}{2\Delta x}) \\ - \sum_{k=0}^{m-1}(\frac{u_{i,j+1}^k - u_{i,j-1}^k}{2\Delta y} + \frac{v_{i+1,j}^k - v_{i-1,j}^k}{2\Delta x})[E_s(\phi^m - \phi^{k+1}) - E_s(\phi^m - \phi^k)]\} \tag{3.56}$$

3. Convergence Study

An unreinforced epoxy-PZT 5H beam assembly is chosen as a test case for convergence study. The material modulus, CTE and CME of epoxy resin are summarized in Table 3.2. The material modulus, piezoelectric and dielectric properties of PZT 5H are summarized below. In the previous section following the parametric study, it was mentioned that the coupled heat and moisture diffusion equations shall be solved by choosing the values of u=0.1, $\lambda\nu = 0.25$, $\lambda = 0.122$. The boundary conditions to which the beam assembly is subjected to are summarized in Eq. (3.24). The grid sizes considered for convergence study are summarized in Table 3.3. With this choice of material properties and grid sizes, the finite difference equations derived in the previous section are solved simultaneously. Figure 3.18 depicts the evolution of temperature and moisture fields in the beam assembly for the above mentioned choice of the constants u, $\lambda\nu$, λ. Figures 3.19- 3.21 depict the vertical displacement of the beam, potential difference developed across PZT layer and the axial stress at a cross section taken at half length for the chosen grid size values. It can be noted from these figures that the vertical displacement per unit length, potential difference and the axial stress converge as the grid element size decreases. The tip vertical displacement, potential difference at half length for all the grid sizes are summarized in Table 3.4. It can be noted that tip vertical displacement and the potential difference values differ by less than 5% for the grid sizes mentioned in 2^{nd} and 3^{rd} rows of Table 3.4. On further decreasing the grid size, the accuracy of the results can further be improved but due the corresponding increase in the computational time and the cost involved with it, the grid size specified in the 3^{rd} row shall be considered for the current study.

Table 3.2. Summary of the properties of epoxy [1]

Elastic Modulus(GPa)	3.5
Poission's ratioν	0.25
CTE (mm/mm/^oC)α	6x10^{-5}
CME(mm/mm/% H_20)β	2x10^{-3}
Thermal Conductivity(W/m/k)	0.1
density(g/cm^3)	2.7
specific heat(J/Kg/^ok)	1300

$$\mathbf{C} = \begin{bmatrix} 126 & 84.1 & 79.5 & 0 & 0 & 0 \\ 84.1 & 117 & 84.1 & 0 & 0 & 0 \\ 79.5 & 84.1 & 126 & 0 & 0 & 0 \\ 0 & 0 & 0 & 23 & & 0 & 0 \\ 0 & 0 & 0 & 0 & 22.35 & 0 \\ 0 & 0 & 0 & 0 & 0 & 23 \end{bmatrix} \text{GPa}$$

$$\mathbf{e} = \begin{bmatrix} 0 & 0 & 0 & 0 & 0 & 17 \\ -6.5 & 23.3 & -6.5 & 0 & 0 & 0 \\ 0 & 0 & 0 & 17 & 0 & 0 \end{bmatrix} \text{Col/m}^2$$

$$\boldsymbol{\varepsilon} = \begin{bmatrix} 15.05 & 0 & 0 \\ 0 & 13.02 & 0 \\ 0 & 0 & 15.05 \end{bmatrix} \text{x}10^{-9}\text{Col/Vm}$$

$$\boldsymbol{\alpha_p} = \begin{bmatrix} 0.4658 & -0.9004 & 0.4658 \end{bmatrix} \text{x}10^{-6} \text{ mm/mm/k}$$

Table 3.3. Summary of grid sizes(mm) chosen for convergence study

ΔX	Δy_1	Δy_2
0.417	0.208	0.417
0.3125	0.125	0.3125
0.278	0.104	0.278

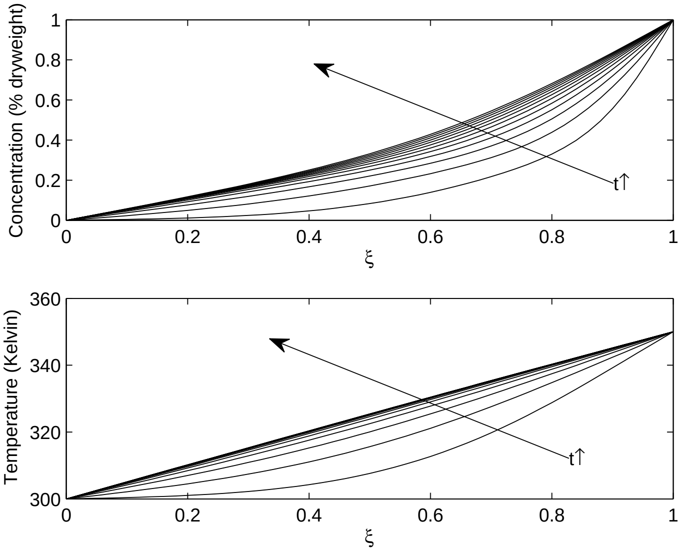

Fig. 3.18. Plot shows the evolution of moisture concentration and temperature fields in the beam assembly when û=0.1, $\lambda\nu = 0.25$, $\lambda = 0.122$. t↑ indicates evolution with time. The dimensionless time parameter $\hat{\theta}$ varies from 0 to 7x10^{-2}.

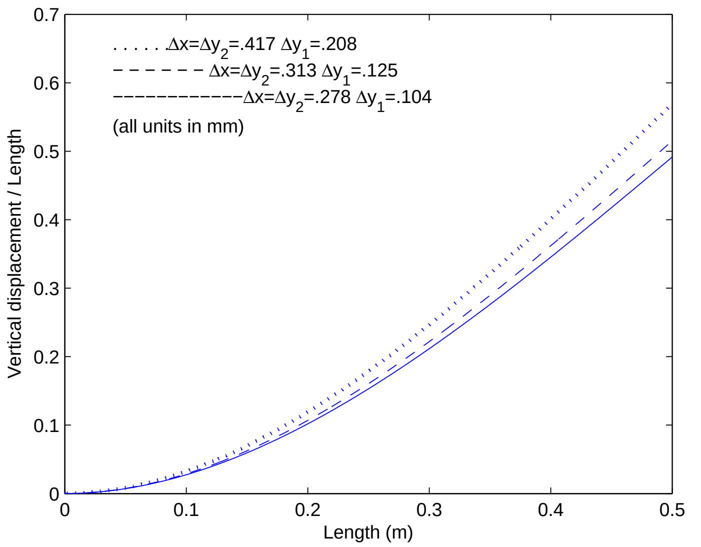

(a) Vertical displacement of the beam when $\hat{\theta} = 0.0058$

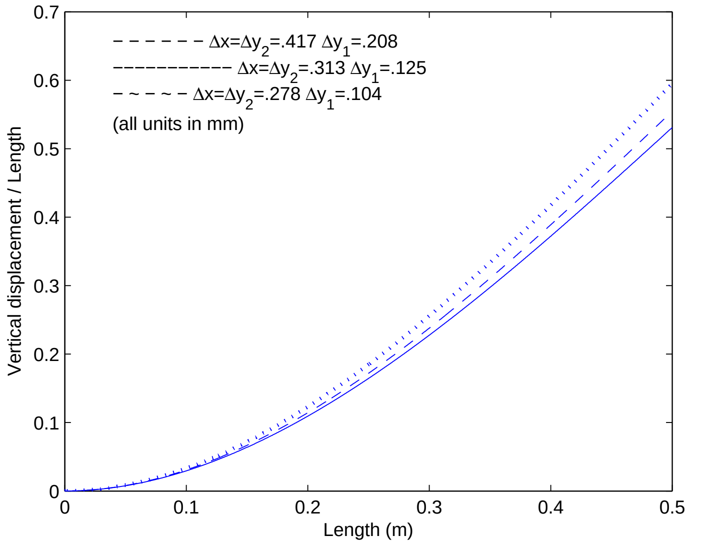

(b) Vertical displacement of the beam when $\hat{\theta} = 0.0116$

Fig. 3.19. Plot shows the vertical displacement per unit length for the grid sizes of (a)$\Delta X = 0.417$, $\Delta y_1 = 0.208$, $\Delta y_2 = 0.417$ (0− − − −) (b)ΔX=0.3125, Δy_1=0.125, Δy_2=0.3125 (——) and (c)ΔX=0.278, Δy_1=0.104, Δy_2=0.278 (- -). The plots are obtained at non-dimensional time $\hat{\theta}$ values of 0.0058 and 0.0116.

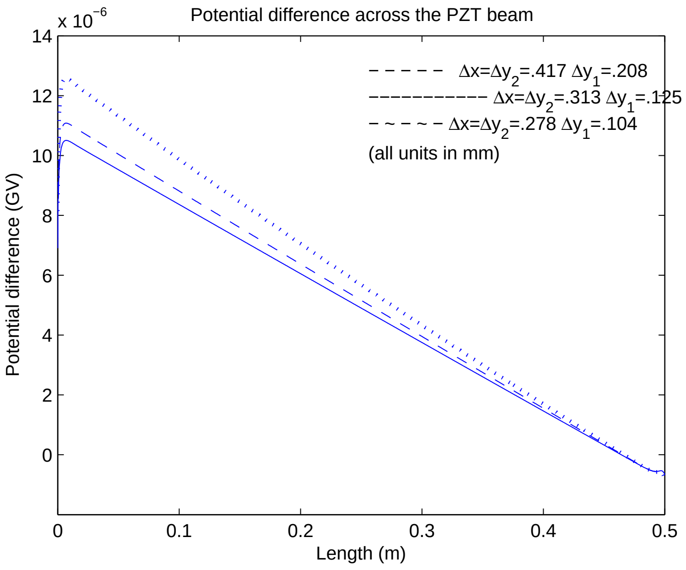

(a) Potential difference across PZT layer when $\hat{\theta} = 0.0058$

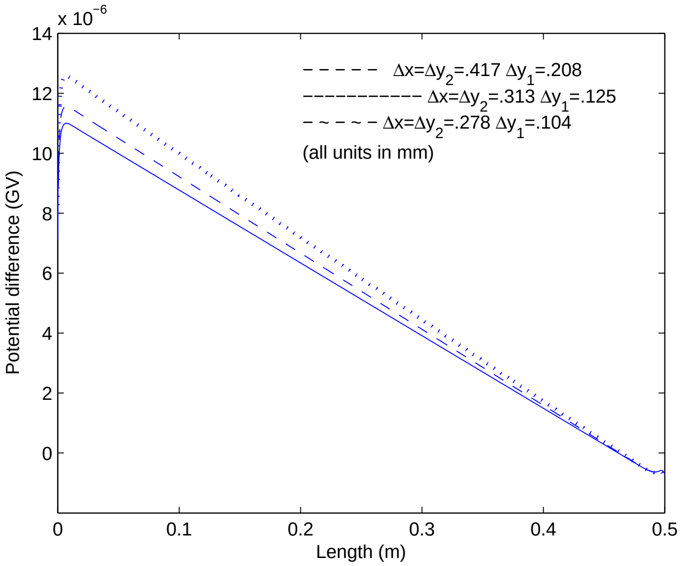

(b) Potential difference across PZT layer when $\hat{\theta} = 0.0116$

Fig. 3.20. Plot shows the potential difference across PZT 5H layer for the grid sizes of (a)$\Delta X = 0.417$, $\Delta y_1 = 0.208$, $\Delta y_2 = 0.417$ (- - - -)(b)$\Delta X = 0.3125$, $\Delta y_1 = 0.125$, $\Delta y_2 = 0.3125$ (——) and (c)$\Delta X = 0.278$, $\Delta y_1 = 0.104$, $\Delta y_2 = 0.278$ (-   -   ). The plots are obtained at non-dimensional time $\hat{\theta}$ values of 0.0058 and 0.0116.

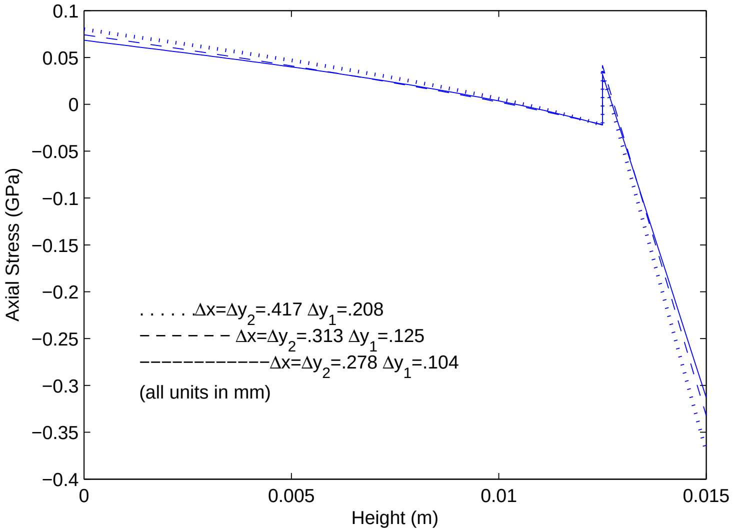

(a) Axial stress at $\hat{\theta} = 0.0058$

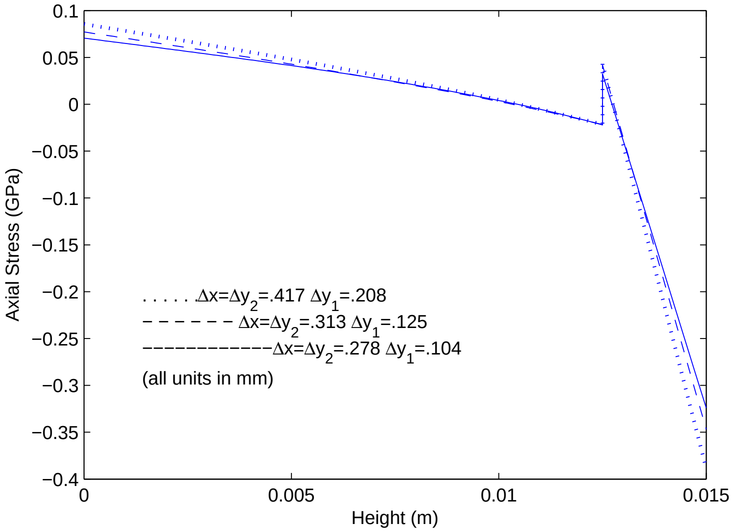

(b) Axial stress at $\hat{\theta} = 0.0116$

Fig. 3.21. Plot shows the axial stress at half length for the grid sizes of (a)$\Delta X = 0.417$, $\Delta y_1 = 0.208$, $\Delta y_2 = 0.417$ (- - - -)(b)$\Delta X = 0.3125$, $\Delta y_1 = 0.125$, $\Delta y_2 = 0.3125$ (——) and (c)$\Delta X = 0.278$, $\Delta y_1 = 0.104$, $\Delta y_2 = 0.278$ (-   -   ). The plots are obtained at non-dimensional time $\hat{\theta}$ values of 0.0058 and 0.0116.

Table 3.4. Summary of tip displacement per unit length and potential difference across PZT layer at θ=0.0058 for the grid sizes summarized in Table 3.3

ΔX	Δy_1	Δy_2	tip vertical displacement/L	Potential difference(GV)
0.417	0.208	0.417	0.575	5.75x10^{-6}
0.3125	0.125	0.3125	0.515	5.1x10^{-6}
0.278	0.104	0.278	0.495	4.9$10^{-6}$

Table 3.5. Summary of the properties of composite beam [2]

E_{11}=E_{33}(GPa)	17.2
E_{22} (Gpa)	6.9
ν_{13}	0.14
ν_{12} =ν_{32}	0.4
ν_{21}=ν_{23}	0.1558
G_{13} (GPa)	1.70
G_{12}=G_{32}	2.76
CTE (mm/mm/^oC)α_{11}=α_{33}	5.2x10^{-6}
α_{22}	21.6x10^{-6}
Thermal Conductivity(W/m/k)	0.49
density(g/cm^3)	1.717
specific heat(J/Kg/^ok)	900

Before numerically solving the cases described in Chapter I, the results predicted by the numerical method are compared with those presented in the work by Song et al. [2]. To this end, Figure 3.22(a) depicting the geometry used by Song et al. is slightly modified for simplicity as depicted in Figure 3.22(b). The properties of the elastic layer are summarized in Table 3.5. The properties of PZT from page 93 are used for study.

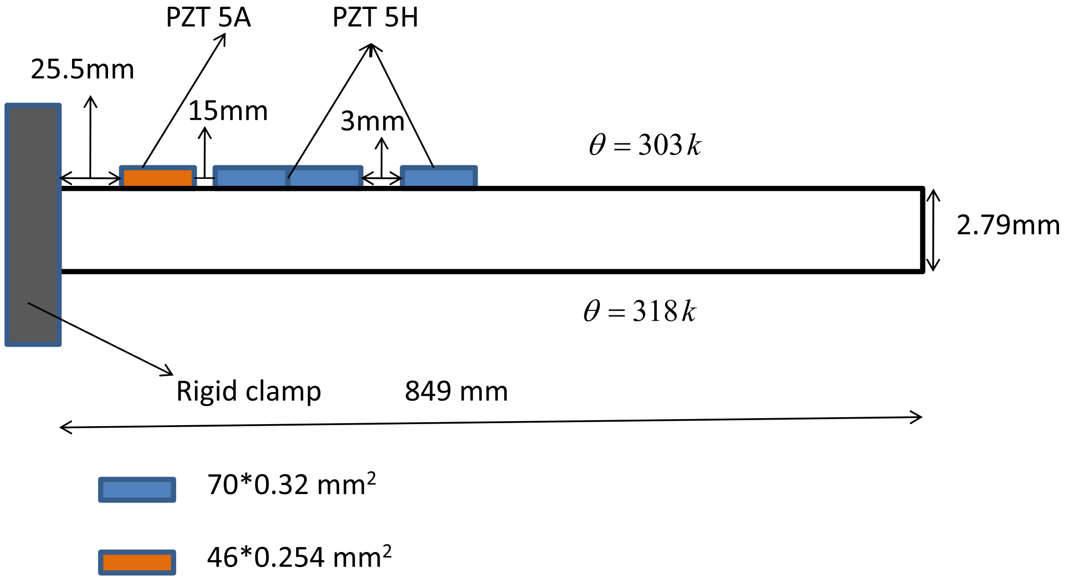

(a) Composite beam with 3 PZT 5H actuators and one PZT 5A sensor

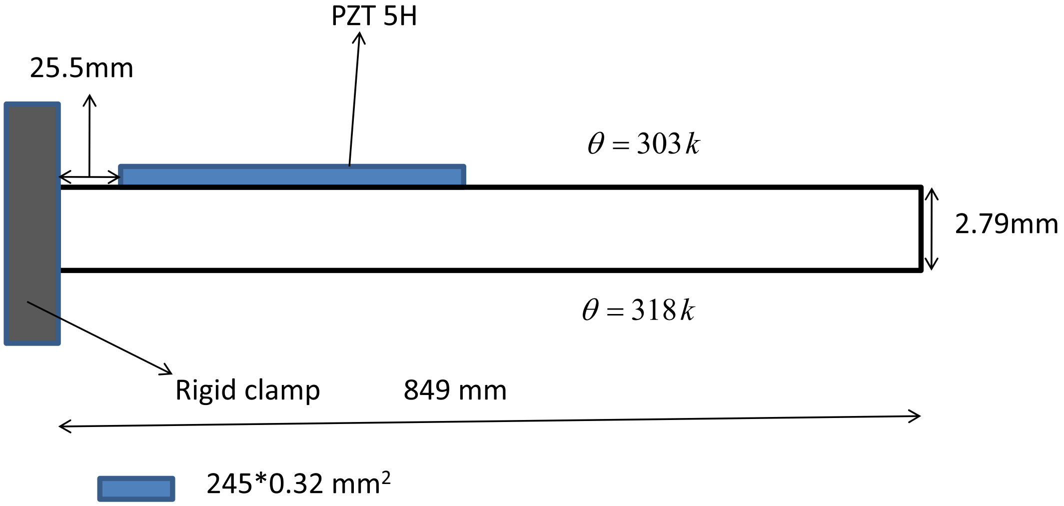

(b) Composite beam with PZT 5H surface bonded actuator

Fig. 3.22. Plot (a) illustrates the geometry used by Song et al. Plot (b) depicts the modified geometry used in the current study.

Table 3.6. Table summarizes the grid sizes considered for convergence study.

Δx	Δ y_1	Δy_2
0.3317	0.35	0.16
0.849	0.35	0.16

Both the geometries in Figure 3.22 are subjected to same boundary conditions. The top surface containing PZT actuators is maintained at 303 k and the bottom surface is maintained at 318 k. The temperature in the composite beam is assumed to in a steady state. Figure 3.23 depicts vertical displacement in the unactuated beam for various gird sizes. To solve the problem numerically the grid sizes in the second row of Table 3.6 are used. Figure 3.24 depicts the plot of vertical displacement of the beam in actuated and unactuated states. It also compares the unactuated vertical displacement of the beam with those reported by Song et al. in [2]. It can be seen that there is a good agreement between both the results. The voltage required to actuate the beam is 45V as compared to 150V required for the geometry considered by Song et al. in [2]. The difference in the magnitudes in the voltages can be attributed to the fact that in the modified geometry, the overall length of actuator is more than that in the original geometry. Also, in the geometry assumed by Song et al. part of the actuation is performed by PZT 5A actuator which is weaker than PZT 5H for actuation purposes. This justifies why lesser voltage is required in the former case. The tip displacement is 11.46 mm in the case with modified geometry as compared to 11 mm in [2]. Thus there is a good agreement between both the values. It is observed that the displacement is suppressed more in the region where PZT actuators are employed as observed in Figure 3.24.

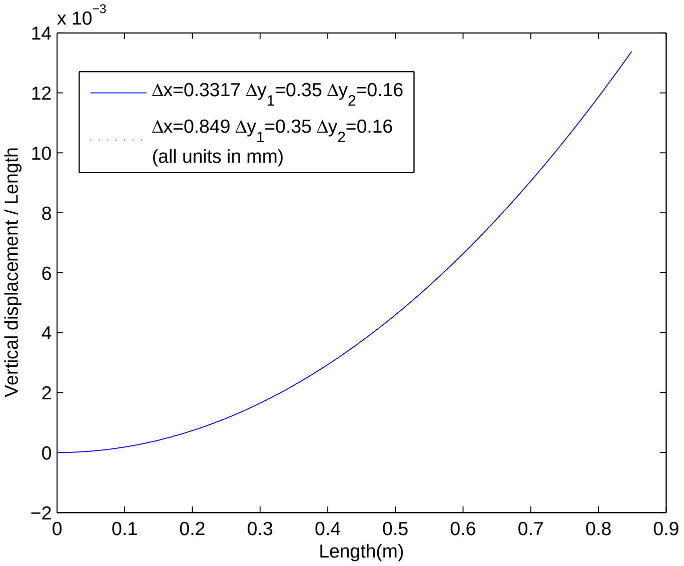

Fig. 3.23. Plot depicts the convergence of the vertical displacement of the beam for various grid sizes.

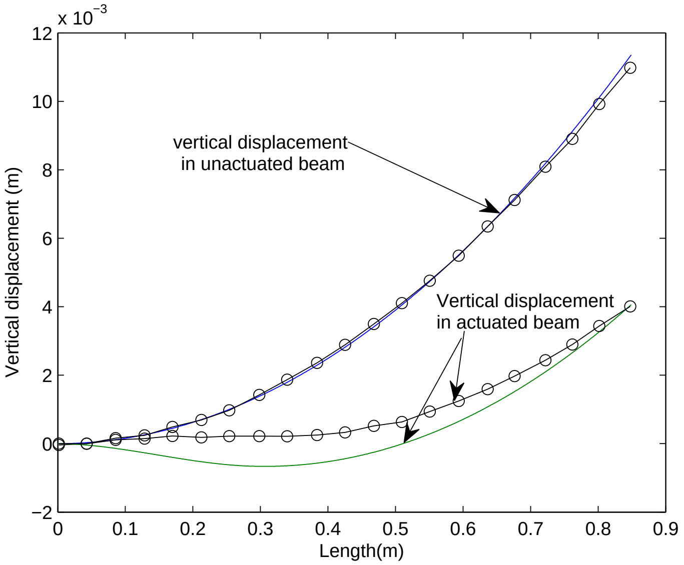

Fig. 3.24. Plot depicts the vertical displacement of the beam in actuated and unactuated states. Curves highlighted by ('o') depict the vertical displacement reported by Song et al. [2].

D. Numerical Solutions to the Cases Considered for Study

In this section, the finite difference equations presented in the earlier subsection are solved numerically with the appropriate boundary conditions for the various materials considered for the study. The cases considered for study are summarized as follows:

- Linearly elastic materials:
    1. Aluminium-PZT 5H beam assembly subjected to transient thermal field.[2]
    2. Isotropic un-reinforced epoxy-PZT beam assembly subjected to transient thermal and moisture fields.
    3. Anisotropic CFRP-PZT beam assembly subjected to transient thermal and moisture fields.
- Linearly viscoelastic material-PZT beam assembly subjected to transient thermal and moisture fields.

1. Aluminium-PZT Beam Assembly Subjected to Transient Thermal Load

The first case considered for study is an aluminium beam of the following dimensions; Length (L)=0.5m, thickness (h_1)=0.0125m. PZT 5H layer of same length but with thickness(h_2)=.0025m is perfectly bonded to the Al beam. The PZT 5H layer is assumed to be poled along direction-2 as shown in Figure 3.1. The material properties of Al are summarized below in Table 3.7. The properties of PZT 5H summarized following Table 3.7 are taken from [28]. The CTE of PZT 5H is denoted by $\boldsymbol{\alpha_p}$. The CME for Al is chosen to be zero because of the negligible moisture absorbability of Al. The boundary conditions of the beam assembly are specified in Eq. (3.24). Figure 3.25 shows the evolution of temperature in the Al layer with time.

---

[2] The moisture dependent deformation of Al is not considered for the moisture diffusion in Aluminium is negligible compared to the diffusion of heat.

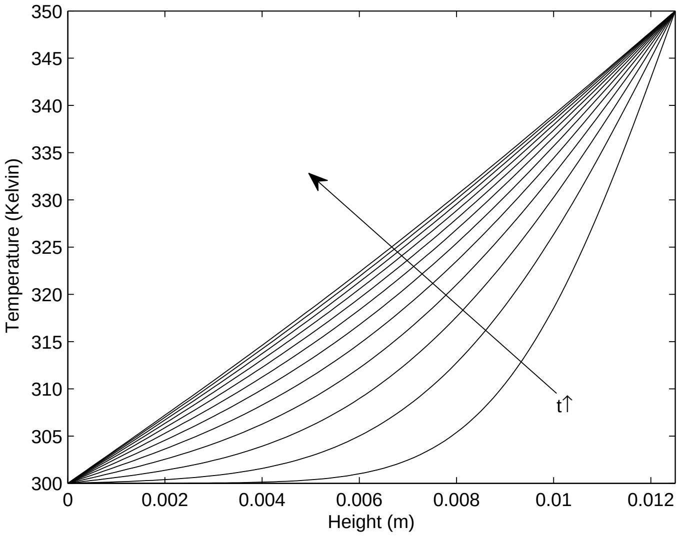

Fig. 3.25. Plot shows the evolution of temperature in the Al layer with time. The non-dimensionalised time parameter $\hat{\theta}$ varies from 0 to 3x10^{-7}. t↑ indicates evolution of displacement with time.

Table 3.7. Summary of the properties of Al [3]

Elastic Modulus(GPa)	70
Poission's ratioν	0.3462
CTE (mm/mm/^oC)α	2.3x10^{-5}
CME(mm/mm/% H_20)β	0
Thermal Conductivity(W/m/k)	200
density(g/cm^3)	2.7
specific heat(J/Kg/^ok)	913

$$\mathbf{C} = \begin{bmatrix} 126 & 84.1 & 79.5 & 0 & 0 & 0 \\ 84.1 & 117 & 84.1 & 0 & 0 & 0 \\ 79.5 & 84.1 & 126 & 0 & 0 & 0 \\ 0 & 0 & 23 & & 0 & 0 \\ 0 & 0 & 0 & 0 & 22.35 & 0 \\ 0 & 0 & 0 & 0 & 0 & 23 \end{bmatrix} \text{GPa}$$

$$\mathbf{e} = \begin{bmatrix} 0 & 0 & 0 & 0 & 0 & 17 \\ -6.5 & 23.3 & -6.5 & 0 & 0 & 0 \\ 0 & 0 & 0 & 17 & 0 & 0 \end{bmatrix} \text{Col/m}^2$$

$$\boldsymbol{\varepsilon} = \begin{bmatrix} 15.05 & 0 & 0 \\ 0 & 13.02 & 0 \\ 0 & 0 & 15.05 \end{bmatrix} \text{x}10^{-9}\text{Col/Vm}$$

$$\boldsymbol{\alpha_p} = \begin{bmatrix} 0.4658 & -0.9004 & 0.4658 \end{bmatrix} \text{x}10^{-6} \text{ mm/mm/k [10]}$$

The system of equations governing the deformation of the beam assembly are converted to the appropriate finite difference equations as presented in Chapter II. The following are the mesh sizes used for solving the system numerically. Along the length span 1800 elements with a grid size of 0.278mm are chosen. Along the height 120 elements each of size 0.104mm are chosen for the Al-layer. Along the height of PZT 5H layer, 9 elements each of size 0.278mm are chosen for study. The vertical displacement of the composite beam, under the influence of thermal load is depicted in Figure 3.26(a). It can be noted that the tip displacement increases of the beam with time. This can be explained as follows. The Al layer has a greater CTE compared to PZT 5H layer. Hence, when the beam assembly is subjected to a uniform temperature increase, Al layer is strained more than the PZT 5H layer. This results in the total beam assembly bending with a curvature towards the PZT 5H layer side. But in the current case, the temperature is non-uniform in the Al layer. From Figure 3.1, it is noted that the temperature is lower at the lower section of Al layer and increases along the thickness direction. Thus thermal strains increase as we move along the thickness direction. This causes the beam to bend towards the surface maintained at lower temperature, i.e with a curvature towards the Al layer side. The net displacement is the resultant of these two counter-acting phenomena. As temperature evolves in the Al layer, the curvature due to bending caused due to the temperature gradient in the Al layer decreases to reach a steady state value. As a result, effect of the bending caused due to the difference in CTE between the two layers increases with time. As a result, the curvature of the beam towards the PZT 5H layer side increases with time which can be noted in Figure 3.26(a). Figure 3.26(b) compares the vertical displacement with and with out the external actuation being applied across PZT 5H layer. It can be noted that the displacement in the latter case has been subdued to a great extent.

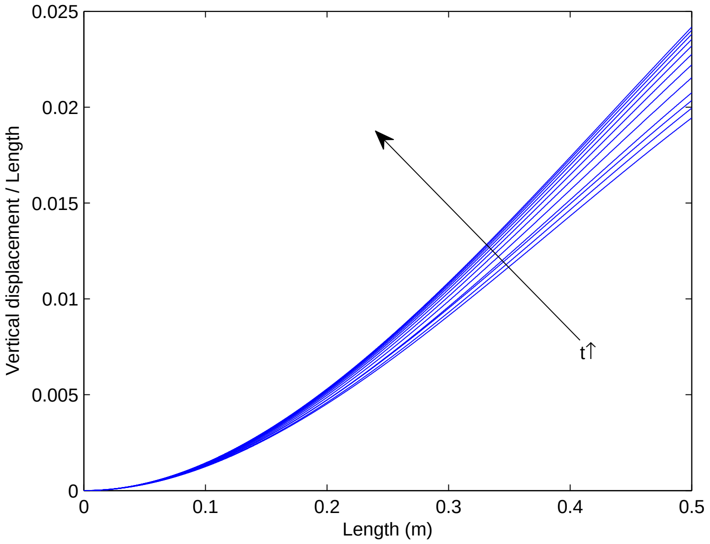

(a) Non-dimensionalized vertical displacement under no external actuation

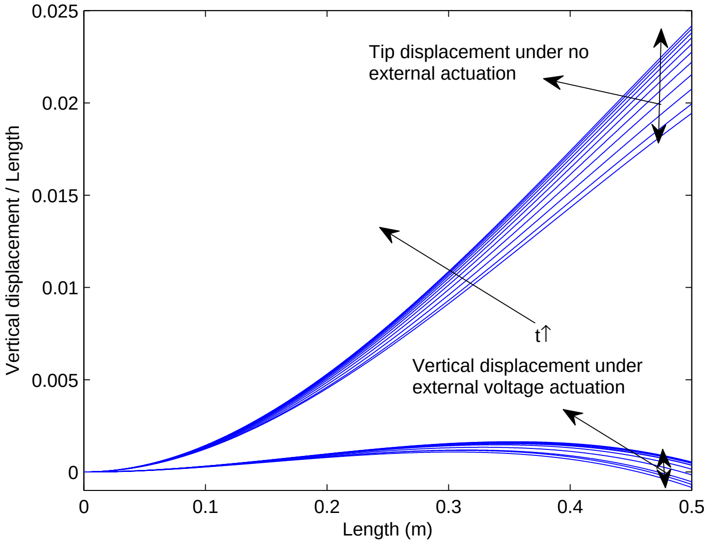

(b) Non-dimensionalized vertical displacement under external voltage

Fig. 3.26. Plots show the evolution of vertical displacement of the Al-PZT beam assembly due to temperature chages when (a)no external voltage is applied across PZT 5H layer (b) external voltage is applied across PZT 5H layer. t↑ indicates evolution of displacement with time.

The Figure 3.27(a) depicts the evolution of axial stress with time at half-length of the beam assembly. It can be noted that at the Al-PZT 5H boundary, the axial stress is discontinuous, as expected. Due to the bending of the beam towards the PZT 5H layer, it can be noted that the axial stresses become more compressive in the Al layer as we move from the bottom surface to the common interface between the two layers. The stresses becoming increasingly tensile with time at the bottom most layer of the beam due to increased bending of the beam assembly with time. The Figure 3.27(b) depicts the axial stress at the half length with of the beam assembly under the effect of actuating voltage. It can be noted that the axial stress is significantly reduced in the presence of actuating voltage.

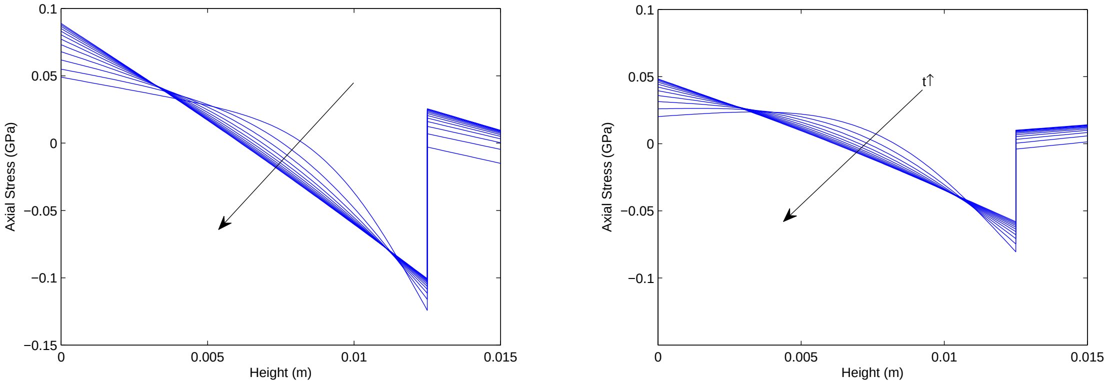

(a) Axial stress at mid section under no external voltage

(b) Axial stress at mid section under external voltage

Fig. 3.27. Plots show the evolution of axial stress σ_{xx} in the Al-PZT beam assembly due to temperature changes when (a)no external voltage is applied across PZT 5H layer (b) external voltage is applied across PZT 5H layer. Arrow indicates evolution of displacement with time.

Figures 3.28(a) and (3.28(b) depict the evolution of shear stress with time, at half-length of the beam assembly in the presence of (a)only thermal load and (b)both thermal load and external actuating voltage, respectively. As expected, the shear stress is continuous at the Al-PZT 5H boundary. It can be noted that the material discontinuity at the Al-PZT 5H boundary, is reflected in the form of a kink in the shear plot at the common boundary. The shear stress is considerably reduced due to the application of external actuating mechanism as shown in Figure 3.28(b).

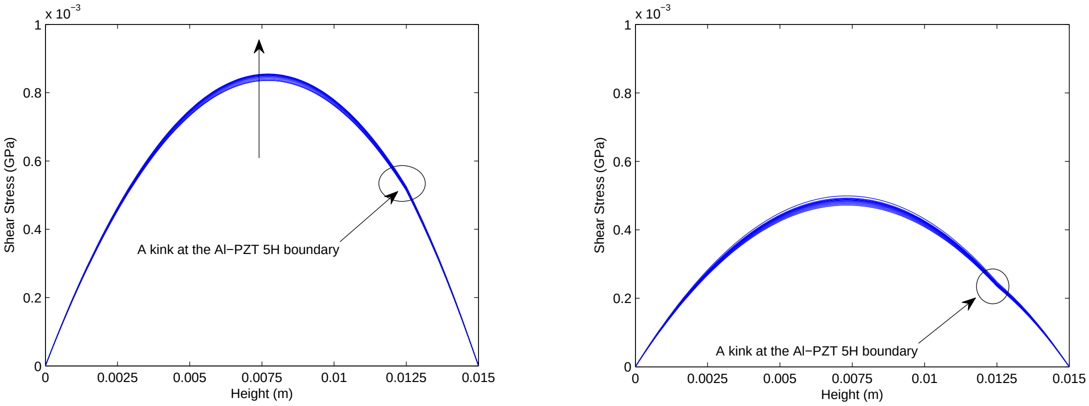

(a) Shear stress at mid section due to temperature changes

(b) Shear stress at mid section due to temperature changes and external actuating voltage

Fig. 3.28. Plots show the evolution of shear stress σ_{xy} in the Al-PZT beam assembly due to temperature changes when (a)no external voltage is applied across PZT 5H layer (b) external voltage is applied across PZT 5H layer. t↑ indicates evolution of displacement with time.

Figures 3.29(a) and 3.29(b) depict the evolution of the electric field and voltage induced across the PZT 5H layer respectively, when the beam assembly is under transient thermal load. It can be noted from the figure that both the electric field and the potential difference vary significantly along the length. Figure 3.30(a) represents the required actuating voltage to minimize the bending of the beam assembly subjected to the given loading conditions. It can be noted that the voltage required for deformation control increases linearly with time. This trend can be explained in terms of the increasing tip displacement with time as shown in Figure 3.26(a). More the tip displacement in unactuated beam, more the external voltage necessary to minimize it. Figure 3.30(b) depicts the electric field developed across the PZT 5H layer when an external actuating voltage is applied across it. It can be noted that the electric field so induced increases with time due to the increase in the required external voltage to minimize the bending of the beam. In practice, electric fields of the order of 1 MV/m in a piezoelectric material lead the system to the verge of non-linearity, in which the case the the problem needs to be addressed in terms of a non-linear theory. Crawley et al. [7] experimentally proved that when G 1195 PZT material is subjected to electric fields of the order of 1MV/m, the induced strain and the applied electric field cannot be related linearly[3]. However, the current study is focussed to analyze the problem in the context of a linearized theory, for simplicity. Therefore, no attempt will be made to incorporate any such non-linear effects.

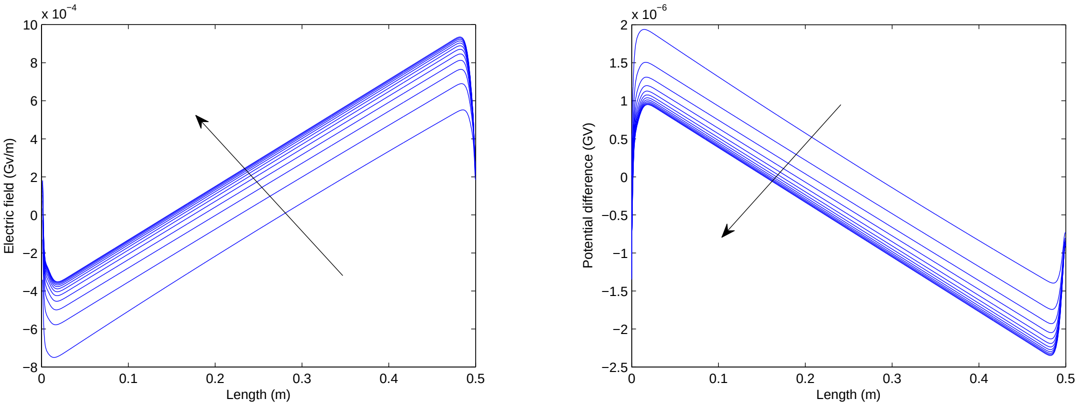

(a) Electric field induced across PZT 5H layer

(b) Potential difference induced across PZT 5H layer

Fig. 3.29. Plots show the evolution of (a)the induced electric field **E** and (b)the induced potential difference across the Al-PZT beam assembly due to temperature changes. t↑ indicates evolution of displacement with time.

---

[3] A prolonged exposure to electric fields of magnitude $>$ 1MV/m might result in the excessive heating up of the piezoelectric material resulting in an eventual loss of piezoelectric properties/failure of the material.

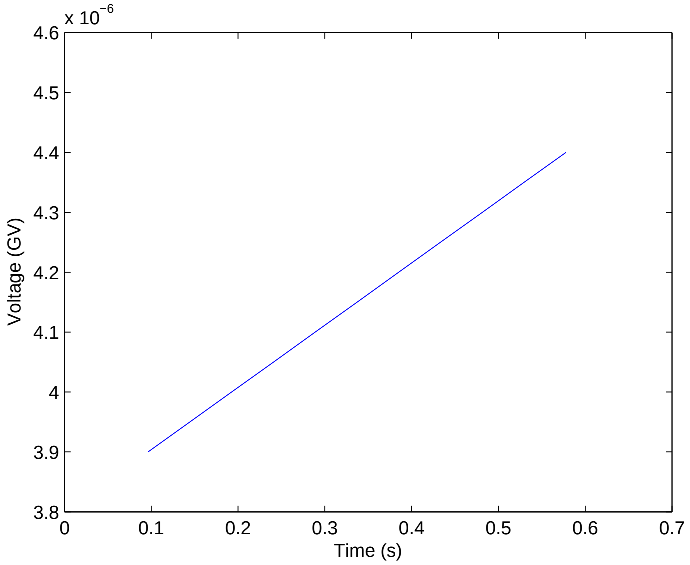

(a) Actuating voltage required across PZT 5H with time

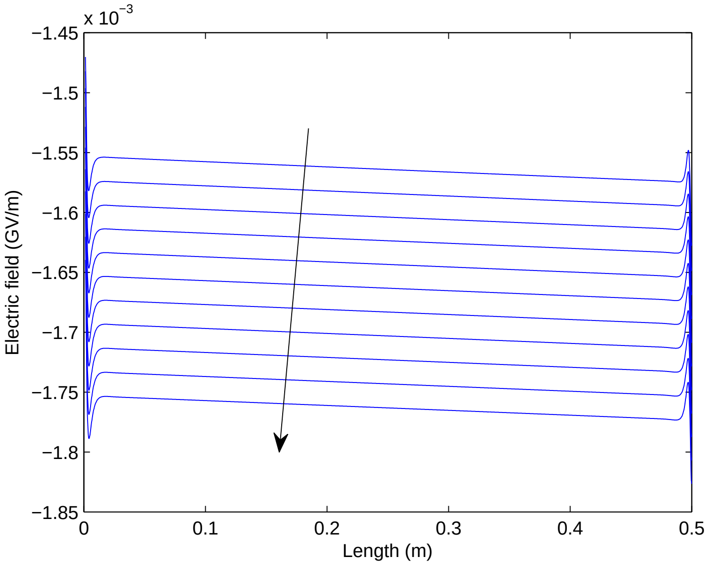

(b) Electric field induced across PZT 5H with time

Fig. 3.30. Plots show the (a)external actuating voltage required with time,to be applied across PZT 5H layer to minimize the bending of the Al-PZT beam subjected to changes in temperature. (b) depicts the evolution of the induced electric field(**E**) across the PZT 5H layer under the effect of an external actuating shown in. t↑ indicates evolution of displacement with time.

2. Epoxy-PZT 5H Beam Subjected to Transient Thermal and Moisture Loading

The second case considered for study is an epoxy beam of the following dimensions; length (L)=0.5m, thickness of (h_1)=0.0125m. PZT 5H layer of same length but with thickness of (h_2)=0.0025m is perfectly bonded to the epoxy beam. The PZT 5H layer is assumed to be poled along direction-2 as shown in Figure 3.1. The material properties of the epoxy are summarized below in Table 3.2. The specific heat of epoxy is taken as 1300J/Kg/^{o}k [29]. The properties of PZT 5H summarized are in page 93. The CME for epoxy is chosen to be of the order of 2.0x10^{-3} based on the values of 3501-6 epoxy resin [30]. The boundary conditions of the beam assembly are specified in Eq. (3.24). The moisture diffusivity of epoxy is the order of 10^{-12} m^2/s to 10^{-14} m^2/s, depending on the temperature [18]. The thermal diffusivity when computed from the values in Table 3.2 is of the order of 10^{-8} m^2/s. So, a choice of Lewis number of the order of 10^4 to 10^6 would be ideal for study. But, with such high Lewis number, the moisture concentration reaches a steady state much later than temperature does[4]. So, we choose a Lewis number of 10 with the following justification. The current study is focussed to simultaneously incorporate the effects of both temperature and moisture. So, the combined effect of temperature and moisture fields is more prominent if the time scales of both the diffusive phenomena do not differ greatly. For instance, in the case where Lewis number >10 is chosen (say, 10^3), the gradients of moisture are very high towards the end with higher moisture concentration as shown in Figure 3.31. A computationally expensive high resolution mesh is required in order to capture these gradients. Also, by choosing a Lewis number of 10, (which is the case with T300/5208 carbon/epoxy composite) it is still maintained that thermal diffusivity is faster than moisture diffusivity.

---

[4] A discussion on this was presented in the parametric study done in the second section of this chapter.

With this justification we choose û (inverse of Lewis number)=0.1 to accelerate the diffusion process and save computing time. Our intention is to mainly examine the effect of simultaneous heat and moisture diffusion on the overall deflection of epoxy beam. The evolution of temperature and moisture fields in this case is depicted in Figure 3.32. The finite difference equations of the corresponding governing equations of the system are solved numerically with the following grid sizes. Along the length span 1800 elements with a grid size of 0.278mm are chosen. Along the height 120 elements each of size 0.104mm are chosen for the epoxy layer. Along the height of PZT 5H layer, 9 elements each of size 0.278mm are chosen for study. The vertical displacement of the composite beam is depicted in Figure 3.33(a). It can be noted that the tip displacement of the beam increases with time. An explanation similar to the one offered in the case of Al-PZT 5H beam assembly can be offered in this case. Figure 3.33(b) compares the vertical displacement with and with out the external actuation being applied across PZT 5H layer. It can be noted that the displacement in the latter case has been subdued to a great extent.

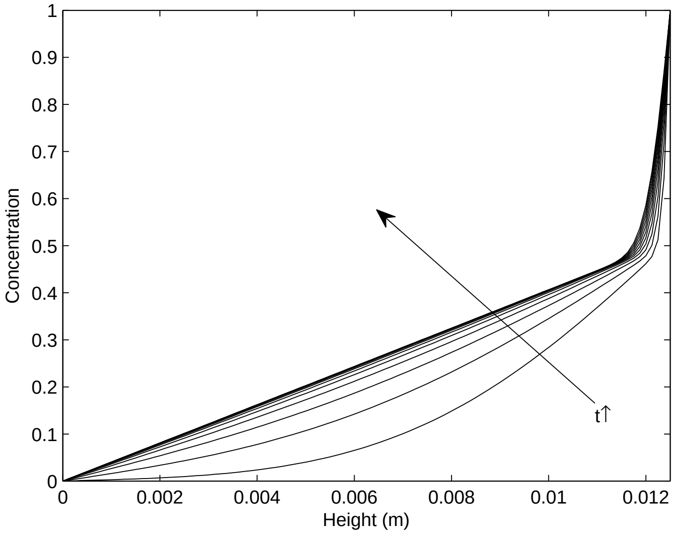

(a) Evolution of Moisture with time

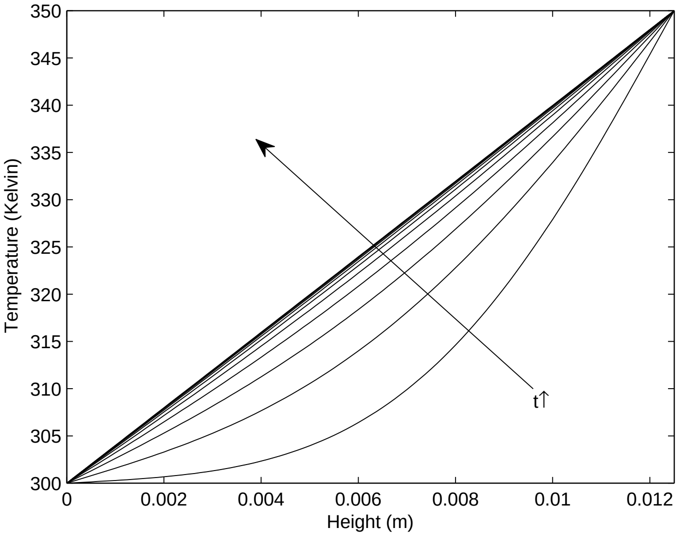

(b) Evolution of Temperature with time

Fig. 3.31. Plots show the evolution of temperature and moisture fields when $\hat{u}=10^{-3}$. (a) Depicts the evolution of moisture field (b) Depicts the evolution of temperature field. It can be noted that near the high concentration boundary, the gradients are large. The non-dimensionalised time parameter $\hat{\theta}$ varies from 0 to $7x10^{-2}$.t↑ indicates evolution with time.

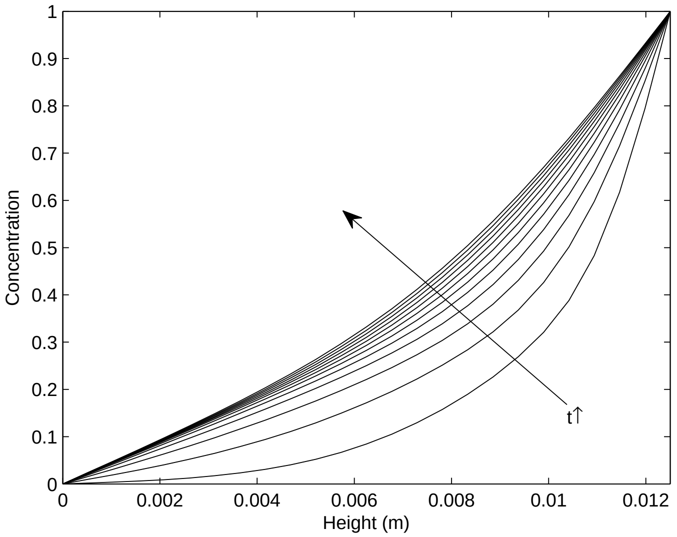

(a) Evolution of Moisture with time

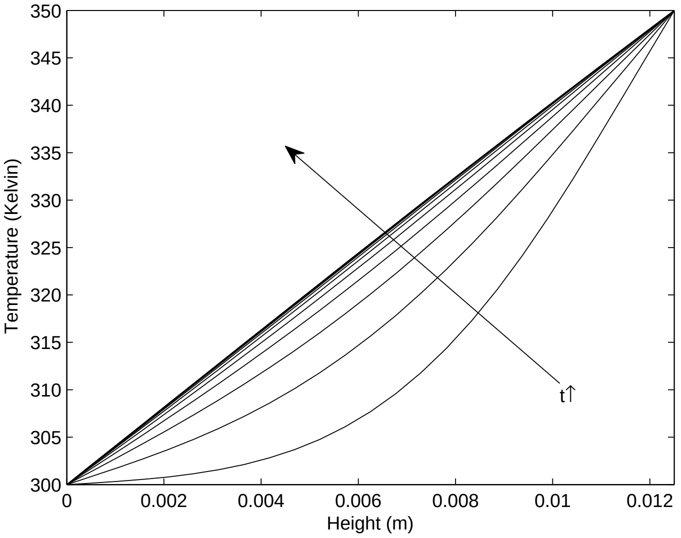

(b) Evolution of Temperature with time

Fig. 3.32. Plots show the evolution of temperature and moisture fields when $\hat{u}=10^{-1}$. (a) depicts the evolution of moisture field (b) depicts the evolution of temperature field. The non-dimensionalised time parameter $\hat{\theta}$ varies from 0 to $7x10^{-2}$. t↑ indicates evolution with time.

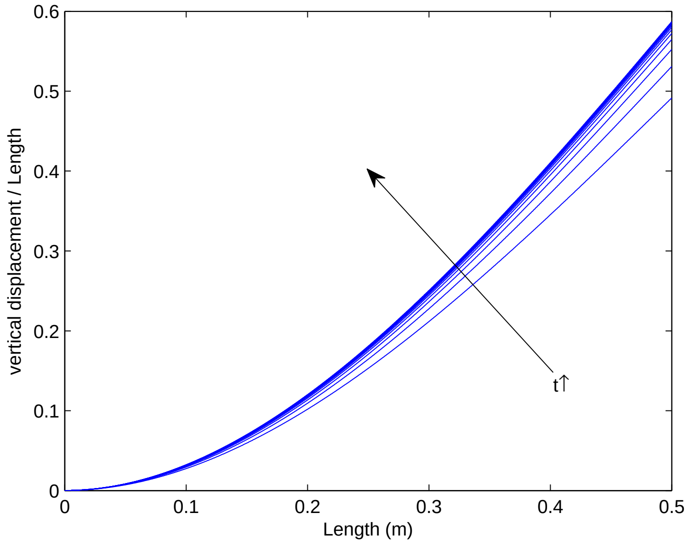

(a) Non-dimensionalized vertical displacement under no external actuation

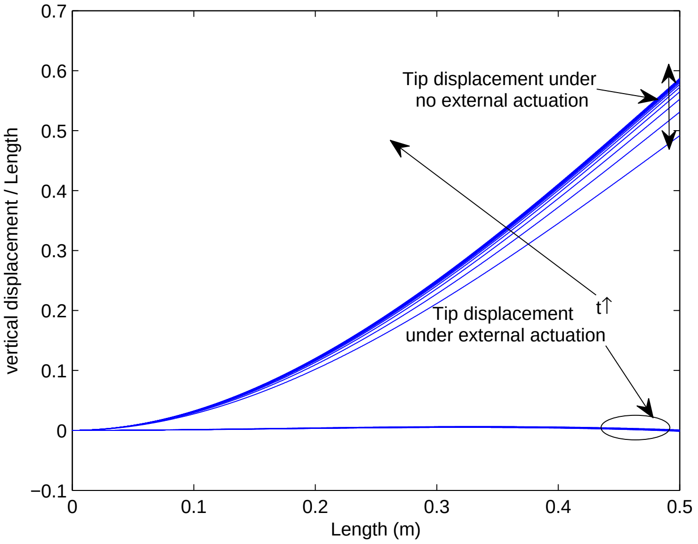

(b) Non-dimensionalized vertical displacement under the influence of an external voltage

Fig. 3.33. Plots show the evolution of vertical displacement of the beam assembly due to transient temperature and moisture changes when (a)no external voltage is applied across PZT 5H layer (b) external voltage is applied across PZT 5H layer. t↑ indicates evolution of displacement with time.

The Figure 3.34(a) depicts the evolution of axial stress with time, at half-length of the beam assembly. The trend observed in this case is similar to what has been observed in Al-PZT 5H beam. It can be noted that at the epoxy-PZT 5H boundary, the axial stress is discontinuous, as expected. Due to the bending of the beam towards the PZT 5H layer, it can be noted that the axial stresses become more compressive in the epoxy layer as we move from the bottom surface to the common interface between the two layers. The stresses becoming increasingly tensile with time at the bottom most layer of the beam due to increased bending of the beam assembly with time. The Figure 3.34(b) depicts the axial stress at the half length with of the beam assembly under the effect of actuating voltage. It can be noted that the axial stress is significantly reduced in the presence of actuating voltage.

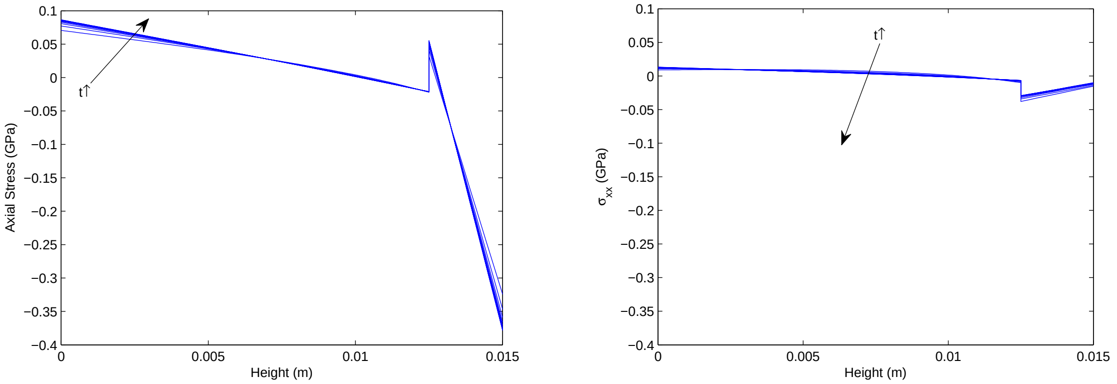

(a) Axial stress at mid section under no external voltage

(b) Axial stress at mid section under external voltage

Fig. 3.34. Plots show the evolution of axial stress σ_{xx} in the epoxy-PZT beam assembly due to transient temperature and moisture changes when (a)no external voltage is applied across PZT 5H layer (b) external voltage is applied across PZT 5H layer. t↑ indicates evolution of with time.

Figures 3.35(a) and 3.35(b) depict the evolution of shear stress with time, at half-length of the beam assembly due to transient temperature and moisture changes and with and with out external actuating voltage. As expected, the shear stress is continuous at the epoxy-

PZT 5H boundary. It can be noted that the material discontinuity at the epoxy-PZT 5H boundary, is reflected in the form of a kink in the shear plot at the common boundary. The shear stress is considerably reduced due to the application of external actuating mechanism as shown in Figure 3.35(b).

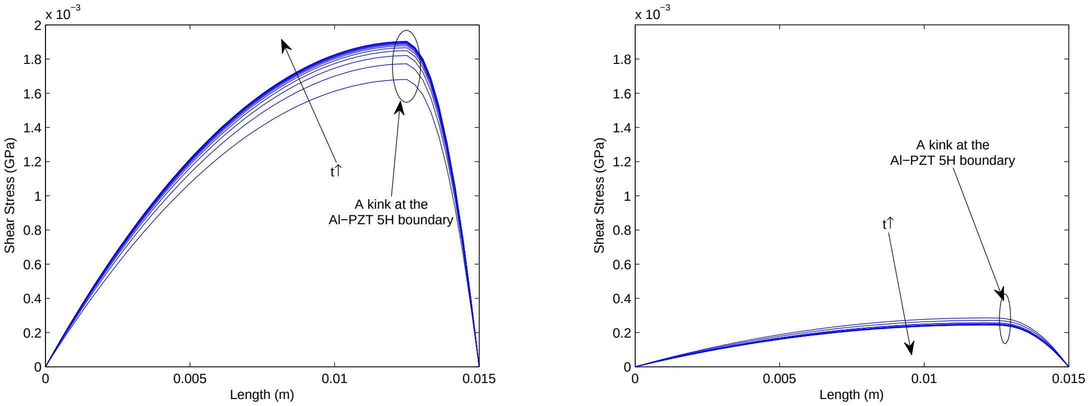

(a) Shear stress at mid section when no external actuation applied

(b) Shear stress at mid section due to actuating voltage

Fig. 3.35. Plots show the evolution of shear stress σ_{xy} in the epoxy-PZT beam assembly due to transient temperature and moisture changes when (a)no external voltage is applied across PZT 5H layer (b) external voltage is applied across PZT 5H layer. t↑ indicates evolution of displacement with time.

Figures 3.36(a) and 3.36(b) depict the evolution of the electric field and voltage induced across the PZT 5H layer respectively, when the beam assembly due to transient temperature and moisture changes. It can be noted from the figure that both the electric field and the potential difference vary significantly along the length. Figures 3.37(a) and 3.37(b) represent the required actuating voltage and the corresponding electric field to minimize the bending in the beam assembly subjected to the given loading conditions. It can be noted from Figures 3.37(b)and 3.36(a) that the electric fields developed in the PZT 5H layer are well over the range in which linear piezoelectric theory can be applied. The corresponding voltages developed are also extremely high. Such high electric fields when applied in direction opposite to the poling direction lead to the change in the polarization direction of the PZT 5H layer. That would indeed be the case with the epoxy-PZT 5H beam.

More the tip displacement in unactuated beam, more the external voltage necessary to minimize it. This can be observed in the Figure 3.37(a). Figure 3.37(b) depicts the electric field developed across the PZT 5H layer when an external actuating voltage is applied across it. It can be noted that the electric field so induced increases with time due to the increase in the required external voltage to minimize the bending in the beam. In practice, electric fields of the order of 1 MV/m in a piezoelectric material lead the system to the verge of non-linearity, in which the case the the problem needs to be addressed in terms of a non-linear theory. Crawley et al. [7] experimentally proved that when G 1195 PZT material is subjected to electric fields of the order of 1MV/m, the induced strain and the applied electric field cannot be related linearly[5]. However, the current study is focussed to analyze the problem in the context of a linearized theory, for simplicity. Therefore, no attempt will be made to incorporate any such non-linear effects.

---

[5] A prolonged exposure to electric fields of magnitude > 1MV/m might result in the excessive heating up of the piezoelectric material resulting in an eventual loss of piezoelectric properties/failure of the material.

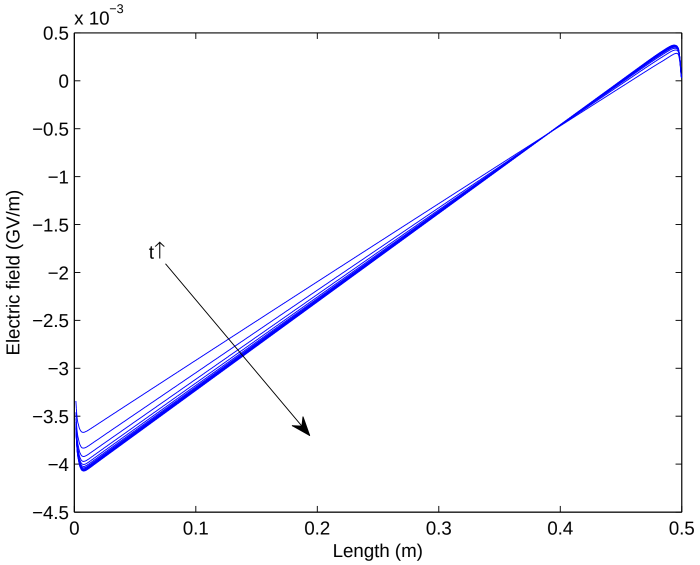

(a) Electric field induced across PZT 5H layer

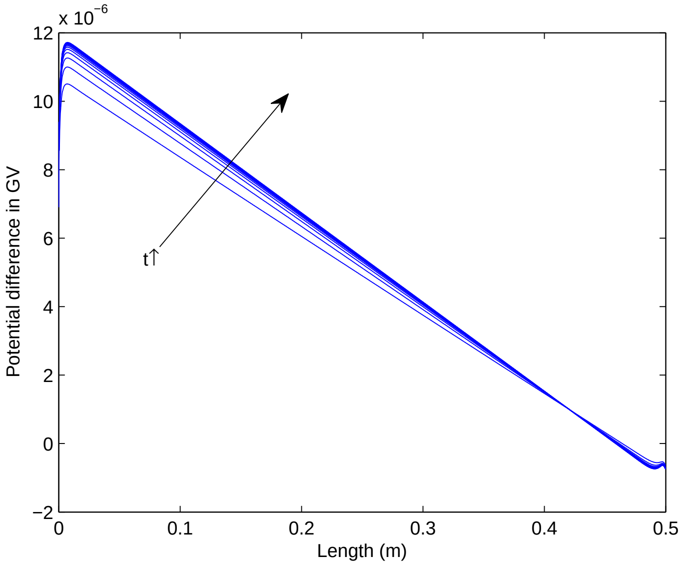

(b) Potential difference induced across PZT 5H layer

Fig. 3.36. Plots show the evolution of (a)the induced electric field **E** and (b)the induced potential difference across the epoxy-PZT beam assembly due to thermal and moisture changes. t↑ indicates evolution of displacement with time.

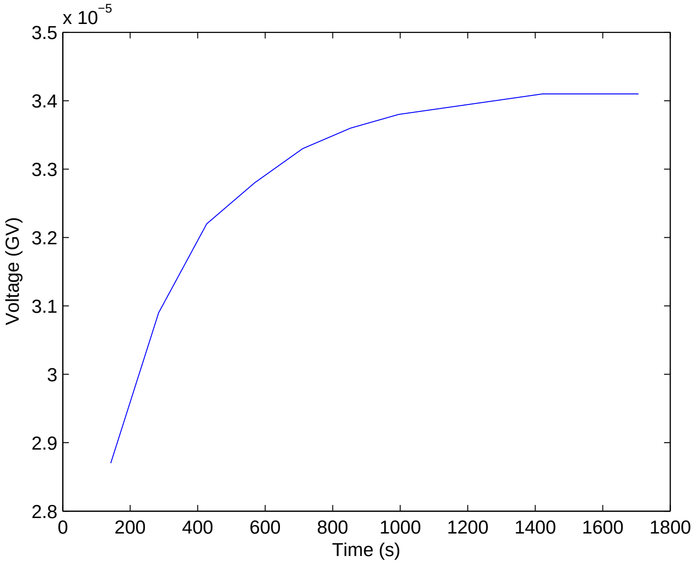

(a) Actuating voltage required across PZT 5H with time

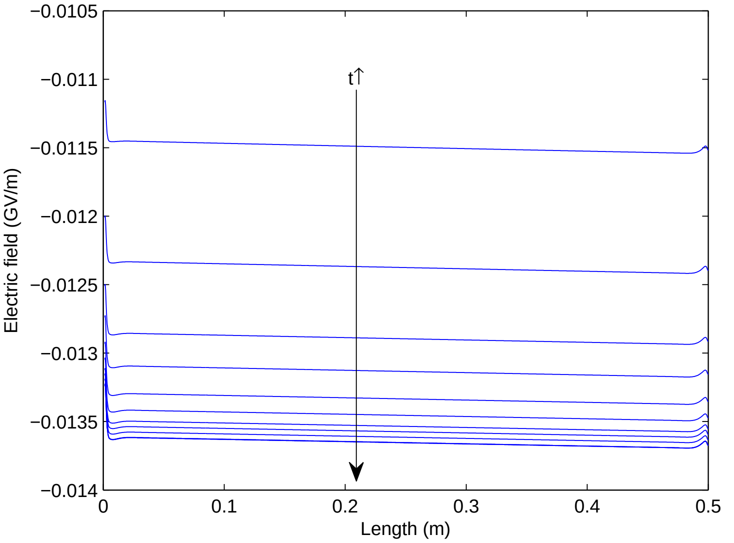

(b) Electric field induced across PZT 5H with time

Fig. 3.37. Plots show the (a)external actuating voltage required with time,to be applied across PZT 5H layer to minimize the bending of the beam under transient temperature and moisture changes. (b) depicts the evolution of the induced electric field(**E**) across the PZT 5H layer under the effect of an external actuating shown in. t↑ indicates evolution of displacement with time.

3. Carbon Fiber Reinforced Polymer (CFRP)-PZT 5H Composite Beam Subjected to Transient Thermal and Moisture Fields

The third case considered for study is a CFRP beam of the following dimensions; Length (L)=0.5m, thickness (h_1)=0.0125m. PZT 5H layer of same length but with thickness(h_2)=0.0025m is perfectly bonded to the CFRP beam. The PZT 5H layer is assumed to be poled along direction-2 as shown in Figure 3.1. The material properties of CFRP are summarized below in Table 3.8. The elastic modulus of CFRP is given below in the matrix form in page 111. The properties of PZT 5H are summarized in the matrix form in page 93. Due to the inherent anisotropy of CFRP, the elastic modulus, CTE and CME are different along the fiber reinforcement direction and normal to it . CFRP exhibits higher elastic modulus and thermal conductivity along the fiber direction but much lower CTE and CME compared to transverse direction due to the presence of carbon fibers. The CME values along and perpendicular to the carbon fiber direction for CFRP are chosen to be of the order of 10^{-6} and 10^{-3} based on the values reported by Poenninger [17]. The boundary conditions of the beam assembly are specified in Eq. (3.24). The moisture diffusivity of CFRP composites in the transverse direction is the order of 10^{-13} m^2/s to 10^{-14} m^2/s, depending on the temperature [18]. The thermal diffusivity along the transverse direction when computed from the values in Table 3.8 is of the order of 10^{-8} m^2/s. So, a choice of Lewis number of the order of 10^4 to 10^6 would be ideal for study. But, with such high Lewis number, the moisture concentration reaches a steady state much later than temperature does as mentioned earlier in the case of epoxy. So, we choose a Lewis number of 10 ($\hat{u}$=0.1) with the same justification given in the case of epoxy-PZT 5H composite beam. The evolution of temperature and moisture fields in this case is depicted in Figure 3.38.

$$\mathbf{C} = \begin{bmatrix} 141.6867 & 3.3735 & 3.3735 & 0 & 0 & 0 \\ 3.3735 & 10.7470 & 2.7470 & 0 & 0 & 0 \\ 3.3735 & 2.7470 & 10.7470 & 0 & 0 & 0 \\ 0 & 0 & 0 & 4.0000 & 0 & 0 \\ 0 & 0 & 0 & 0 & 4.1000 & 0 \\ 0 & 0 & 0 & 0 & 0 & 4.1000 \end{bmatrix} \text{GPa}$$

Table 3.8. Summary of the properties of CFRP [1]

CTE along fiber direction(mm/mm/k)α_1	0.5x10^{-6}
CTE along transverse direction(mm/mm/k)α_2=α_3	27x10^{-6}
CME along fiber direction(mm/mm/%H_2O)β_1	1x10^{-6}
CME along transverse direction(mm/mm/%H_2O)β_2 =β_3	1x10^{-3}
Axial thermal Conductivity(W/m/k)	10
Transverse thermal Conductivity(W/m/k)	0.5
density(g/cm^3)	1.6
specific heat(J/Kg/^ok) [31]	1200
Transverse thermal diffusivity(m^2/s) [31]	0.42x10^{-6}

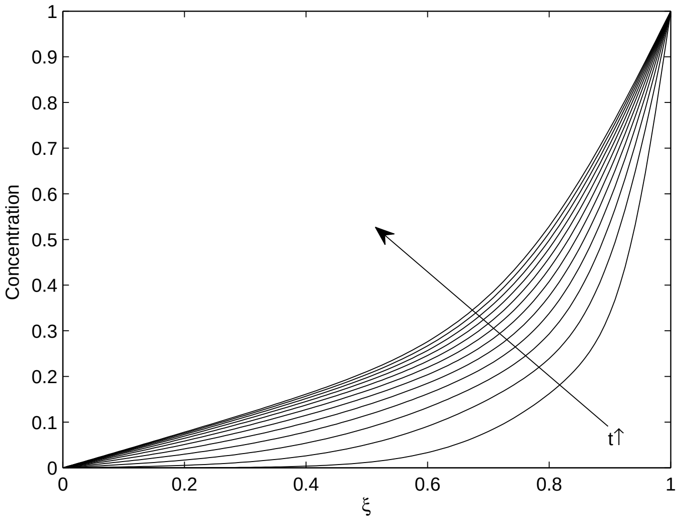

(a) Evolution of moisture with time

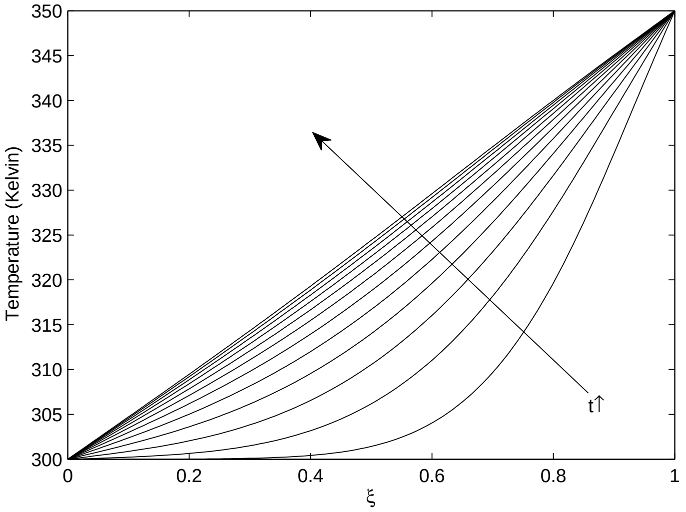

(b) Evolution of temperature with time

Fig. 3.38. Plots show the evolution of temperature and moisture fields when u=10^{-1}. (a) Depicts the evolution of moisture field (b) Depicts the evolution of temperature field. The non-dimensionalised time parameter $\hat{\theta}$ varies from 0 to 7x10^{-2}.t↑ indicates evolution with time.

The finite difference equations of the corresponding governing equations of the system are solved numerically with the following grid sizes. Along the length span 1800 elements with a grid size of 0.278mm are chosen. Along the height 120 elements each of size 0.104mm are chosen for the CFRP layer. Along the height of PZT 5H layer, 9 elements each of size 0.278mm are chosen for study. The vertical displacement of the composite beam is depicted in Figure 3.39(a). It can be noted that the tip vertical displacement of the beam is much lower in this cases compared to the earlier two cases owing to the smaller axial CTE of CFRP composite material compared to Al and un-reinforced epoxy materials. Also, it is noted that the tip vertical displacement decreases with time contrary to what is observed in the earlier two cases. This could be attributed to the anisotropic thermal response of CFRP material which can be noted from Table 3.8 where the CTE in fiber direction and direction normal to it are two orders of magnitude apart. Figure 3.39(b) compares the vertical displacement with and with out the external actuation being applied across PZT 5H layer. It can be noted that the displacement in the latter case has been subdued to a great extent.

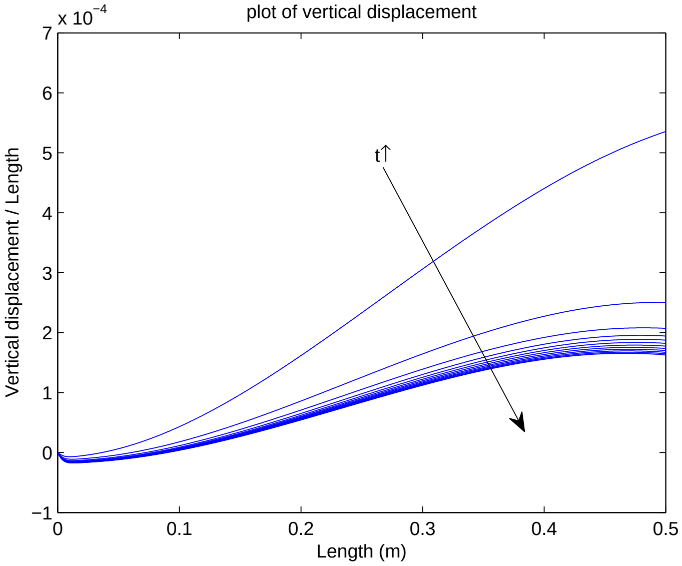

(a) Non-dimensionalized vertical displacement under no external actuation

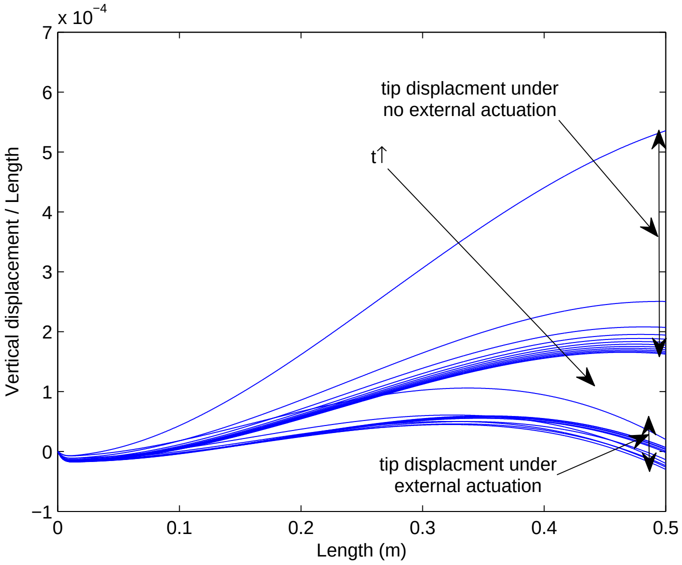

(b) Non-dimensionalized vertical displacement under external voltage

Fig. 3.39. Plots show the evolution of vertical displacement of the CFRP-PZT beam assembly under thermal load when (a)no external voltage is applied across PZT 5H layer (b) external voltage is applied across PZT 5H layer. t↑ indicates evolution of displacement with time.

The Figure 3.40(a) depicts the evolution of axial stress with time, at half-length of the beam assembly. The trend observed in this case is similar to what has been observed in the earlier two cases. It can be noted that at the CFRP-PZT 5H boundary, the axial stress is discontinuous, as expected. Due to the bending of the beam towards the PZT 5H layer, it can be noted that the axial stresses become more compressive in the CFRP layer as we move from the bottom surface to the common interface between the two layers. The stresses becoming increasingly tensile with time at the bottom most layer of the beam due to increased bending of the beam assembly with time. The Figure 3.40(b) depicts the axial stress at the half length with of the beam assembly under the effect of actuating voltage. It can be noted that the axial stress is significantly reduced in the presence of actuating voltage.

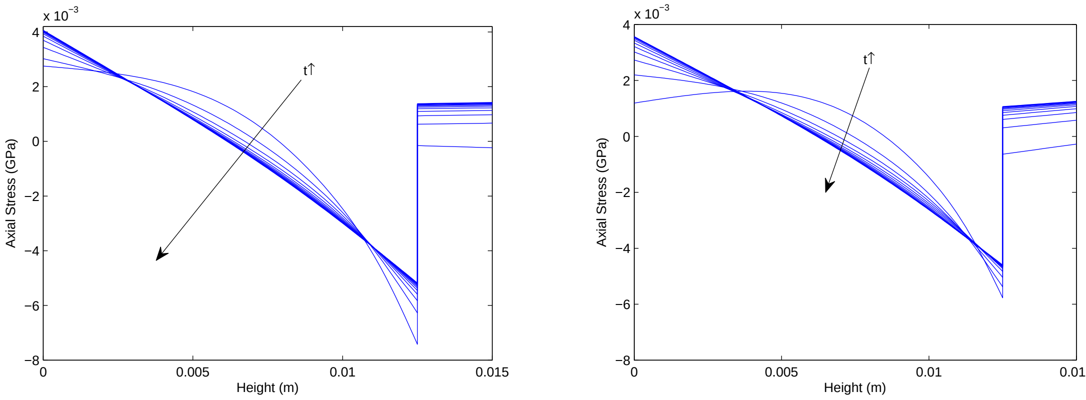

(a) Axial stress at half length under no external voltage

(b) Axial stress at half length under external voltage

Fig. 3.40. Plots show the evolution of axial stress σ_{xx} at half length in the CFRP-PZT beam assembly under thermal load when (a)no external voltage is applied across PZT 5H layer (b) external voltage is applied across PZT 5H layer. t↑ indicates evolution of with time.

Figures 3.41(a) and 3.41(b) depict the evolution of shear stress with time, at half-length of the beam assembly due to thermal and moisture changes and (a) under no external actuation (b) under external actuating voltage. As expected, the shear stress is continuous at the CFRP-PZT 5H boundary. It can be noted that the material discontinuity at the CFRP-PZT 5H boundary, is reflected in the form of a kink in the shear plot at the common boundary. The shear stress is considerably reduced due to the application of external actuating mechanism as shown in Figure 3.41(b).

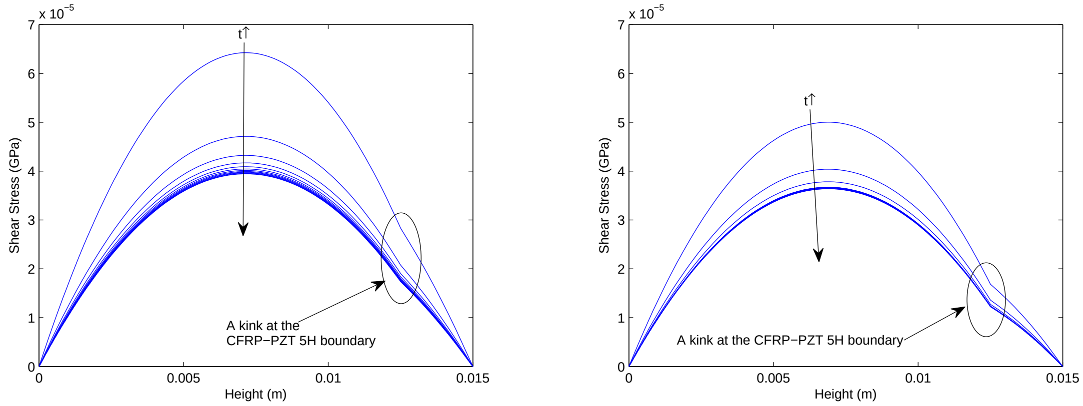

(a) Shear stress at mid section when no external actuating voltage applied

(b) Shear stress at mid section due to actuating voltage

Fig. 3.41. Plots show the evolution of shear stress σ_{xy} in the CFRP-PZT beam assembly subjected to transient temperature and moisture changes (a)no external voltage is applied across PZT 5H layer (b) external voltage is applied across PZT 5H layer. t↑ indicates evolution of displacement with time.

Figures 3.42(a) and 3.42(b) depict the evolution of the electric field and voltage induced across the PZT 5H layer respectively, when the beam assembly is subjected to transient thermal and moisture changes. It can be noted from the figure that both the electric field and the potential difference vary significantly along the length. Figures 3.43(a) and 3.43(b) represent the required actuating voltage and the corresponding electric field to minimize the bending of the beam assembly subjected to the given loading conditions. The external actuating voltage is noted have an opposite polarity which increasing magnitude than that necessary in the earlier discussed cases.

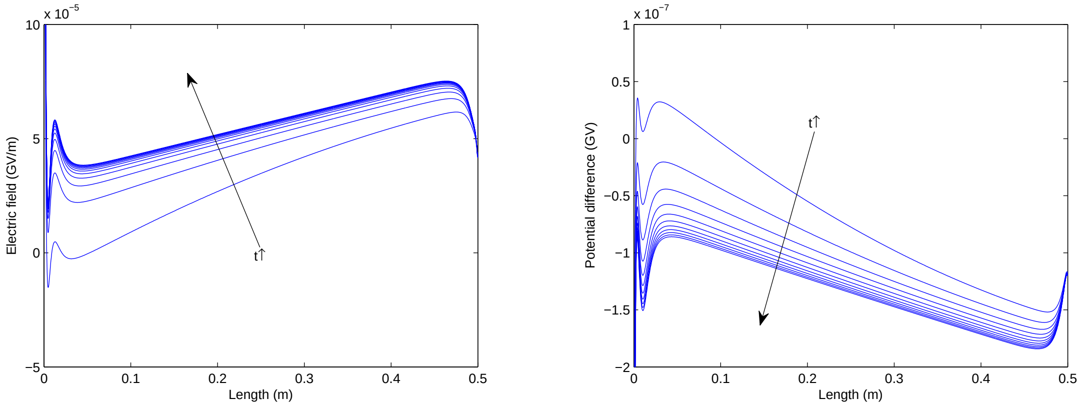

(a) Electric field induced across PZT 5H layer

(b) Potential difference induced across PZT 5H layer

Fig. 3.42. Plots show the evolution of (a)the induced electric field **E** and (b)the induced potential difference across the CFRP-PZT beam assembly due to transient temperature and moisture changes. t↑ indicates evolution of displacement with time.

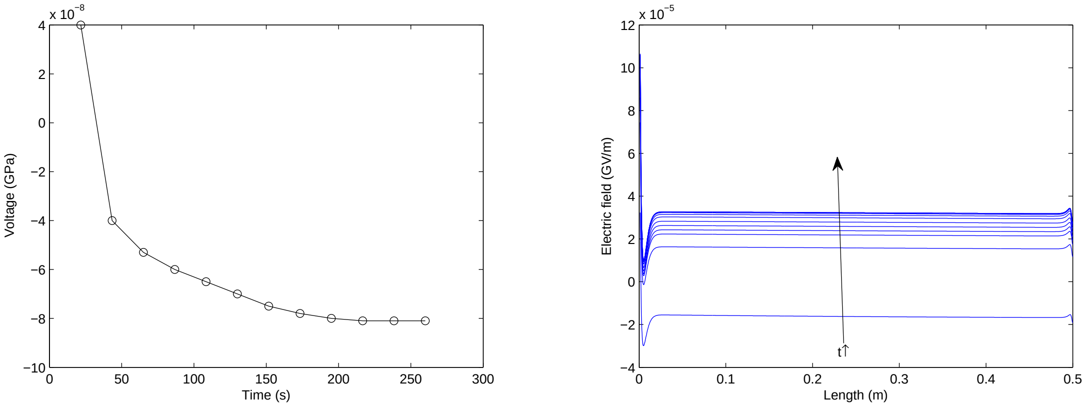

(a) Actuating voltage required across PZT 5H with time

(b) Electric field induced across PZT 5H with time

Fig. 3.43. Plots show the (a)external actuating voltage required with time, to be applied across PZT 5H layer to minimize the bending in the beam caused due to transient temperature and moisture changes (b) depicts the evolution of the corresponding electric field(**E**) across the PZT 5H layer due to the external actuating voltage. t↑ indicates evolution of with time.

4. Viscoelastic Epoxy-PZT 5H Composite Beam Subjected to Transient Thermal and Moisture Fields

In this subsection, the response characteristics of a linearly viscoelastic-PZT beam subjected to thermal and moisture changes is studied. To this end, the finite difference equations (3.36), (3.40), (3.41), (3.42), (3.46), (3.47) to (3.52) are solved at all nodal points considered in the domain to obtain the displacement and voltage fields in the beam. First, we begin by validating the numerical method implemented for this case. This is done by comparing the results obtained numerically and analytically for the case of a linearly viscoelastic cantilever beam subjected to uniform transverse load at two different temperatures. This is then followed by implementing the numerical method to address the problem under study.

The case of a viscoelastic epoxy-PZT 5H composite beam under heat and moisture diffusion effects is an extension of the earlier case of epoxy-PZT 5H beam under transient thermal and moisture changes. Here the epoxy material is assumed to exhibit linear viscoelastic behavior. Also, it is assumed to be a TSM for simplicity. The elastic, thermal and moisture effect related properties of epoxy are summarized in Table 3.2. The elastic, thermal and piezoelectric properties of PZT 5H are summarized in the matrix form in page 93. The stress relaxation modulus of viscoelastic epoxy like material takes the following form:

$$E_s(t,\theta,C) = E_s(\int_o^t \frac{ds}{a(\theta,C,\theta_o,C_o)}, \theta_o, C_o) \tag{3.57}$$

where 'a' represents the shift factor, initial temperature and initial concentration are denoted by θ_o and C$_o$ respectively. We assume $\theta_0 = 300k$ and C$_o = 0$ for current study. The shift factor is assumed to be the following function of temperature θ, and concentration C.

$$a(\theta,C) = 1 - k_1\frac{(\theta-\theta_o)}{\theta_o} - k_2(C - C_o)$$
$$\text{where} \;\; k_1 = 0.9,\; k_2 = 0.2 \tag{3.58}$$

To validate the numerical scheme implemented, two cases are considered where analytical solutions are known a priori . The two cases are as follows:

1. A linearly viscoelastic beam subjected to a uniform transverse load (q) at temperature $\theta = \theta_o = 300k$ and $C = C_o = 0$.

2. A linearly viscoelastic beam subjected to a uniform transverse load (q) at temperature $\theta = 350k$ and $C = C_o = 0$.

The following values of load and material properties are assumed.

$$E_s(t, \theta, C, \theta_o, C_o) = 1.75(1 + e^{\int_o^t \frac{ds}{t_o a(\theta, C, \theta_o, C_o)}}) \tag{3.59}$$

$$\frac{q}{E_s(0, \theta_o, C_o)} = 1.0\text{x}10^{-5} \tag{3.60}$$

where t_o denotes the relaxation time. For cases 1 and 2, the shift factor defined in Eq. (3.58) takes the following values :

$$\begin{aligned} &\text{Case 1} \quad a = 1 \\ &\text{Case 2} \quad a = 0.85 \end{aligned} \tag{3.61}$$

The tip vertical displacement and axial stress at half length of a linear viscoelastic cantilever beam subjected to a uniform transverse load is given as follows [5].

$$v(t) = \frac{qL^3 E_c(t, \theta, C, \theta_o, C_o)}{8I} \tag{3.62}$$

$$\sigma_{xx}(t) = \frac{q(L - x)^2 y}{2I} \tag{3.63}$$

where E_c denotes the creep compliance, I represents second moment of the cross section about z-axis, L represents the length and q represents the force per unit length. The ratio of tip vertical displacement of the beam of time to the initial tip displacement and the axial stress at mid section of the beam, at various instances of time obtained numerically and analytically are summarized in Table 3.9. It can be noted that there is a good agreement between the both the results. However, the initial displacement v(0) predicted numerically and analytically are 0.45m and 0.48m respectively. Figures 3.44 and 3.45 depict the evolution of vertical displacement and axial stress at midsection in the beam at aforementioned temperatures. It can be noted that the axial stress predicted numerically is in good agreement with the result predicted analytically.

Table 3.9. Comparison of numerically and analytically obtained results for tip vertical displacement of a viscoelastic cantilever beam under uniform transverse load at two different temperatures. $\theta = 300k$, $\theta = 350k$

	v(t)/v(0)			
time(t/t$_o$)	$\theta = 300k$		$\theta = 350k$	
	Numerical result	Analytical result	Numerical result	Analytical result
0	1.0	1.0	1.0	1.0
0.5	1.0244	1.0247	1.0286	1.0290
0.10	1.0482	1.0488	1.0563	1.0571
0.15	1.0714	1.0723	1.0833	1.0845
0.20	1.0941	1.0952	1.1095	1.1110
0.25	1.1161	1.1175	1.1349	1.1368
0.30	1.1377	1.1393	1.1596	1.1618
0.35	1.1587	1.1605	1.1836	1.1861
0.40	1.1792	1.1813	1.2069	1.2097
0.45	1.1993	1.2015	1.2296	1.2326
0.50	1.2188	1.2212	1.2526	1.2548

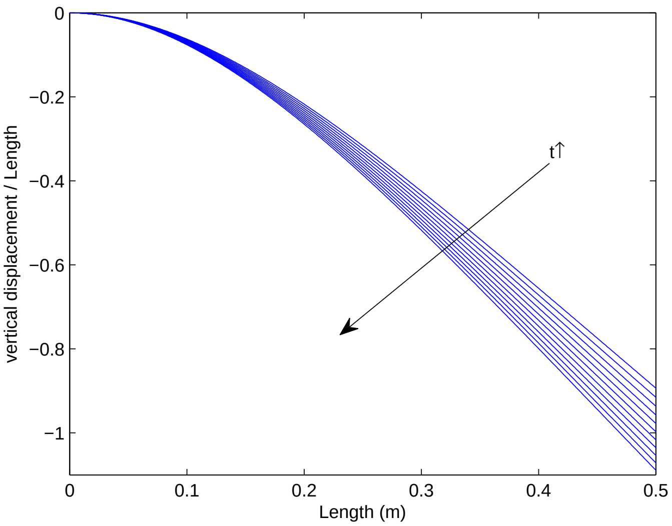

(a) Tip vertical displacement per unit length of the beam

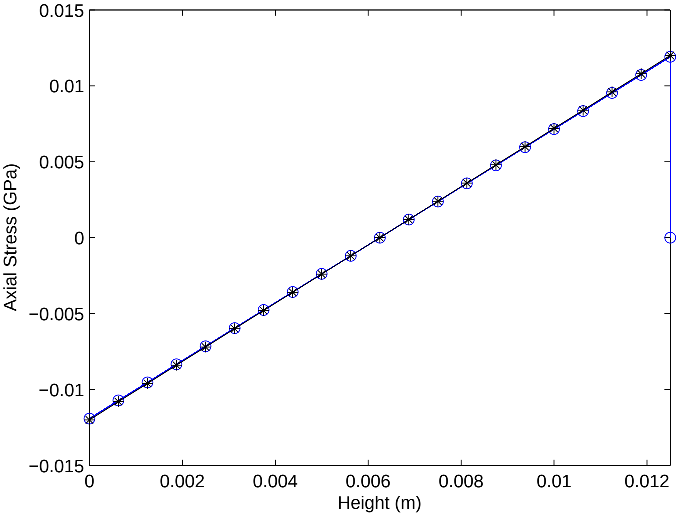

(b) Axial stress in the beam at half length (*)indicates analytical solution (o) indicates numerical solution

Fig. 3.44. The plot (a) shows the evolution of tip vertical displacement and the plot (b) compares the axial stress at mid section obtained analytically represented by (*) and numerically represented by (o)for the viscoelastic beam under uniform transverse load at initial temperature θ_o=300k. t↑ indicates the direction of time evolution. t varies from 0-50s with Δt/t$_o$=5s.

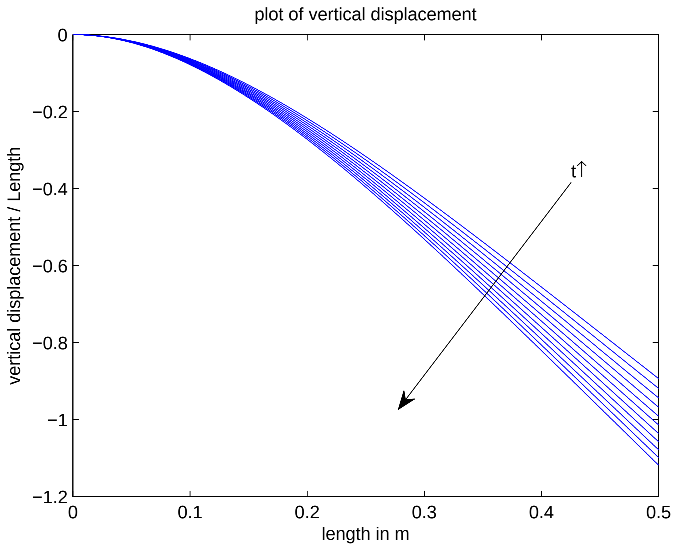

(a) Tip vertical displacement per unit length of the beam

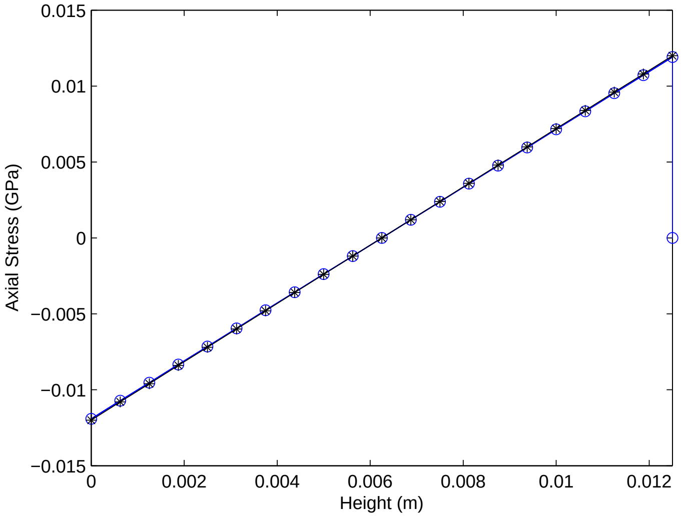

(b) Axial stress in the beam at half length (*)indicates analytical solution (o) indicates numerical solution

Fig. 3.45. The plot (a) shows the evolution of tip vertical displacement and the plot (b) compares the axial stress at mid section obtained analytically represented by (*) and numerically represented by (o)for the viscoelastic beam under uniform transverse load at initial temperature θ_o=350k. t↑ indicates the direction of time evolution. t varies from 0-50s with Δt/t$_o$=5s.

For the case under study the following properties are considered for the viscoelastic material. The properties summarized in Table 3.10 are same as those of epoxy material. The stress relaxation modulus of the material is assumed to be form specified in Eq. (3.59) with shift factor assuming the form specified in Eq. (3.58).

Table 3.10. Summary of the properties of viscoelastic epoxy [1]

Poission's ratio ν	0.25
CTE (mm/mm/$^oC)\alpha$	6x10^{-5}
CME(mm/mm/% $H_20)\beta$	2x10^{-3}
Thermal Conductivity(W/m/k)	0.1
density(g/cm^3)	1.2
specific heat(J/Kg/^ok)	1300
Relaxation time t$_o$ (s)	3000

The relaxation time specified in Table 3.10 is assumed to be of the same order as the time taken for the temperature and moisture fields to reach a steady state, for simplicity. To this end, t$_o$ is chosen to be 3000s. The PZT 5H layer is assumed to be poled along direction-2 as shown in Figure 3.1. The properties of PZT 5H are summarized in the matrix form in page 93. So, we choose a Lewis number of 10 with the same justification given in the case of epoxy-PZT 5H composite beam. Figures 3.46(a) and 3.46(b) depict the evolution of temperature and moisture fields in the viscoelastic material. Figure 3.47 depicts the plot of stress relaxation modulus with time at temperatures 300k and 350k. It can be noted that at an increase in temperature speeds up the relaxation process. The dimensions considered for study are as follows: Length (L)=0.5m, thickness (h_1)=0.0125m. PZT 5H layer of same length but with thickness(h_2)=0.0025m is perfectly bonded to the viscoelastic beam. The length span is divided into 1800 elements each of length 0.278mm and the thickness of viscoelastic material is divided into 100 elements of thickess 0.125mm. The thickness of PZT later is divided into 9 elements of thickness 0.278mm. In what follows, the vertical displacement, axial and shear stresses at half length of the beam, electric field and voltage across PZT layer are numerically obtained for the actuated and unactuated beams until temperature and moisture fields reach steady state i.e. $0 < t < 1800$. For $t > 1800$, the any changes in the field values can be purely attributed to the viscoelastic effects. Therefore this is addresses separately.

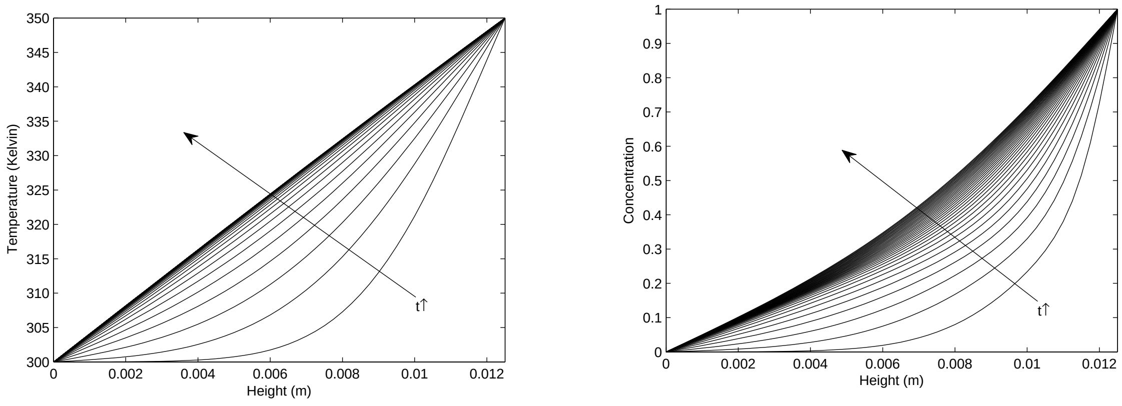

(a) Evolution of temperature with time (b) Evolution of concentration with time

Fig. 3.46. The plot (a) shows the evolution of temperature and the plot (b) shows the evolution of concentration in the viscoelastic material. t↑ indicates the direction of time evolution. t varies from 0-1800s with Δt=70s.

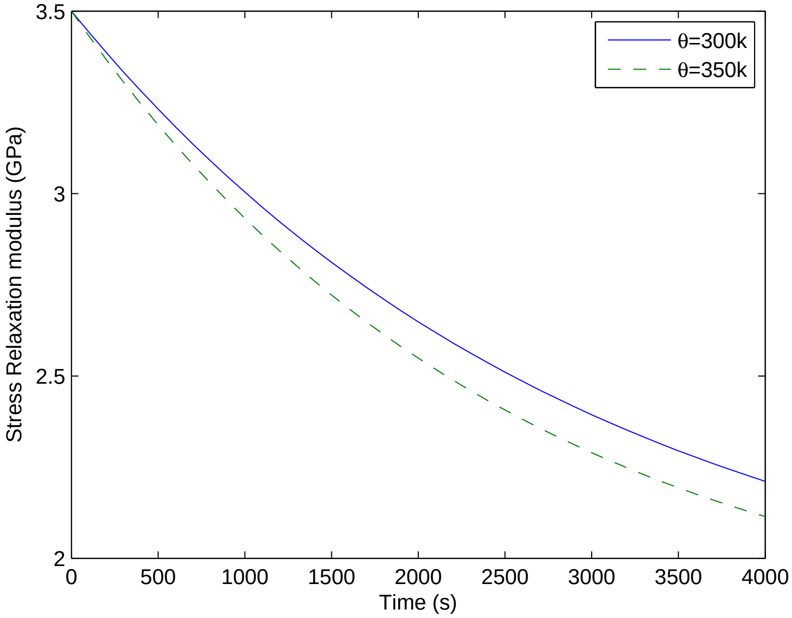

Fig. 3.47. Plot shows the stress relaxation modulus at 300k and 350k.

The vertical displacement of the composite beam as time varies is depicted in Figure 3.48(a). It can be noted that the tip vertical displacement increases with time. Under the influence of an external actuating voltage the vertical displacement of the beam is suppresses largely as depicted in Figure 3.48(b). It can be noted that the tip vertical displacement is more in this case compared to the case of elastic epoxy-PZT 5H composite beam as shown in Figure 3.33. This could be attributed to the softening of the viscoelastic material as temperature evolves as follows. As the temperature increases in the viscoelastic material, the relaxation modulus of layers below the layer CD in Figure 3.1(b) becomes progressively lesser with time thus offering lesser resistance to thermal expansion of the higher temperature layers above it. Thus bending is more pronounced here compared to the case where material doesn't soften with time. It will be observed that due to relatively more bending in this case compared to the case of elastic epoxy-PZT 5H layer, the external actuating voltage required to minimize deformation in this case is slightly higher as well.

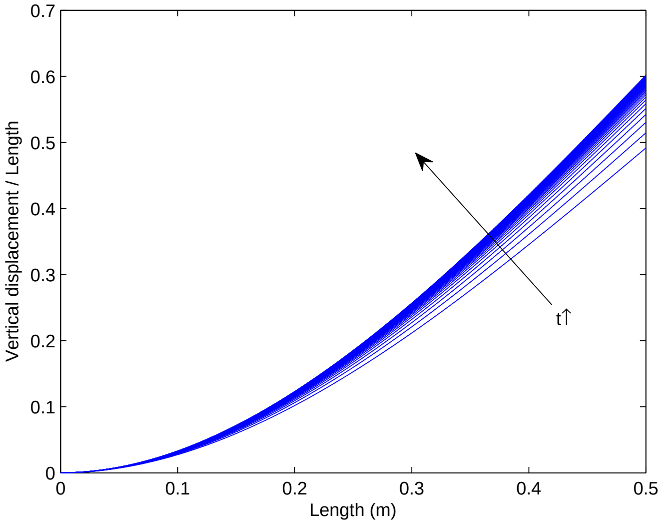

(a) Non-dimensionalized vertical displacement of the beam with time

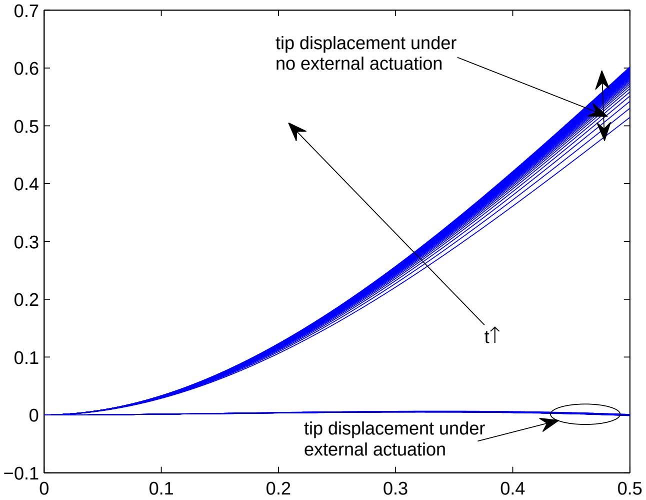

(b) Comparison of the Non-dimensionalized vertical displacement of the beam with and with out the influence of an external actuating voltage

Fig. 3.48. Plots show the evolution of vertical displacement of the viscoelastic epoxy-PZT beam assembly due to transient thermal and moisture changes when (a)no external voltage is applied across PZT 5H layer (b) external voltage is applied across PZT 5H layer. t↑ indicates evolution of displacement with time. t varies from 0-1800s with Δt=70s.

The axial stress at half length of the beam is depicted in Figure 3.49(a) due to temperature and moisture changes where no external actuation is applied. Figure 3.49(b) depicts the axial stress at half length when external voltage is applied across PZT 5H beam. It can be noted that the axial stress is largely reduced in the latter case.

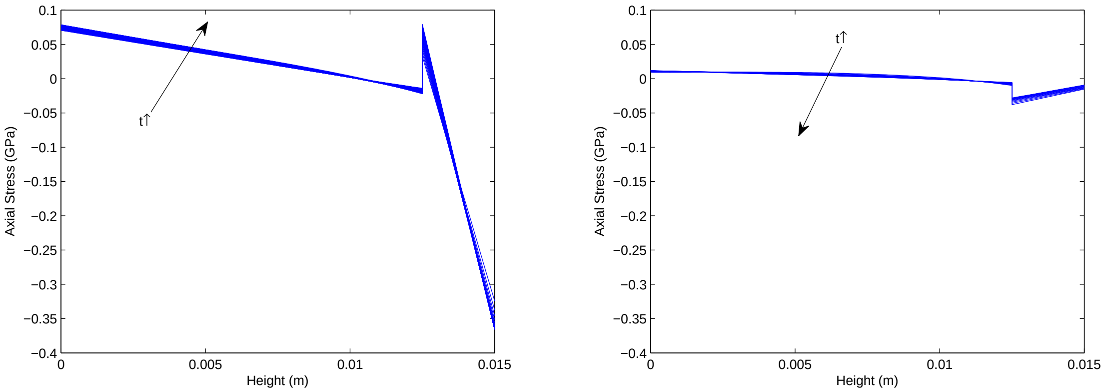

(a) Axial stress at mid section under no external voltage

(b) Axial stress at mid section under external voltage

Fig. 3.49. Plots show the evolution of axial stress σ_{xx} in the viscoelastic epoxy-PZT beam assembly due to transient temperature and moisture changes when (a)no external voltage is applied across PZT 5H layer (b) external voltage is applied across PZT 5H layer. t↑ indicates evolution of with time.

The shear stress at half length of the beam is depicted in Figure 3.50(a) due to temperature and moisture changes. Figure 3.50(b) depicts the same when an external voltage is applied across PZT layer. It can be noted that the shear stress is largely suppressed in the composite beam.

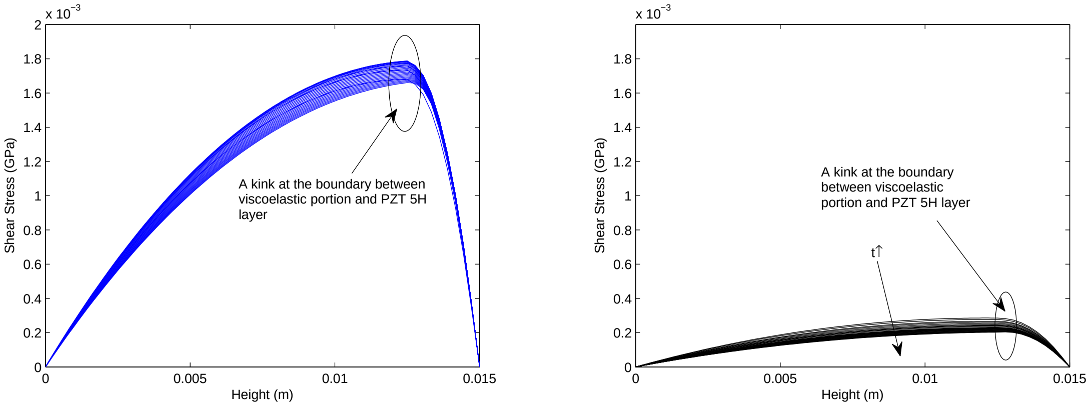

(a) Shear stress at mid section under due to thermal load

(b) Shear stress at mid section due to actuating voltage

Fig. 3.50. Plots show the evolution of shear stress σ_{xy} in the viscoelastic epoxy-PZT beam assembly due to transient temperature and moisture changes when (a)no external voltage is applied across PZT 5H layer (b) external voltage is applied across PZT 5H layer. t↑ indicates evolution of displacement with time.

The electric field and voltage developed across the PZT layer due to the bending of the beam and temperature changes are depicted in Figures 3.51(a)and 3.51(b). Both the electric field and voltage in the PZT layer vary along the length with a maximum at the fixed end. Also, the voltage developed across the PZT layer also are very high. When PZT material is subjected to such high electric field acting opposite to its poling direction, the dipoles in the PZT material reorient themselves along the direction of external electric field. Such effects care not accounted for in the current study. The magnitude of electric field is well over the range in which the linear piezoelectricity can be appealed to and there is a need to address the problem in the context of a non-linear framework which will not be done in this thesis.

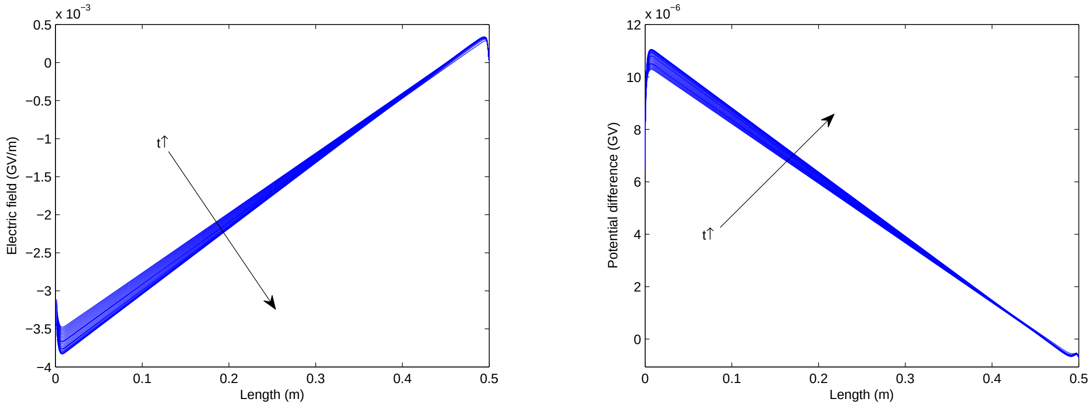

(a) Electric field induced across PZT 5H layer

(b) Potential difference induced across PZT 5H layer

Fig. 3.51. Plots show the evolution of (a)the induced electric field **E** and (b)the induced potential difference across the viscoelastic epoxy-PZT composite beam due to temperature and moisture changes. t↑ indicates evolution of displacement with time.

The voltage required to suppresses the deformation in the composite beam and the corresponding electric field are depicted in Figures 3.52(a) and 3.52(b). It can be noted that the voltage required to suppress the deformation increases with time due to the increase in bending with time of the unactuated beam.

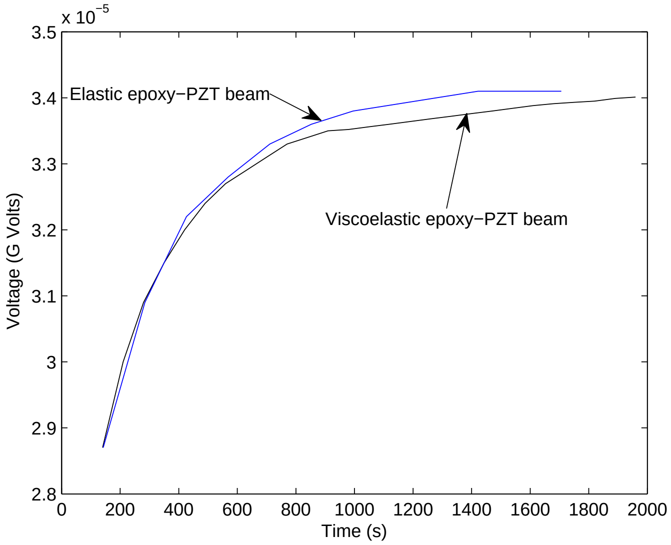

(a) Actuating voltage required across PZT 5H with time

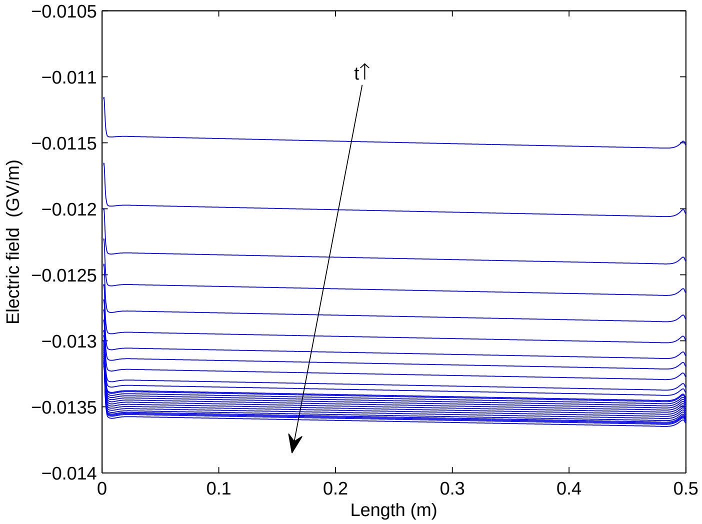

(b) Electric field induced across PZT 5H with time

Fig. 3.52. Plots show the (a)external actuating voltage required with time, to be applied across PZT 5H layer to minimize the bending of the beam under transient temperature and moisture changes for elastic and viscoelastic response of epoxy material. (b) depicts the evolution of the induced electric field(**E**) across the PZT 5H layer under the effect of an external actuating shown in. t↑ indicates evolution of displacement with time.

CHAPTER IV

CONCLUSION AND FUTURE WORK

The implementation of perfectly bonded surface piezoelectric actuators to minimize the temperature and moisture induced deformation in elastic and viscoelastic cantilever beams was studied.The coupled hygrothermal and mechanical constitutive equations for the elastic material have been derived from the basic conservation laws and the second law of thermodynamics. The field equations for a linearized theory are obtained by assuming sufficiently small deformation field. In the linearized theory, the effect of temperature and moisture fields on the strain field was incorporated through the coefficients of thermal and moisture expansion (CTE, CME). The constituive equations for the viscoelastic material were derived appealing to the correspondence principle. The viscoelastic material was asuumed to be thermorheologically simple. A parametric study was performed to study the degree of coupling between the temperature and the moisture diffusive phenomena. This numerical study provided useful insights about the dependence of temperature and moisture fields on the ratio of moisture and thermal diffusivities and the coupling constant. A discussion on the choice of piezoelectric material chosen for actuation was presented.

A numerical method based on the finite difference was implemented for the field equations. The numerical method was verified by solving the problem of bending in a cantilever beam under a uniform distributed surface load. The results obtained numerically were in good agreement with the results analytically obtained. A convergence study was performed to obtain optimum values of grid sizes for use for the current problem. The response of composite beams comprised of aluminium-PZT 5H, unreinforced epoxy-PZT 5H, CFRP-PZT 5H and linearly viscoelastic epoxy-PZT 5H under transient temperature and moisture changes were obtained numerically. Based on these results, the external actuation required across PZT 5H layer to minimize deformation in the composite beams were obtained numerically.

By controlling the deformation in the composite beam with this external voltage it is shown that the tip displacement and the magnitude of axial stresses were reduced significantly. Numerically obtained results were in good agreement with experimental results.

In case of Aluminium-PZT composite beam, the effect of moisture was ignored due to the negligible diffusion of moisture through aluminium. The tip displacement of the composite beam is seen to increase steadily to a reach a constant value when temperature field reaches a steady state. A similar trend was observed in the case of epoxy-PZT 5H composite beam. But the magnitude of electric field predicted in the PZT 5H layer suggests that the system response cannot be adequately addressed by a linearized theory due to the non-linear behavior of the PZT material at high magnitudes of electric fields. So, the problem needs to be addressed in a proper non-linear framework. In case of the CFRP-PZT 5H layer, the tip displacement is observed to decrease to a steady state value. This could be attributed due to the anisotropy of the CFRP material where the CTE, CME are minimum along fiber direction and maximum along the transverse direction.

In viscoelastic material-PZT 5H composite beam the deformation in an unactuated state was observed to be greater than the elastic-PZT 5H beam. But, relatively lesser actuating voltage was required in the former case to minimize bending in the beam.

A. Future Work

The current study analyzed the use of piezoelectric actuators to control the deformation of various composite beams under temperature and moisture effects. The PZT material was assumed to be perfectly to the elastic/viscoelastic beam. In practice, piezoelectric materials are used in the form of patches at specific locations on the beam. So, one could solve the current problem by assuming that several piezoelectric surface bonded patches distributed along the length are used for actuation. The elastic material properties, CTE and CME were assumed to be constants in this study for simplicity . This might not be case as it has been reported in several studies that the material properties can be dependent on field variables such as stress, strain, temperature and moisture fields. To this end, one could assume field variable dependent material properties to address the current problem. In such a case, the viscoelastic material can no longer be assumed as TSM. In this study, the stress and strain fields are assumed to be dependent on temperature and moisture changes (through CTE and CME) but vice-versa has not been considered. One could address a fully coupled problem where temperature and moisture evolution in the body is dependent on stress and strain fields and also vice-versa. The current study doesn't account for any mechanical loads acting on the composite beam. One could also solve the current problem incorporating the effect of external mechanical loads on the system.

REFERENCES

[1] C. Harper, *Handbook of Plastics, Elastomers, and Composites.* New York: McGraw-Hill Professional, 2002.

[2] G. Song, X. Zhou, and W. Binienda, "Thermal deformation compensation of a composite beam using piezoelectric actuators," *Smart Materials and Structures*, vol. 13, no. 1, pp. 30–37, 2004.

[3] K. Potter, *Resin Transfer Moulding.* London: Chapman and Hall, 1997.

[4] M. Kutz, *Mechanical Engineers' Handbook.* New York: John Wiley and Sons, Inc., 2005.

[5] A. Wineman and K. Rajagopal, *Mechanical Response of Polymers: An Introduction.* New York: Cambridge Univ. Press, 2000.

[6] E. Crawley and J. De Luis, "Use of piezoelectric actuators as elements of intelligent structures," *AIAA Journal*, vol. 25, no. 10, pp. 1373–1385, 1987.

[7] E. Crawley and E. Anderson, "Detailed models of piezoceramic actuation of beams," *Journal of Intelligent Material Systems and Structures*, vol. 1, no. 1, pp. 4–25, 1990.

[8] Y. Zhou and H. Tiersten, "An elastic analysis of laminated composite plates in cylindrical bending due to piezoelectric actuators," *Smart Materials and Structures*, vol. 3, no. 3, pp. 255–265, 1994.

[9] H. Lee and D. Saravanos, "Coupled layerwise analysis of thermopiezoelectric composite beams," *AIAA Journal*, vol. 34, no. 6, pp. 1231–1237, 1996.

[10] S. Ahmad, C. Upadhyay, and C. Venkatesan, “Electro-thermo-elastic formulation for the analysis of smart structures,” *Smart Materials and Structures*, vol. 15, no. 2, pp. 401–416, 2006.

[11] Y. Weitsman, “Effects of fluids on polymeric composites-a review,” *Polymer Matrix Composites*, vol. 2, pp. 369–401.

[12] G. Springer, *Environmental Effects on Composite Materials. Volume 3.* Lancaster, PA: Technomic Publishing Co., Inc., 1988.

[13] Y. Weitsman, “Coupled damage and moisture-transport in fiber-reinforced, polymeric composites,” *International Journal of Solids and Structures*, vol. 23, no. 7, pp. 1003–1025, 1987.

[14] A. Muliana, K. R. Rajagopal, and S. C. Subramanian, “Degradation of an elastic composite cylinder due to the diffusion of a fluid,” *Journal of Compoiste Materials*, vol. 43, no. 11, pp. 1225–1249, 2009.

[15] H. Bouadi and C. Sun, “Hygrothermal effects on the stress field of laminated composites,” *Journal of Reinforced Plastics and Composites*, vol. 8, no. 1, pp. 40–54, 1989.

[16] L. Cai and Y. Weitsman, “Non-Fickian moisture diffusion in polymeric composites,” *Journal of Composite Materials*, vol. 28, no. 2, pp. 130-154, 1994.

[17] A. Poenninger and B. Defoort, “Determination of the coefficient of moisture expansion (CME),” in *Proc. of the 9th Int. Symp. on Materials in a Space Environment, 2003*, Noordwijk, The Netherlands, June 2003, pp. 567–572.

[18] W. Wright, “The effect of diffusion of water into epoxy resins and their carbon-fibre reinforced composites,” *Composites*, vol. 12, no. 3, pp. 201–205.

[19] F. Schwarzl and A. Staverman, “Time-temperature dependence of linear viscoelastic behavior,” *Journal of Applied Physics*, vol. 23, no. 8, pp. 838–843, 2009.

[20] K. Rajagopal and A. Wineman, “Applications of viscoelastic clock models in biomechanics,” *Acta Mechanica*, vol. 213, no. 3–4, pp. 255–266, 2010.

[21] D. Flaggs and F. Crossman, “Analysis of the viscoelastic response of composite laminates during hygrothermal exposure,” *Journal of Composite Materials*, vol. 15, no. 1, pp. 21–40, 1981.

[22] G. Sih and S. Shih, “Transient hygrothermal stresses in composites: coupling of moisture and heat with temperature varying diffusivity,” *International Journal of Engineering Science*, vol. 18, no. 1, pp. 19–42, 1980.

[23] G. Sih, A. Ogawa, and S. Chou, “Two-dimensional transient hygrothermal stresses in bodies with circular cavities: moisture and temperature coupling effects,” *Journal of Thermal Stresses*, vol. 4, no. 2, pp. 193–222, 1981.

[24] P. Henry, “Diffusion in absorbing media,” *Proceedings of the Royal Society of London. Series A, Mathematical and Physical Sciences*, vol. 171, no. 945, pp. 215–241, 1939.

[25] R. Hartranft and G. Sih, “The influence of the soret and dufour effects on the diffusion of heat and moisture in solids,” *International Journal of Engineering Science*, vol. 18, no. 12, pp. 1375–1383, 1980.

[26] G. Sih, J. Michopoulos, and S. Chou, *Hygrothermoelasticity.* Dordrecht,The Netherlands: Kluwer Academic Publishers, 1986.

[27] H. Tiersten, “On the nonlinear equations of thermo-electroelasticity,” *International Journal of Engineering Science*, vol. 9, no. 7, pp. 587–604, 1971.

[28] J. Yang, *An Introduction to the Theory of Piezoelectricity.* New York: Springer, 2005.

[29] M. Richardson. (2010) Kaye & laby tables of physical and chemical constants. [Online]. Available: http://www.kayelaby.npl.co.uk/general_physics/2_3/2_3_6.html

[30] D. Cairns and D. Adams, "Moisture and thermal expansion properties of unidirectional composite materials and the epoxy matrix," *Journal of Reinforced Plastics and Composites*, vol. 2, no. 4, pp. 239–255, 1983.

[31] N. Avdelidis, D. Almond, A. Dobbinson, B. Hawtin, C. Ibarra-Castanedo, and X. Maldague, "Aircraft composites assessment by means of transient thermal NDT," *Progress in Aerospace Sciences*, vol. 40, no. 3, pp. 143–162, 2004.

VITA

Ramachandra Srinivasa Chaitanya Kuravi was born in India. He received his B.Tech. degree in mechanical engineering from the Indian Institute of Technology, Guwahati in 2008. He pursued his graduate studies in Mechanical Engineering at the Texas A&M University, College Station from August 2008 to December 2010. He received M.S. degree in mechanical engineering in May 2011. He was a member of the Non-Linear Mechanics Laboratory in the Texas A&M University during this period.

He may be reached at the following address:

Department of Mechanical Engineering
3123 TAMU
Texas A&M University
College Station TX 77843-3123

The typist for this thesis was the author himself.